UNIVERSITÀ
DI PAVIA

PhD IN BIOMEDICAL SCIENCES
DEPARTMENT OF BRAIN AND BEHAVIORAL SCIENCES
UNIT OF NEUROPHYSIOLOGY

FUNCTIONAL ANALYSIS AND TRANSCRIPTOME PROFILE OF MENINGES AND SKIN FIBROBLASTS FROM HUMAN AGED DONORS

PhD Tutor: Dr. Cristina Cereda

PhD dissertation of
Fantini Valentina

Curriculum Neuroscience
Cicle XXXIV - a.a. 2018 – 2021

Abstract

The number of elderly people is expected to rise to 1.5 billion by 2050 in the world, accounting for 16% of the global population, suggesting that one in every six people would be 65 or older. For this reason, the need to study the characteristics of aging in depth is becoming increasingly important. Aging is linked to a steady reduction in cognitive and physical abilities, as well as an increased risk of diseases like cancer, diabetes, cardiovascular, musculoskeletal, and neurological problems. Because of their enormous impact on healthspan and quality of life, neurodegeneration and accompanying cognitive decline are particularly relevant among the different age-related illnesses.

The use of the different cellular models in the study of a variety of diseases has been converged on fibroblasts, versatile, adaptable cells. The feasible accessibility of fibroblasts allows the researchers to study the disease biomarkers, assess the reprogramming ability, and analyze aging and cellular senescence. Some evidence clearly asses that fibroblasts are not all the same. Colombo and colleagues (1994) hypothesized that the meninges fibroblasts might have a different fibroblast cell population than the epidermis because of the different embryonic development. DeSisto and colleagues (2021), using a scRNA-seq study on rat embryos, backed up this theory by showing how the meninges have a lot of cellular heterogeneity, which is important for embryonic development and central nervous system (CNS) homeostasis. Nonetheless, there is no evidence of the significance of meninges fibroblasts in adults.

Based on this evidence, the goal of this study was to compare the molecular and cellular properties of fibroblasts from adult human donors' meninges (MFs) to those of fibroblasts from the same donors' skin (SFs) to identify the key aspects of this non-neuronal cell that is equally involved in CNS processes.

To get this finding, we began observing the cell cultures on day 0 and tracked their progress in several ways. The frequency of cell escape from the tissue was the first difference observed. From the day of explant culture, we monitored the appearance of 10-20 cells, and we marked the progress. From 19 MFs and 13 SFs, the mean of days of appearance cells shows a difference of 5 days later for the SFs, in particular, MFs appeared after 12 days and SFs after 17 days. We noticed also that the two cell types had a different cell attachment time after a routinary detachment procedure. We monitored the cells every two hours for 8 hours, and after 24 hours, and we assessed that SFs reach 50% of cell-attached after 2-4 hours, whereas MFs after 8 hours reach only 18%. Linked to this result, we also measured the metabolic activity during 14 days of culture, indirect measurement of the cells proliferative state. SFs result in more metabolic activity, and thus the proliferation rate. MFs

maintain a regular cell activity, with no increment. Continuing the observation of the two cell cultures, we noticed that they had different shapes and orientations. With an ImageJ tool Directionality (NIH), we measured the alignment, very well characterized in SFs, but completely absent in MFs. All of these characteristics demonstrated that MFs and SFs are distinct cell types.

Starting from previous data on literature, we measured four markers, two specifics for fibroblasts (serpinh1 and fibronectin) and the other two for a neuronal phenotype (nestin and β-III-tubulin). Both MFs and SFs show fibronectin and serpinh1 fibroblasts marker, and also β-III-tubulin as well. The nestin is the only marker present exclusively in MFs and not in SFs, suggesting a possible involvement of the MFs in the neuronal processes.

We decided to try a direct conversion of MFs and SFs (using neural stem cell lines as a control) to investigate if MFs could become neurons without going through a stage of pluripotency. This experiment does not provide us with the expected results. The protocol resulted optimal for the neural stem cells used as control, but not for the MFs and SFs.

To gain a better understanding of these two cell types, we chose to do more in-depth research, examining the entire transcriptome, focusing on fibroblast cells.

We compared 12 cell lines, deriving from 6 donors, 6 couple of MFs, and SFs. Principal component analysis (PCA) obtained using all differentially expressed genes (DEGs) dataset in MFs compared to SFs shows a neat different expression profile, and a total of 1145 DEGs were identified in MFs, 591 messenger RNA (mRNAs), and 554 noncoding RNAs (ncRNAs). The pathway analysis of deregulated genes revealed the main involvement of the ECM-receptor interaction, with the downregulation of two types of integrin α (ITGA1 and ITGA4) and three types of collagens α (COL6A1, COL6A2, and COL6A3). As adhesion receptors, integrins control various steps in signaling pathways that regulate behaviors as diverse as cytoskeletal architecture, cell proliferation, differentiation, apoptosis, and migration. Gene Ontology (GO) enrichment analysis shows the involvement of two biological processes linked with a previous work of Colombo and colleagues (1994), the dysregulation of the cAMP metabolic process and the cellular response to forskolin. Both of them show the involvement of three types of adenylate cyclase, ADCY1, ADCY5, and ADCY6, all upregulated. These genes have been associated with behavioral abnormalities, intellectual impairments, and increased stress sensitivity, showing that they are critical for maintaining healthy CNS homeostasis. The overexpression of genes linked with cellular response to forskolin in MFs compared to SFs could indicate increased susceptibility to cyclic AMP (cAMP), as well as increased susceptibility to forskolin. Because forskolin and other small molecules (SMs) are used to promote direct reprogramming and transdifferentiation of fibroblasts into neurons, this evidence, along

with the high expression of nestin, could indicate a propensity for reprogramming in this cell type. The cAMP metabolic process shows also the downregulation of two phosphodiesterases, PDE3B and PDE4B, i.e., enzymes involved in cAMP hydrolysis. The up-regulation of ADCY1, ADCY5, and ADCY6 and the down-regulation of PDE3B and PDE4B could further demonstrate how MFs have considerable reprogramming potential. ADM, a part of the cAMP metabolic process, was found downregulated in MFs. ADM interacts with cytoskeletal components including microtubules to protect neurons, promote cAMP synthesis, and mediate proper neuron proliferation and morphological development.

In conclusion, our findings revealed that MFs and SFs have distinct characteristics in terms of culture, morphology, proliferation, protein marker expression, and transcriptome profile, showing that they are two separate cell types. Furthermore, the discovery of nestin expression in MFs, as well as the up-regulation of pathways involved in the cellular response to forskolin and cAMP metabolism, opens the door to more research into MFs' ability to differentiate into mature neurons, potentially leading to new personalized treatments for major neurodegenerative diseases.

Summary

List of Tables

List of Figures

1. Background

1.1 Aging Population

The shift from communicable, infectious disease to non-communicable, chronic illnesses has resulted in a significant rise in life expectancy over the last century. This, combined with a drop in fertility, has resulted in a shift from a population predominantly made up of older and aging people. The World Health Organization (WHO) predicts that civilization will continue to age in the next years (Figure 1A). The prevalence of many age-related disorders has massively enhanced due to the rapid growth of older populations globally, particularly in developed countries. These illnesses' prevalence is projected to rise at the same time, hurting one's quality of life, and have serious consequences for the individual, family, and society [1]. In 2019, the world's population of people aged 65 reached 703 million, from 6 % in 1990 to 9 % in 2019. In 2050, the number of elderly people is expected to increase to 1.5 billion reaching 16 %, implying that one in every six individuals on the planet will be 65 or older [2] (Figure 1B). Therefore, the need to study the characteristics of aging in depth is becoming increasingly important.

Aging is commonly defined as a time-dependent progressive loss of an individual's physiological integrity that finally leads to reduced physical function [3] [4]. Traditionally, aging has not been viewed as a genetically designed adaptation, more recently, biological currents have pointed to two basic theories: planned aging and damage or error-based theories. The first argues that the structural and functional capacity of human cells is deteriorating due to an innate biologic program [5]. The latter emphasizes the cumulative damage that causes intrinsic aging in living organisms [6].

Human aging is associated with a continuous decline in cognitive and physical capacities, as well as a higher risk of developing diseases such as cancer, diabetes, cardiovascular, musculoskeletal, and neurological diseases [7].

Neurodegeneration and concomitant cognitive decline are particularly important among the various age-related disorders because of their significant impact on health span and quality of life. Thus, it is critical to consider the basic mechanisms of aging and their role in the beginning and progression of neurodegenerative illness in order to create effective therapies [8].

1.2 The biology of aging

Recent advancements in aging science have been exceptional, notably the discovery that the rate of aging is influenced by genetic pathways and metabolic mechanisms

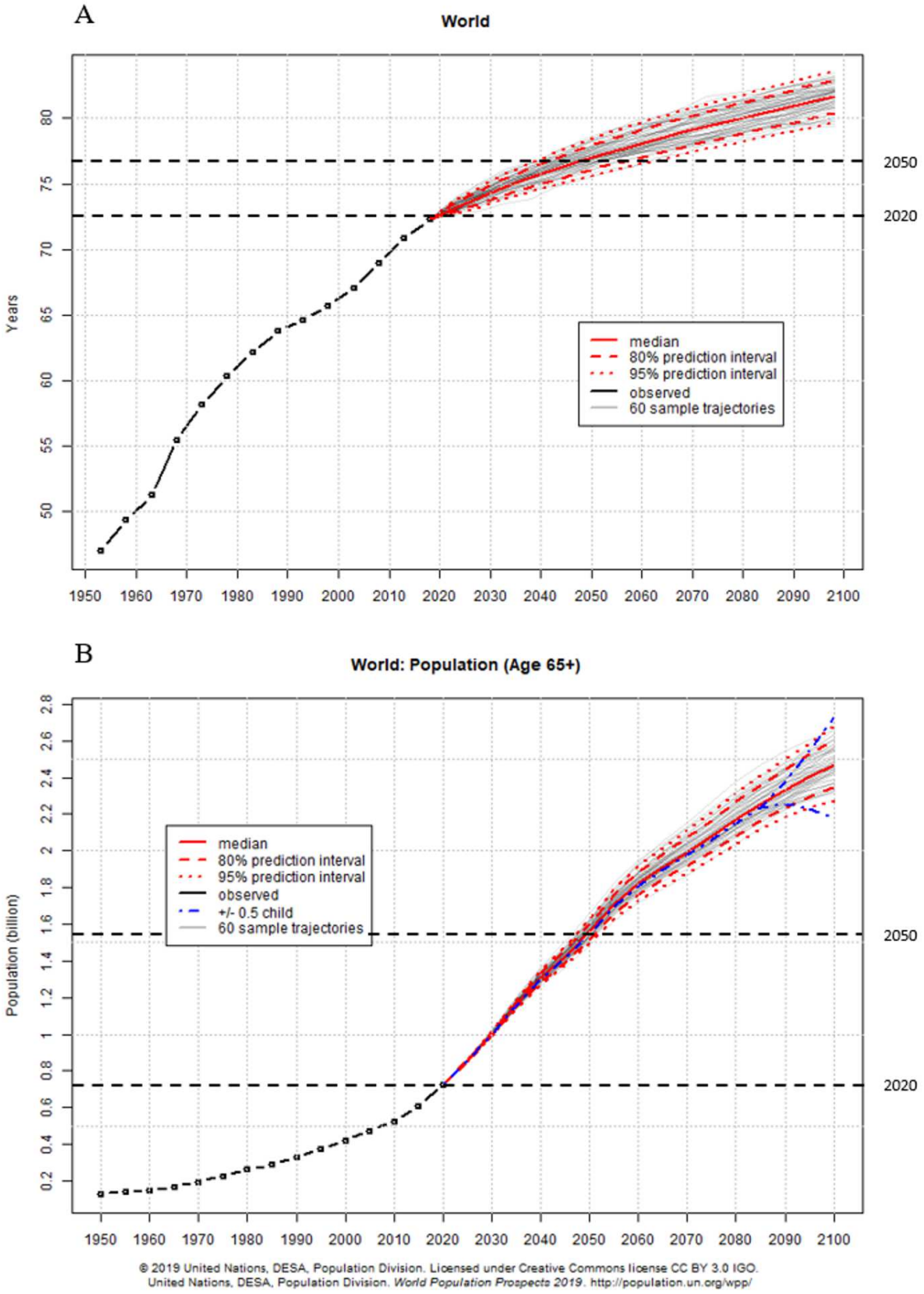

Figure 1: Probabilistic projections elaborated by the Department of Economic and Social Affairs (DESA) of the United Nations. (A) Probabilistic projection of life expectancy (Both sexes). (B) Probabilistic projection of Population over 65 years. Modified from the World Population Prospects 2019 (http://population.un.org/wpp)

that have remained unchanged throughout evolution. Lopez-Otin and colleagues in 2013 proposed nine hallmarks that contribute to the process of aging, categorized them into primary, antagonist and integrative hallmarks. (1) Genomic instability, (2) telomere attrition, (3) epigenetic changes, and a (4) loss of proteostasis are the primary hallmarks. Compensatory or antagonistic responses to the primary damage include (5) unregulated nutrition sensing, (6) mitochondrial failure and (7) cellular senescence. These responses initially minimize the damage, but they can eventually become harmful to themselves. The integrative hallmarks, (8) stem cell depletion and (9) altered intercellular communication, come from accumulated damage caused by the primary and antagonistic hallmarks, and are ultimately accountable for the functional decrease associated with aging (Figure 2) [4] [9].

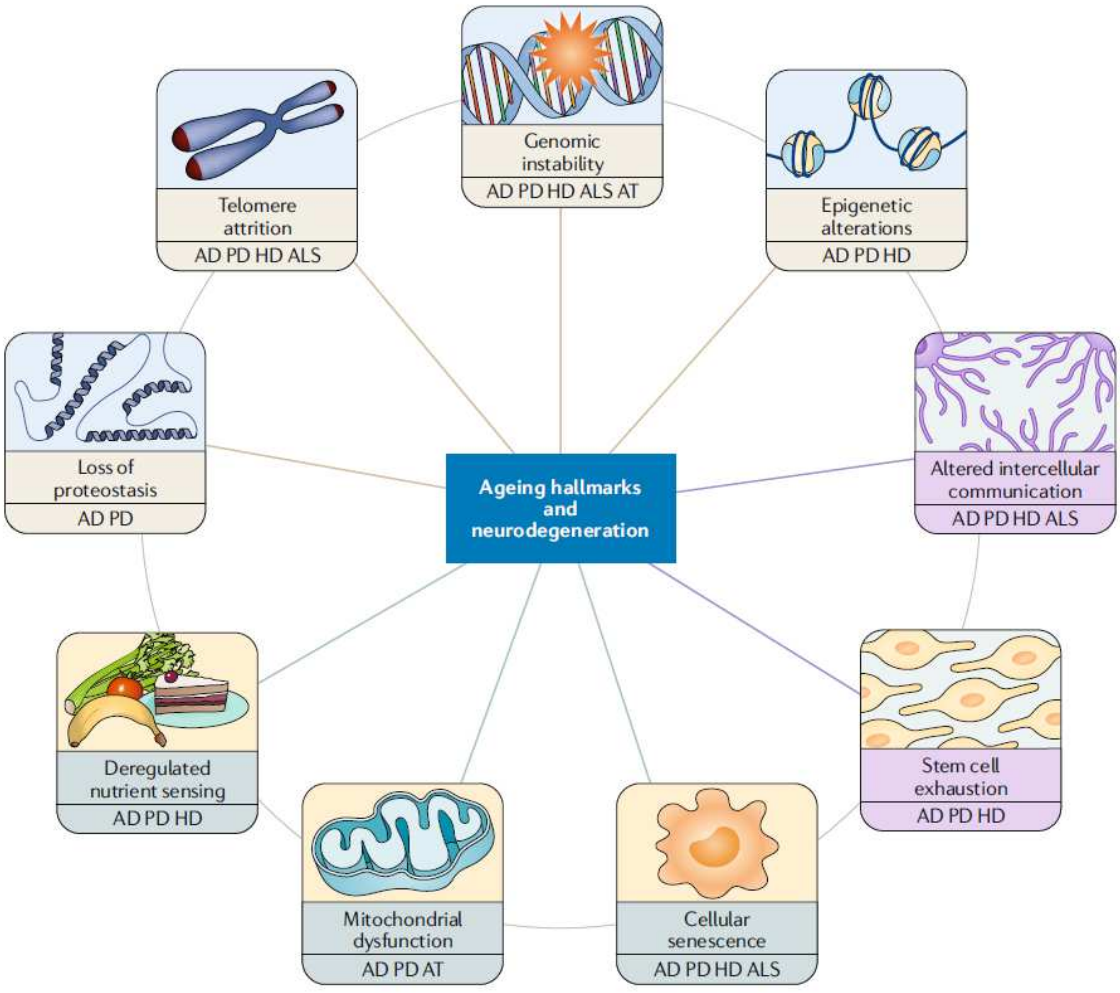

Figure 2: Nine hallmarks of aging in neurodegenerative diseases: genomic instability, telomere attrition, epigenetic alterations, mitochondrial dysfunction, deregulated nutrient sensing, loss of proteostasis, cellular senescence, stem cell exhaustion and altered intercellular communication. AD: Alzheimer disease; ALS: amyotrophic lateral sclerosis; AT: ataxia telangiectasia; HD: Huntington disease; PD: Parkinson disease [8]

1.2.1 Primary hallmarks of aging

1.2.1.1 Genomic instability

The buildup of genetic damage throughout life is a common denominator of aging [10] [4]. Exogenous physical, chemical, and biological forces, as well as endogenous hazards such as DNA replication mistakes, spontaneous hydrolytic reactions, and reactive oxygen species (ROS), all pose constant challenges to DNA integrity and stability [11]. Point mutations, chromosomal gains and losses, translocations, gene disruption, and telomere shortening are among the genetic lesions caused by extrinsic or intrinsic damages. To reduce the severity of these lesions, organisms have evolved a complex network of DNA repair mechanisms that can handle the majority of nuclear DNA damage [12] [13]. Base excision repair (BER), nucleotide excision repair (NER), mismatch repair, DNA double-strand break repair (DSBR), and direct reversal are the five major DNA repair processes [14][15]. Not only does DNA damage cause genomic instability, but it also triggers signaling cascades that spread throughout the cell. Poly [ADP-ribose] polymerase 1 (PARP-1) is induced by persistent DNA damage, which causes PARylation (the production of PAR polymers at locations of DNA damage or changes) and depletion of NAD+. Sirtuins, DNA repair, mitophagy, and mitochondrial health all require the cofactor NAD+. Sirtuin 3, Sirtuin 1, and Sirtuins 1 and 6, respectively, promote efficient BER, NER, and DSBR [16]. DNA damage causes cellular senescence and inflammation, which exacerbates neurodegeneration associated with aging [8].

1.2.1.2 Telomere attrition

This DNA damage appears randomly in the DNA, but some chromosomal regions, for example, telomers, appear to be vulnerable to age-related degradation [17] [4] [18] [19]. DNA polymerase, the enzyme that acts as DNA duplicator, cannot duplicate completely the terminal ends of DNA molecules, a function reserved for telomerase, a specialized DNA polymerase. This enzyme is not expressed in most mammalian cells, causing the cumulative loss of telomere-protective sequences from the end of the chromosome, explainable with the Hayflick limit. Hayflick limit is the limited proliferative capacity of mammalian cells, that cause cellular senescence [20].

1.2.1.3 Epigenetic changes

The epigenetic alteration also affects cells and tissues during the lifespan [4]. These alterations involved DNA methylation, post-translational histones modification, and chromatin remodeling through different types of enzymes: DNA methyltransferases, histone deacetylases, acetylases, demethylases, and methylases. Different is also

the age-associated epigenetic pattern, for example, the increase of H4K20 trimethylation, H3K4 trimethylation, or H4K16 histone acetylation, as well as decreased H3K27 trimethylation or H3K9 methylation [21] [22] [23] [24].

1.2.1.4 Loss of proteostasis

The balance and quality of the proteome is also an important checkpoint to preserve the functionality of cells and tissues [4]. The proteome is regulated by the heat shock protein, involved in the mechanisms of protein stabilization and folding, and by the mechanisms of protein degradation, proteasome, and lysosome [25] [26] [27]. All of this machinery works to keep misfolded proteins from accumulating and to ensure and restore their proper folding [27]. In eukaryotic cells, proteostasis is maintained through correct regulation of the proteasome and autophagy [4], as well as the ubiquitination machinery and lysosomal system. Proteins that have been ubiquitinated are frequently degraded. Autophagy is an intracellular degradation system that allows misfolded or unfolded proteins, as well as damaged organelles, to be degraded by lysosomes, lowering inflammatory cytokine secretion [28]. Aging is the main cause of proteostasis alteration, contributing to the development of some age-related proteinopathies, such as AD and PD [29].

1.2.2 Antagonistic hallmarks of aging

1.2.2.1 Unregulated nutrition sensing

The growth hormone (GH), produced by the anterior pituitary, and the secondary mediator insulin-like growth factor 1 (IGF-1), produced in response to GH, are involved in the somatotrophic axis in mammals. IGF-1 activates the same intracellular signaling pathway as insulin, which alerts cells to the presence of glucose. The insulin and IGF-1 signaling (IIS) pathway is the most evolutionarily conserved aging-controlling mechanism, with several substrates including the FOXO family of transcription factors and the mTOR complexes, all of which are implicated in aging and have been conserved Polymorphisms or mutations that deregulate the IIS pathway are linked to longevity [30] [31] [32]. Overall, the evidence supports the idea that increased anabolic signaling accelerates aging and decreased nutritional signaling prolongs life [31] [33].

1.2.2.2 Mitochondrial failures

The mitochondrial disfunction accelerate the aging process in mammals [34] [35] [36], and the efficiency of the respiratory chain tends to deteriorate as cells and organisms age, resulting in increased electron leakage and decreased ATP synthesis

[33]. Damaged mitochondria increase the formation of ROS, which is linked to the natural aging process as well as the bulk of recognized neurodegenerative disorders [37]. Apart from ATP production, mitochondria are involved in a variety of intercellular functions, including lipid biosynthesis, calcium signaling, and cell death, all of which are important in the progression of neurodegenerative disease [38]. Mitochondrial function in the brain deteriorates with age, and it is thought to be a substantial and early contribution to the aging process [8].

1.2.2.3 Cellular senescence

Cellular senescence is the main cellular alteration, originally described by Hayflick in 1961, characterized by the irreversible stop of the cell cycle of skin fibroblasts in culture. [20]. Cell senescence is triggered by a variety of events and is linked to DNA damage, particularly telomere attrition [39]. Senescent cells actively suppress cell cycle progression, preventing a compromised genome from being replicated. The senescence-associated secretory phenotype (SASP) describes how senescent cells change their metabolism, shape, and secretory profile. The SASP, which comprises pro-inflammatory cytokines, chemokines, and proteases, varies by cell type and senescence inducer [40] [41]. Senescent cell accumulation with age could be due to an increase in the rate of senescent cell formation and/or a decrease in their rate of clearance, such as a result of a weakened immunological response [4].

1.2.3 Integrative hallmarks of aging

1.2.3.1 Stem cell depletion

Stem cell depletion is a result of the above-mentioned aging hallmarks and is likely one of the leading causes of tissue regeneration capacity decrease and, as a result, organismal aging. Immunosenescence has already been linked to some of this loss [42]. Dermal mesenchymal stem cells (dermal MSCs), found in the inner layer of the dermis, and epidermal stem cells (ESCs), found in the basal epidermal layer, are the pillars of skin homeostasis. Dermal MSCs can differentiate into subcutaneous adipocytes, osteoblasts, and chondrocytes [43] [44], whereas ESCs are responsible for epidermal cell renewal as a result of their ability to differentiate into distinct cell lineages of the skin, such as keratinocytes and melanocytes [45]. With age, ESCS and dermal MSCS production and differentiation decline, resulting in a slowing of skin cell renewal and a reduction in skin healing potential [46] [44].

1.2.3.2 Altered intercellular communication and immune function

Aside from cell-autonomous changes, aging also involves changes in intercellular communication, whether endocrine, neuroendocrine, or neural communication [47] [48] [49] [50]. As inflammatory reactions increase, immunosurveillance against pathogens and premalignant cells declines, and the composition of the peri- and extracellular environment changes, neurohormonal signaling (e.g., renin-angiotensin, adrenergic, insulin-IGF-1 signaling) tends to be deregulated in aging, affecting the mechanical and functional properties of all tissues, including the skin [49] [4].

1.3 Brain aging and neurodegenerative diseases

Learning and memory, attention, decision-making speed, sensory perception (vision, hearing, touch, smell, and taste), and motor coordination all deteriorate as the brain's functional capacities decline with age, as they do with other organ systems [51] [52] [53]. As a result of cognitive slowdown and hearing loss, older persons frequently have trouble understanding rapid speech, as well as poor comprehension of syntactically complicated phrases and impaired word retrieval skills [51].
Individuals in their sixth, seventh, and eighth decades are more likely to develop a neurodegenerative disorder, the most frequent of which are AD and PD [54] [55] [56] [57]. The incidence of these two illnesses rises inexorably with age [58] [59]. In 2010, an estimated 30 million people were affected by AD, with that figure expected to rise to nearly 106.2 million by 2050 [60].
Physiological aging causes a steady loss in cognitive and motor functions associated with the cholinergic and dopaminergic systems, respectively, inside the central nervous systems (CNS) [61]. However, in AD and PD, this deterioration can lead to a total atrophy of neurons belonging to the two systems [62] [63]. As a result of the reduction of gray and white matter, as well as the swelling of the ventricles, the human brain decreases in volume as it ages [64] [65].
In most brains, population-based autopsy studies of elderly people who had not been diagnosed with a neurological disease consistently report the presence of amyloid plaques, neurofibrillary tangles, Lewy bodies, inclusions of TAR DNA-binding protein 43 (TDP-43), synaptic dystrophy and neuron loss. Individuals differ substantially in terms of these characteristics, with certain lesions dominating specific areas of the brain or being restricted to specific regions. It's unclear what produces these lesions, or whether they're precursors to neurodegeneration and disease, or merely the result of brain aging [66] (Figure 3).
Other subcellular structures, such as stress granules, lipofuscin, Marinesco bodies, and Hirano bodies, accumulate in aging brains, either in the extracellular space (for

example, corpora amylacea) or inside glial cells or neuronal cells [67] [68] [69][70] [71]. Although most of these structures are poorly understood and their role in neurodegeneration is unknown, they are likely to have an impact on normal brain function.

Early and mid-life environmental factors can influence the cause of depression,

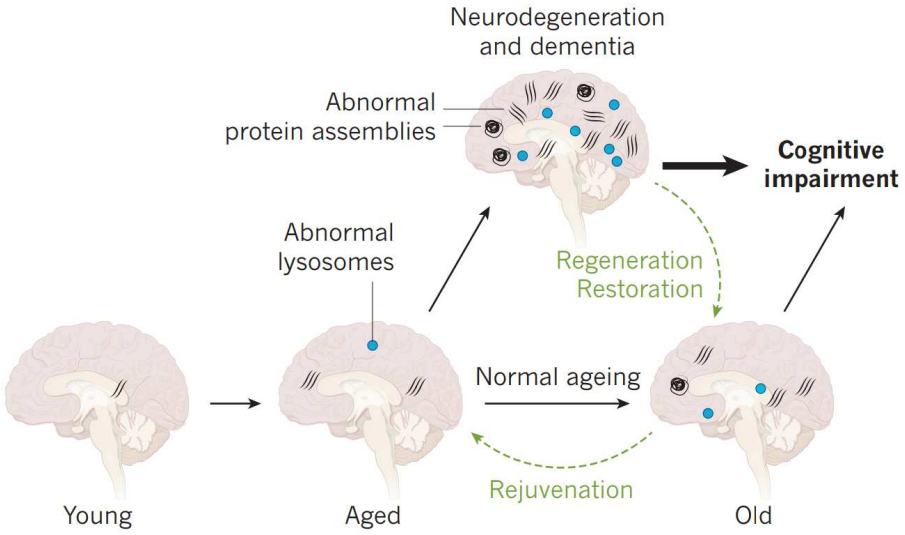

Figure 3: A representative image of the relationship between normal aging and neurodegenerative disease, with a focus on aberrant lysosomes and protein assemblies [72]

brain function and neurodegenerative illness later in life. Traumatic brain injury (TBI) and emotional trauma during early or mid-life, for example, can raise the risk of late-life cognitive impairment and AD and PD, comparable to joint injuries and the risk of osteoarthritis later in life [73].

Stroke, also known as cerebral ischemia, strictly related to the CNS and aging, is a medical condition characterized by a transient cessation of blood flow within a brain artery caused by a clot. Sudden weakness, loss of facial sensibility, confabulation, decreased eyesight, and paralysis of the side of the body opposite the cerebral ischemia are some of the symptoms [74] [75]. A necrotic ischemic core, characterized by dead neurons, forms at the site of ischemia, surrounded by an ischemic penumbra, a halo in which ischemic damage is partial and neurons undergo delayed death [76]. Ischemic damage is characterized by aging-related changes, such as energy deprivation, mitochondrial dysfunction, oxidative stress, DNA damage, and inflammation [77].

1.3.1 Alzheimer's disease

AD is the most common neurodegenerative disease in humans. Late-life memory and learning difficulties, disorientation, mood swings, and behavioral disorders are the most common clinical characteristics of AD. Defects in at least three proteins

have been identified as risk factors for AD: the amyloid precursor protein (APP), presenilin 1, and presenilin 2 [78]. Familial (early-onset) AD has been associated with mutations in the genes encoding these proteins. Sporadic (late onset) AD has a significantly greater (and rising) prevalence and is likely to be the result of the complex interplay between hereditary and environmental variables. The most common genetic risk factor for sporadic AD has been discovered to be the ϵ 4 allele of the apolipoprotein E gene (APOE) [79].
AD is characterized by the neuropathological deposition of Aβ peptide–containing amyloid plaques (Aβ plaque) and neurofibrillary tangle (NFTs) aggregates of hyperphosphorylated or misfolded tau protein [80] [81]. A β is a short aberrant proteolytic fragment (36–43 amino acids of APP) generated by cleavage of APP by β-secretase and γ-secretase in a sequential manner [82].
Cholinergic dysfunction, Aβ plaques, tau aggregation, inflammation, DNA damage, and mitochondrial dysfunction are some of the fundamental causes of Alzheimer's disease, which are currently being debated [8] (Figure 4).
These changes hurt neurons, resulting in cognitive impairment and neurodegeneration. Cell types that are prone to senescence during normal aging appear to be altered in AD. Microglia from Alzheimer's patients, for example, had shorter telomeres than age-matched controls [83].

1.3.2 Parkinson's disease

Neuronal loss in the substantia nigra causes striatal dopamine insufficiency, and intracellular inclusions containing aggregation of α-synuclein are hallmarks of PD. Neuromuscular dysfunction that affects movement amplitude and speed, rigidity, and/or rest tremor are all diagnostic markers of PD. Multiple routes and mechanisms are involved in the molecular etiology of PD, including synuclein proteostasis, oxidative stress, mitochondrial function, calcium homeostasis, axonal transport, and neuroinflammation [84]. All patients with PD have α-synuclein aggregates in their neurons. Synuclein monomers interact to create oligomers, which subsequently combine to form tiny and then large insoluble synuclein fibrils, which are neurotoxic and associated with cytoplasmic inclusions called Lewy bodies [85]. α-synuclein aggregation and mitochondrial dysfunction appear to be synergistic aspects of PD, with mitochondrial dysfunction being hypothesized to increase α-synuclein aggregation in degenerating neurons of PD patients [86] (Figure 4).

1.3.3 Other neurodegenerative diseases

Amyotrophic lateral sclerosis (ALS) is a severe neurological disease that affects people of all ages. ALS is a rare and fatal neurodegenerative illness that causes muscu-

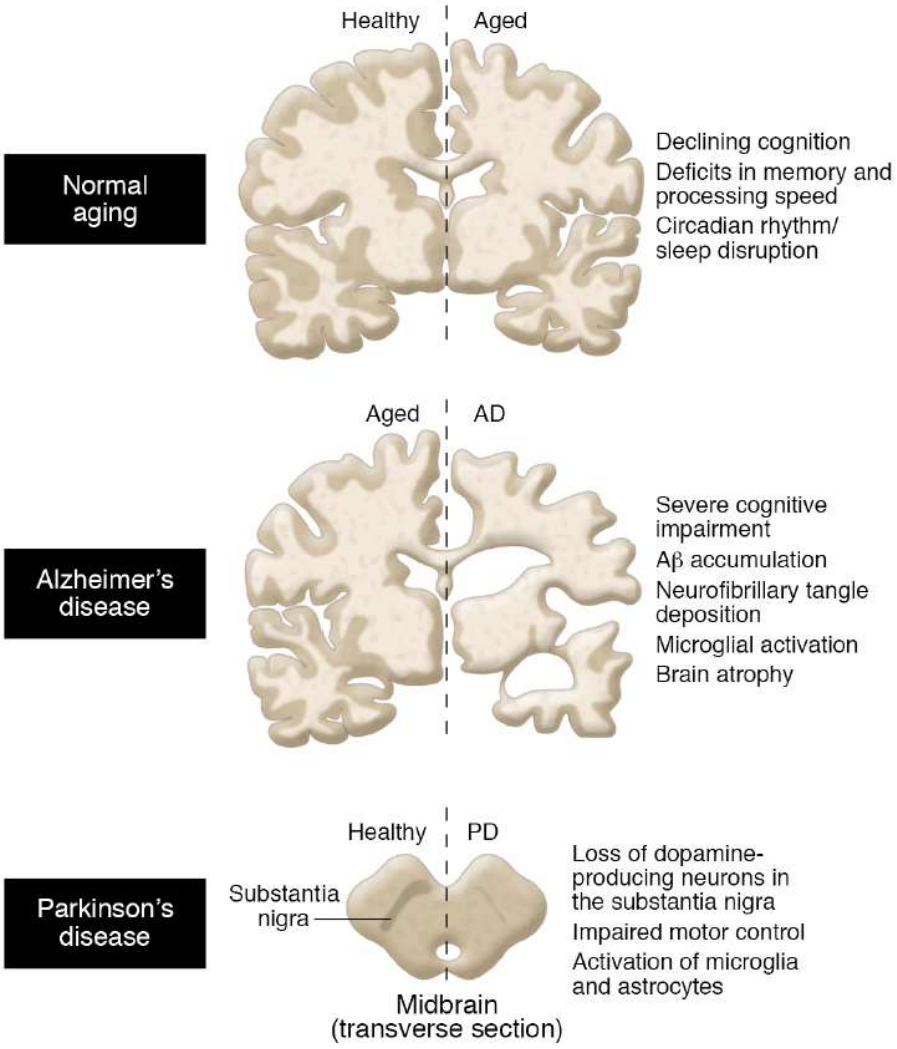

Figure 4: Normal aging and CNS disease have molecular correlations that aren't completely understood. More research into the senescence markers that distinguish healthy aging from neurodegenerative diseases like Alzheimer's and Parkinson's disease could shed light on the role of senescent cells in disease pathogenesis [87]

lar denervation and paralysis due to the degeneration and death of cortical, bulbar, and spinal motor neurons within 3–5 years of diagnosis [88]. TDP-43 inclusions are linked to all sporadic forms of ALS (sALS) and about 90% of familiar ALS (fALS), with the exception of fALS caused by SOD1 and FUS mutations, which are characterized by SOD1- or FUS-containing inclusions, respectively [89] [90] [91]. Inclusion of TDP-43 cause impairment in different processes, such as protein homeostasis, transport through nucleus and cytoplasm, endosomal transport, vesicular transport, mitochondrial function, structure and function of the axon, DNA repair, oligodendrocyte function, and neuroinflammation [92].

Huntington's disease (HD) is a neurological disease caused by an enlarged polyglutamine-encoding CAG tract in the Huntingtin (HTT) gene, which is translated into a mutant HTT (mtHTT) protein [93]. The caudate and putamen, as well as the cerebral cortex, become dysfunctional and die as a result of mtHTT disrupting various processes in the cell. Psychiatric, cognitive, and increasing movement problems are all symptoms of HD [94]. Aging contributes to HD in two ways: (1) events that occur during the aging process sensitize neurons to the mtHTT insult and actively contribute to disease onset and/or progression, or (2) events that occur during the aging process sensitize neurons to the mtHTT insult and actively contribute to disease onset and progression [95].

Multiple sclerosis (MS) is a persistent demyelinating disorder of the CNS that usually begins in young adulthood and is immune-mediated. In more than 80% of patients, MS begins with a relapsing-remitting multiple sclerosis course marked by recurring acute bouts of neurological impairments followed by recovery that becomes less effective over time. The secondary progressive multiple sclerosis phase is characterized by growing impairment without relapse [96]. According to epidemiological studies, age is the biggest predictor of the transition from the recurrent phase of the disease, which is mostly inflammatory, to the secondary progressive phase, which is primarily neurodegenerative [97] [98]. MS pathophysiology is characterized by oxidative stress, mitochondrial dysfunction, and cytokines such as TGF-β [99] [100] [101] [102].

1.4 Cellular senescence in the brain cells

Cell senescence has been linked to many biological processes, including tumor suppression and promotion, embryonic development, chronic inflammation, aging, and neurodegenerative diseases [103] [104] [105]. Epigenetic alterations, telomere attrition, DNA damage, and mitochondrial dysfunction, for example, can all cause cellular senescence, which can lead to unregulated nutrition sensing and proteostasis problems. Stem cell exhaustion and persistent inflammation are two of the conse-

quences of cellular senescence [106]. Cellular senescence is defined in cell biology as a state characterized by persistent cell cycle arrest [107], as well as the release of the cell cycle inhibitor p16INK4a and increased β-galactosidase activity, both of which are useful biomarkers for detecting cell senescence in tissues [108] [109]. Additional modifications in senescent cells include γH2AX and DNA segments with chromatin alterations reinforcing senescence (DNA-SCARS) in nuclear foci, indications of DNA damage response (DDR) activation, increased lipofuscin accumulation, and macro-H2A expression [87] [110] [8].The pro-inflammatory microenvironment induced by pro-inflammatory SASP has been shown to damage surrounding cells [111]. However, not all senescent cells exhibit one or more of these characteristics. Distinct cell types or senescence-inducing stimuli have been shown to reveal different markers in cells [112].

While it is best known for its anti-cancer stress response, current research has revealed that it also has a pro-degenerative function in AD and tauopathies [113] [114] [115]. As a result, cellular senescence may play a role in the inverse relationship between the risk of neurodegeneration and the risk of cancer [116]. Senescent cells have been found in brain tissues, which are extremely vulnerable to numerous stimuli such as ROS and neuroinflammation [117] [118]. Multiple brain cell types, such as neurons, microglia, astrocytes, oligodendrocytes, and endothelial cells, collaborate to allow the brain to conduct daily tasks. Senescence in the above-mentioned brain cells has been shown in research to lead to chronic low-grade inflammation without any evident pathogen, comparable to that seen in peripheral tissue [119] [120]. The accumulation of senescent cells in the brain causes a decrease in pre and postsynaptic densities, dendritic spines and synapses, self-renewal and differentiation capability, blood-brain barrier (BBB) dysfunction, and increased neuroinflammation, which leads to memory loss and cognitive impairments in the elderly [121] (Figure 5). However, it's still unclear what changes and underlying mechanisms or signaling pathways in the aging brain can cause senescence, and how they relate to neurodegenerative illnesses [122].

Neurogenesis ability of senescent neural stem cells has been found to be reduced elsewhere, which could affect neuron production. Senescent microglia, on the other hand, may proliferate in the brain, but senescent neurons may cause senescence in other cell types. Senescent endothelial cells may contribute to BBB disruption. Senescent oligodendrocytes may also alter neurotransmission and reduce myelination in neurons. Finally, as astrocytes become senescent, the antioxidant and energy supply to neurons may be reduced [122].

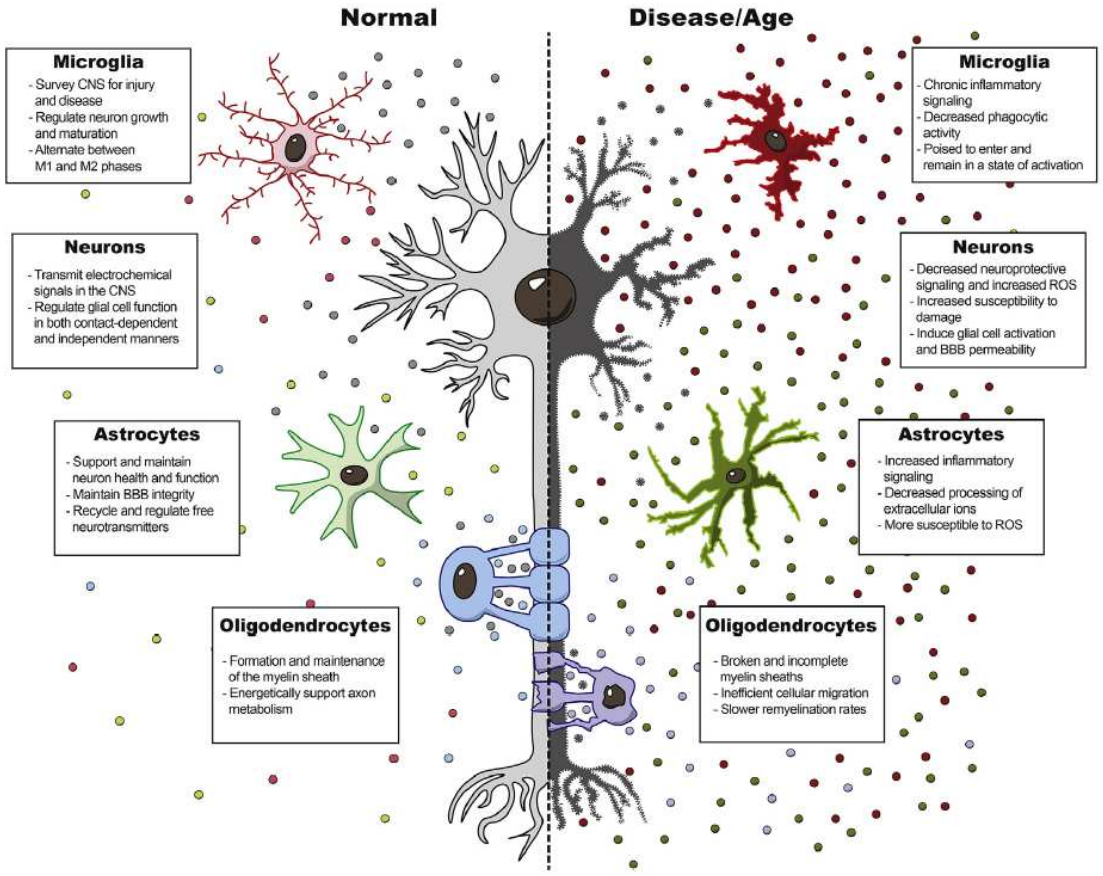

Figure 5: Cellular senescence in the brain. For optimal neurologic function within the brain, many CNS cells play complementary and synergistic roles (left). These cells may actively degrade function in circumstances of age-related or disease-induced dysfunction by promoting inflammation and degradation (right) [123]

1.4.1 Cellular senescence and fibroblasts

The fibroblast is one of the most commonly employed cell types for in vitro studies of cellular senescence events [124]. Fibroblasts are frequently used as a starting point for reprogramming to induced pluripotent stem cells (iPSCs), a process with various implications in regenerative medicine and rejuvenation methods [125] [126]. Several works have sought to determine this cell type's reprogramming capacity, and it has been demonstrated that fibroblasts from mouse skin have varying degrees of reprogramming efficiency depending on the donor subject's age [127]. Although fibroblasts from younger specimens are more effective at reprogramming, it has been observed that the number of myofibroblasts in cell cultures of fibroblasts from older specimens with a higher volume of these fibroblasts correlates directly with reprogramming efficiency. Furthermore, investigations in which myofibroblast and non-activated fibroblast cultures are exchanged reveal that the secretome of activated fibroblasts can control reprogramming in non-activated fibroblasts [127]. IL-6, TNFα, and IL-1, in particular, are able to influence reprogramming in different ways: IL-6 appears to boost reprogramming efficiency, whilst TNFα and IL-1 tend to decrease it, in both young and old fibroblasts. Further data suggest that aging increases cellular heterogeneity, which has an impact on wound healing processes, with fibroblast subpopulations allowing for slow or fast recovery. Activated aged fibroblasts, in particular, have an enrichment of cytokine-related secretory pathways and processes that are involved in the production of extracellular matrix (ECM) components, resulting in positive modulation of tissue contractility, inflammatory processes, and wound healing processes [128] [129] [130]. However, senescent fibroblasts border the component of activated fibroblasts, which increase in quantity and interact in a complex manner with myofibroblasts, negatively influencing the dynamics of the rebuilding of the wounded tissue. The wound healing process can become overly active, resulting in fibrosis, or underactive, resulting in ulcers. Investigating aging mechanisms could thus be useful in developing customized therapeutics and preventing the beginning of certain degenerative disorders in senior people [127].

1.5 Fibroblasts

1.5.1 Embryonic origin and physiological role

Fibroblasts are mesenchymal cells that play multiple roles during development and in adulthood. They are primarily responsible for the synthesis of ECM components and play an important role in wound healing [131].
The epithelium-mesenchymal transition, which drives the transition of the epiblast

into primary mesenchyme during gastrulation, is where fibroblasts begin to grow within the organism. The primary mesenchyme will then give rise to the mesoendoderm, from which endoderm and mesoderm will emerge, forming the embryonic or germinative layer together with the ectoderm. The mesoderm develops into the mesenchyme, which gives rise to adult fibroblasts and other tissues like connective tissue, bone, cartilage, the circulatory system, and the lymphatic system[132] [133] (Figure 6).

Fibroblasts are primarily involved in ECM formation and play a critical role in tis-

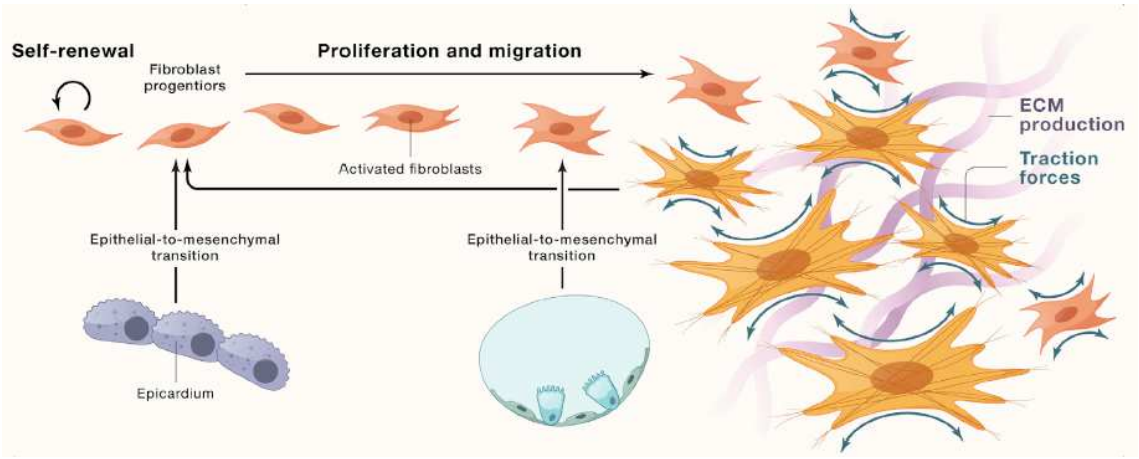

Figure 6: The epithelium-mesenchymal transition active the proliferation and migration of fibroblast progenitors, activating them, to their final shape, capable of producing ECM and giving strength to the tissue [133]

sue integrity by synthesizing molecules like collagen I, fibronectin, and elastin [128] [132]. This results in the formation of the stroma, a structural framework that is necessary for the right arrangement of arteries, blood, and lymphatics, as well as the proper guidance of nerve fibers [131].

During tissue repair, fibroblasts can also develop into a contractile phenotype known as the myofibroblast, which regulate biomechanical remodeling and contraction via traction force [134] onto the enormous amounts of new ECM they create by expressing contractile proteins like αSMA [135] [136]. Beyond contraction, myofibroblasts help to modify the surrounding tissue environment by modulating resident immune cell activities and phagocytosing dead cells [137] [138] [139]. Other types of specialized mesenchymal cells can also change their lineage and become myofibroblasts. Pericytes, for example, are mesenchymal cells that surround blood vessels and are transcriptionally distinct from fibroblast populations [140]. In mouse models, pericytes can migrate out of their perivascular location, develop myofibroblast properties, and contribute to excessive ECM deposition (Figure 7) [141] [142] [143].

Wound healing happens after these inflammatory processes, and it is a multi-step process that includes cell proliferation, migration, ECM deposition, resolution, and

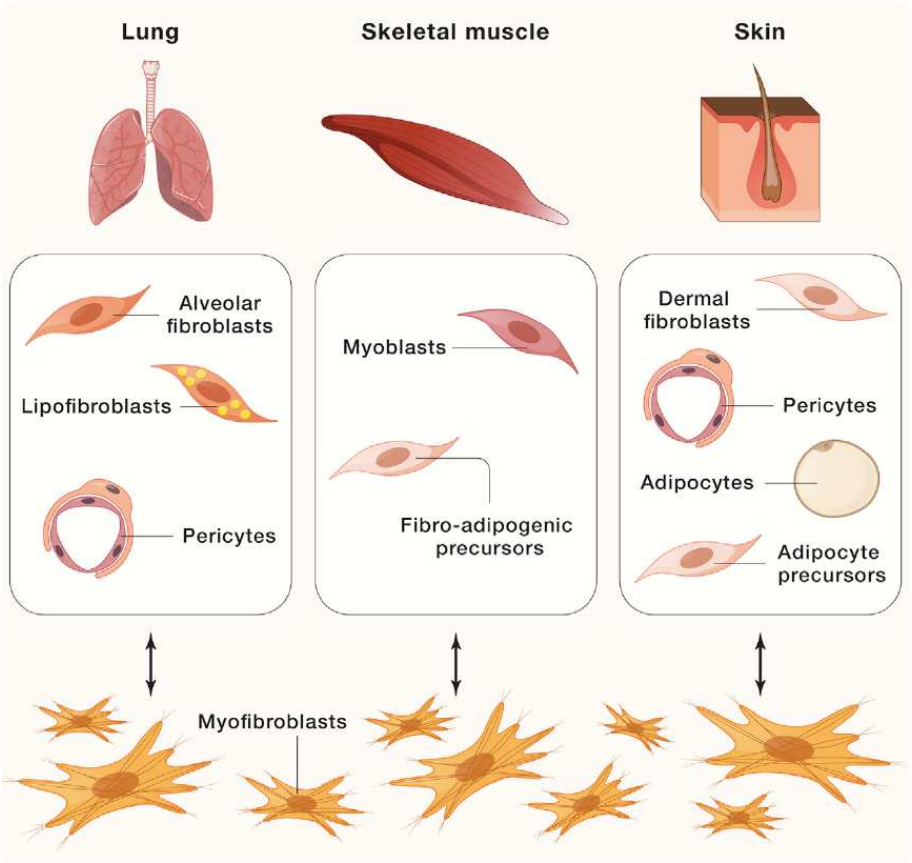

Figure 7: Myofibroblasts can arise from a number of different cells. Reversible conversion to a myofibroblast state can occur in activated tissue resident mesenchymal cells, such as specialized fibroblast progenitors, pericytes, and adipocytes. As an example, the lungs, skeletal muscle, and skin are shown [133]

remodeling. Keratinocytes can operate as a source of growth factors in skin wounds, promoting fibrogenesis and angiogenesis in the wounded tissue. The fibrogenesis processes are driven by fibroblasts, which migrate quickly to the site of injury and proliferate [144]. Myofibroblasts provide contractile power to the wound to maintain wound closure, whereas fibroblasts provide structural integrity to the wound granulation tissue by supplying ECM proteins, primarily collagen and fibronectin. The presence of fibroblasts and myofibroblasts in the wound ensures fibrogenesis: their removal or death by apoptosis causes healing and the creation of scar tissue [145] [146]. In terms of cellular ultrastructure, fibroblasts take on a stellate shape with elongated and branched processes in most cases [147]. They also have a significant endoplasmic reticulum (ER) and Golgi apparatus, which indicates high metabolic activity [148], and may attach to and interact with ECM components and culture substrates [149]. Thus, ECM can interact with fibroblasts and govern their proliferation and collagen synthesis in addition to being generated by them [150].

1.5.2 Gene expression and anatomical localization

Despite their embryonic origins, fibroblasts differ in their anatomical sites and microenvironments. Site-specific expression profiles of genes associated to cell proliferation, differentiation, ECM formation, and cell migration have been discovered in fibroblasts from various tissues by gene expression analyses [131] [149]. Adult fibroblasts are explanted from the upper limbs, abdomen, back, scalp, foreskin, thigh, gingiva, and toe to evaluate these variations. In addition, fibroblasts are isolated from fetal lungs and skin to see if there are any variations based on developmental stage. Fibroblasts exhibit the same morphology in vitro and are uniformly positive for vimentin, a mesenchymal marker, according to studies. In vivo, differences in the expression levels of cell migration signals, which were originally identified as guidance molecules for appropriate axon growth exclusively in the CNS, are discovered. In vitro, discrepancies exist for site-of-origin typical ECM genes such as collagen I and V, which are expressed in fetal skin fibroblasts but not in fetal lung fibroblasts [131]. Further variations in topographic localization in humans are due to differences in the expression of specific homeobox (HOX) genes during embryonic development. The expression of these genes ensures optimal tissue morphogenesis and site-specific cell differentiation. In mouse and human models, differences in HOX gene expression have been reported in skin fibroblasts generated from the extremities and trunk, as well as non-skin fibroblasts [149].

1.5.3 Interactions with the external environment

Extrinsic factors and interactions with ECM components contribute to fibroblast cellular heterogeneity [128]. Several studies have shown that in co-cultures of fibroblasts and keratinocytes, the latter can induce the production of IL-6 and FGF7 by fibroblasts, while factors secreted by fibroblasts can influence keratinocyte growth and differentiation, implying the establishment of a bidirectional cellular interaction [151] [152]. However, there are still some questions about the signaling pathways that underpin the various cellular identities of fibroblasts. The fibroblast as a cell type is indeed regulated by a complicated interplay.
TGF-β, WNT, and platelet-derived growth factor (PDGF) signaling (Figure 8), as well as inflammatory cytokines such as tumor necrosis factor alpha (TNF-α), interleukin-1 (IL-1), and IL-6 signaling, all contribute to the formation of myofibroblasts [133]. The self-renewal of fibroblast lineages via proliferation is required for their development and long-term maintenance. PDGF signaling is required for fibroblasts to have this important characteristic. PDGF ligands are homo- and heterodimers of four distinct polypeptide chains, from A to D, that operate locally inside tissues and can be produced by fibroblasts or other cell types [153]. The TGF-β pathway is responsible for the majority of myofibroblast activation [154], and human fibrotic tissue has higher expression of TGF-β ligands in the lungs, skin, and skeletal muscle (reviewed in Lodyga and colleagues [155]). The classical WNT pathway controls fibroblast fate specification during development and can influence fibrosis and regeneration in adult tissues. On their target cells, canonical WNT ligands bind to complexes of low-density lipoprotein receptors (LRPs) and Frizzled receptors (Figure 8) [156].
Through multiple mechanisms that allow them to adapt and respond to mechanical stress, skin fibroblasts play a critical role in maintaining the structural integrity of the skin. One of these is the involvement of the focal adhesion kinase (FAK), a kinase that is activated by skin injury, and the extracellular signal-regulated kinases (ERK) pathway, which is critical for mechanical stress-driven wound healing processes [157].

1.6 Skin: anatomy and physiological role

The epidermis, dermis, and hypodermis are the three layers that compose the skin. Several proteomics investigations have revealed that the skin contains roughly 160 proteins, including various collagen isoforms, ECM proteins, keratin, and cellular proteins such as vimentin, actin, myosin, and tubulin [158][159].

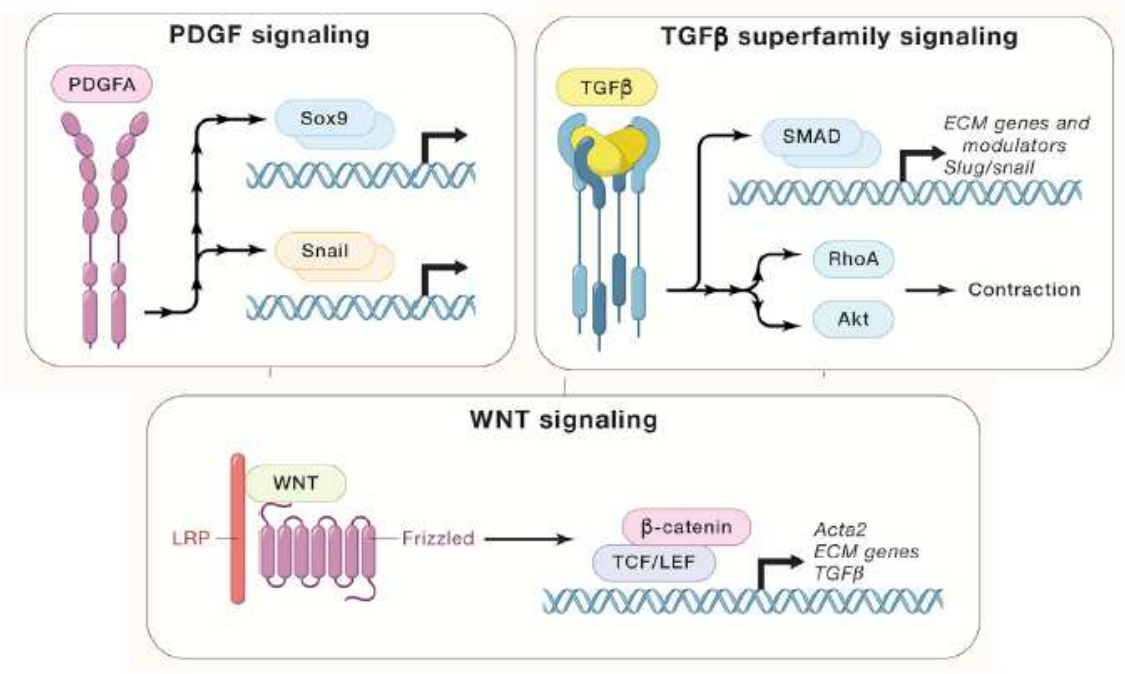

Figure 8: The PDGF, TGF-β, and WNT signaling pathways play important roles in modulating fibroblast activities [133]

1.6.1 Epidermis

The epidermis is the skin's thinnest and most physiologically active layer. To protect the body against atmospheric agents, chemical and physical agents, and microbes, the epidermis' superficial layer, or stratum corneum, goes through a keratinization process. Below the stratum corneum, we find, in order, the stratum granulosum, the stratum spinosum, and finally the basal or germinal layer. All these layers are composed of keratinocytes with a different phenotype. In the stratum corneum, we find enucleated keratinocytes embedded in a lipid matrix [160] [161].

Corneocytes are the main elements of the layer and are made up of dead keratinocytes. Live keratinocytes are found in the stratum granulosum, which are connected by tight connections. The granular layer's keratinocytes and the corneocytes above them form a barrier that limits water loss while selectively controlling the molecules that can travel through it. The granular layer contains lamellar bodies, which are ellipsoid secretory granules that can sequester proteins and antimicrobial peptides (AMPs) before releasing them into the extracellular space between the granular layer and the stratum corneum [162]. The basal or germinal layer, located at the base of the epidermis, is constantly renewing. Keratinocytes ascend the epidermis from the basal layer to the stratum corneum during the differentiation phase, where they take on the phenotype of denucleated squamous cells. This process of proliferation and differentiation is necessary for the epidermis to function properly, and it is disrupted in inflammatory skin disorders including psoriasis and

atopic dermatitis [163]. Desquamation, the loss of the most superficial corneocytes, is the final stage of this process. Desquamation is a mechanism that allows continual cell renewal while also preventing germs from colonizing the epidermis, preventing bacterial penetration and infection. Chemically, the epidermis' protective function is ensured by the presence of AMPs and lipids, both of which are released, either constitutively or in response to stimulation, by immune cells such as Langerhans cells and T cells (Figure 9) [164].

1.6.2 The dermis and the role of fibroblasts

The dermis is a connective tissue that lies beneath the epidermis and is separated from it by the basement membrane. It is mostly made up of fibroblasts, which create collagen, elastin, and other ECM components that help to maintain the skin's structural integrity. When interacting with microbial components, dermal fibroblasts produce cytokines (IL-6, IL-8, and TNF-α), growth factors (Vascular endothelial growth factor, VEGF; Transforming growth factor beta 1, TGF-β1; Heparin-binding EGF-like growth factor, HB-EGF), and Matrix metalloproteinases (MMPs), which operate as immunomodulators [165]. Immune cells such as macrophages, mast cells, and dendritic cells occupy the dermis in healthy settings [166]. These cells can migrate into the skin using scaffolding made of collagen and elastin fibers generated by fibroblasts in the presence of inflammatory conditions [167]. In addition, leukocytes recruited from the bloodstream infiltrate the dermis under these conditions, providing an additional layer of protection to compensate for the body's poorer defense by this layer compared to the epidermis [168].
Mast cells release antimicrobial substances, which are also found in the dermis. These can generate cathelicidin granules within them, which are released in the event of a skin injury or infection and either prevent the pathogen from spreading or stimulate keratinocyte proliferation and the process of angiogenesis to aid tissue regeneration [169] [170] [171]. Keratinocytes also create β-defensins type 2 (hBD2) during wound healing, which can provide further protection from infections and enhance fibroblast migration [172]. To guarantee appropriate wound healing and avoid new infections, the interaction between dermal fibroblasts and epidermal keratinocytes is crucial [173]. Furthermore, fibroblast contact with microbial components and the consequent release of cytokines and growth factors may aid this process by inducing angiogenesis [173] [174]. Adipocytes, which are required for the recruitment of fibroblasts to the injury site, play a significant role [175]. In rare situations, the fibroblasts themselves develop into adipocytes to boost their response to pathogens, a trait that is lost with age, rendering the body more susceptible to skin infections (Figure 9) [176].

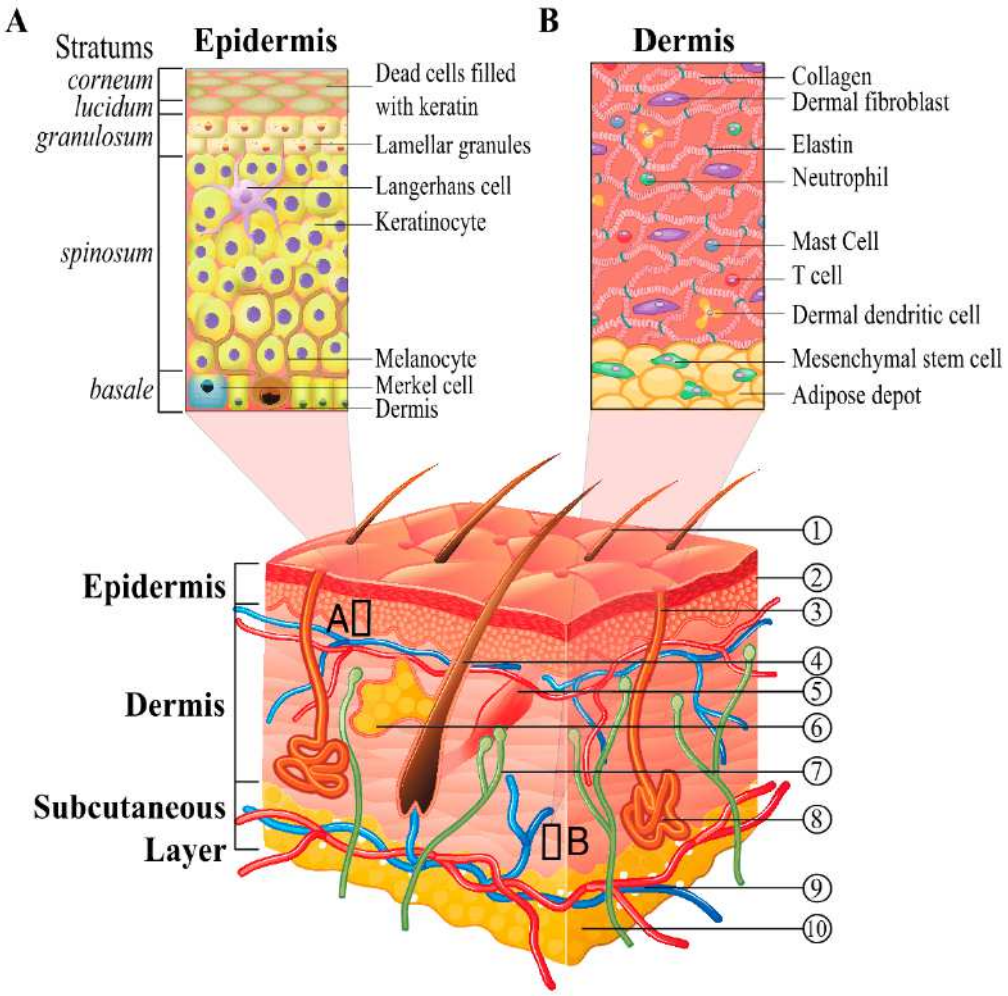

Figure 9: Skin architecture of Epidermis (A) and Dermis (B). (1) hair shaft; (2) stratum corneum; (3) sweat-pore; (4) hair follicle; (5) arrector pili muscle; (6) sebaceous gland; (7) nerve; (8) eccrine sweat gland; (9) cutaneous vascular plexes; (10) adipose depot [177]

1.6.3 Hypodermis

The hypodermis is the innermost layer of skin. This layer is primarily made up of loose connective tissue and large pockets of fatty tissue that isolate and protect the skin depending on the location. Proteoglycans and glycosaminoglycans, which can hold fluid and give the hypodermis mucosa-like qualities, are abundant in the hypodermis [159]. Fibroblasts, adipocytes, and macrophages are the most common cell types found in the hypodermis. Fibroblasts, adipocytes, and macrophages are the primary cell types found in the hypodermis. The latter are involved in obesity-related adipocyte homeostasis, tissue remodeling, and adipose-induced thermogenesis after cold exposure and exercise [178] [179] [180]. G-protein-coupled receptors that govern lipolysis and adiponectin and leptin release are abundant in the hypodermis [181]. The hypodermis is made up of fibrous tissue that is organized into a network of mostly vertically aligned fibers. Their meeting results in the creation of a three-dimensional structure with voids that act as interstitial fluid stores [159]. This structure is also effective at providing structural integrity to the skin as well as resistance to tension, expansion, and compression forces. When the osmotic pressure in the capillaries rises, such as during inflammatory conditions, the hypodermis' ECM, which is particularly rich in hyaluronic acid, glycosaminoglycans, and proteoglycans, acts as a sponge for interstitial fluid [182].

1.7 Meninges: anatomy and physiological role

The meninges are three layers of connective tissue that line the brain and spinal cord. They are membranous and concentric. They are classified as dura mater, arachnoid, and pia mater, with pachymeninges (dura mater; the prefix "pachi-" refers to particularly thick parts) and leptomeninges (arachnoid and pia mater; the prefix "lepto-" refers to thin, fine elements) subdivided (Figure 10). Their major roles are to protect the brain physically and to help establish the BBB. All three meninges are derived from the primitive meninges, a precursor layer made up of materials generated from the head mesenchyme and neural crest. The primordial meninges are separated into two layers: an inner endomeninges layer and an outward ectomeninges layer. The endomeninge is made up of both mesoderm and ectoderm and gives rise to the arachnoid and pia mater, whereas the ectomeninge is made up of just mesoderm and gives birth to the dura mater and neurocranial bones [183] [184].

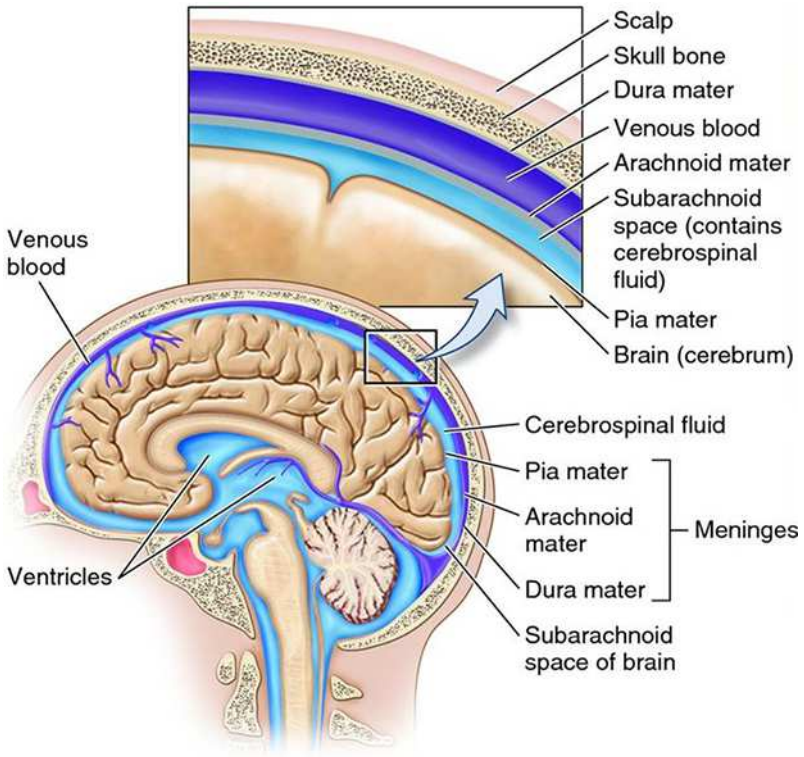

Figure 10: Anatomy of the skull and the meninges (Brain Atlas)

1.7.1 The dura mater

The dura mater is the outermost meninges, and it is made up of two layers: the periosteum, which is adhered to the skull and contains blood vessels, lymph vessels, and nerve endings; and the meningeal layer, which is responsible for the formation of the processes that divide the telencephalon into several compartments. The falx cerebri and the tentorium cerebelli are the most notable of these [184]. These two layers are difficult to identify physically, but changes in the presence of fibroblasts and collagen, which are reduced in the meningeal layer, can be seen histologically [185]. A distinct layer of fibroblasts called the dural border cell layer exists within the dura mater layer and is referred to as the dural border cell layer. Although not morphologically distinguishable, the periosteum and meningeal layers of the dura mater are often separated by dural venous sinuses, spaces into which blood from cerebral veins and cerebrospinal fluid (CSF) from arachnoid granulations drains. The internal jugular vein is then sustained by the dural venous sinuses [186] [187].

1.7.2 Arachnoid

The arachnoid encloses the subarachnoid area, which is filled with CSF and next to the pia mater and symbolizes the intermediate meninges. Because of the underlying cerebral circumvolutions and furrows, the subarachnoid space has a varied width: at

the furrows, the width increases. CSF is found in higher quantities in the cisternae, which are positioned near the brainstem and at the base of the skull [184]. The arachnoid is a non-vascularized meninge made up of two layers of cells. The arachnoid barrier cell layer is found in contact with the dura mater, specifically the dural rim cell layer, and is characterized by densely packed cells held together by tight junctions and desmosomes. These characteristics render the barrier impermeable to CSF. The arachnoid reticular layer is the second, deepest layer, which is more porous. Trabeculae, long linear cellular structures that operate as a bridge between the arachnoid barrier and the pia mater, are found within it. The pia mater lines the blood arteries that branch between these trabeculae [188]. Arachnoid villi are specialized structures that are responsible for CSF absorption and are found within the arachnoid. Arachnoid granulations or cavernous nodules, which extend within the dura mater to the venous sinuses [189] and are also important for CSF reabsorption to counteract any increase in pressure [190], are larger variants of arachnoid villi.

1.7.3 The pia mater

The pia mater is the meninge's deepest layer. It is a connective tissue layer that lines the encephalon and spinal cord and is highly vascularized. The pia mater's membrane also spreads into furrows and fissures, and desmosomes and communication junctions connect the pia mater's constituent cells [191]. Externally, the pia mater borders the blood arteries that flow across the surface of the brain, ensuring anatomical distinction between the subarachnoid space and the subpial and perivascular spaces [188]. Virchow-Robin spaces (VRS), extensions of the subpial space with the purpose of draining interstitial fluid, surround small arteries and arterioles that perforate the cerebral surface [184].

1.8 The influence of the meninges on neurocranium and brain development

The neurocranium, like the meninges, is derived from the primitive meninges in mammals, and these components interact constantly during development [192] [193] [194]. The release of numerous chemicals, including TGF-β, FGFs, and BMPs, by the dura mater, appears to have an instructional role in the processes of neurocranium development [195] [196] [197]. The resolving role of the dura mater, arachnoid, and pia mater in brain growth is equally important. The meninges, in particular, can control the migration and placement of neurons by secreting chemotactic chemicals. CXCL12 is one of them, and it is induced by FOXC1 [198] [199]. Neurons and

neural progenitors that express suitable receptors like CXCR4 and CXCR7 settle in the parts of the brain beneath the meninges. Cajal-Retzius cells and interneurons of the cerebral cortex, neural progenitors of the dentate gyrus, and neural progenitors of the cerebellum are examples of cells that are subject to this control [200] [201] [202] [203] [198] [204]. Radial glial cells give out processes that serve as scaffolds for the migration of neurons from the ventricular zone to the brain surface during physiological brain development [205]. To establish stability, the terminals of these processes adhere to the pia mater basement membrane. The terminations of glial processes detach early in mutant mice with a defective basement membrane, and neurons are distributed abnormally in the cerebral cortex and cerebellum [206] [207] [208] [209] [210] [211] [212]. The meninges also play an important role in the asymmetric division of neural progenitors into neurons, which happens during differentiation. FOXC1 and retinoic acid (RA) are essential actors in this process. The rate of symmetric divisions increases in mice lacking meninges, which are FOXC1 mutants. As a result, the cerebral cortex has grown in size but is devoid of specialized neurons. Because exogenous administration of RA can reestablish a normal cortical state, it's been postulated that RA from the meninges is necessary for healthy neurogenesis [213]. Furthermore, RA interacts with the Wnt/β-catenin pathway in endothelial cells to guarantee adequate cerebral vascularization under physiological settings. Thus, in mice mutant for FOXC1, the absence of RA after meningeal deficiencies induces vascularization problems characterized by increased vessel volume and decreased vessel number [214] [215]. In the end, the meninges provide a home for neural stem cells [216]. In particular, cells expressing Nestin, a stemness marker, have been seen in leptomeninges generated from mice at various stages of development [217] [218]. It was feasible to confirm that these cells can develop into cortical neurons through the use of various experimental methods [219].

1.9 The role of the fibroblast in the meninges

Colombo and colleagues, in 1994, produced one of the earliest contributions to the characterization of fibroblasts from meninges, particularly in respect to fibroblasts from the skin [220]. Meningeal fibroblasts, like astroglial cells, ensure correct neuron migration for cortical plate building during neocortex formation by cAMP-dependent cytoskeleton remodeling [221] [222].
Based on these findings, Colombo and colleagues hypothesized that the embryonic origins of fibroblasts from the meninges, as well as the extracellular microenvironment - primarily CSF - to which they are exposed, determine structural and functional differences in this cell population when compared to fibroblasts from the skin. Cell cultures of fibroblasts from the leptomeninges and skin were then given condi-

tioned media, the first of which was Astroglial Conditioned Medium (ACM), and the second of which was DMEM/F12 enhanced with 0.5 mM cAMP (Figure 11) [220].

DeSisto and colleagues were able to develop a molecular profile of meningeal fibroblasts using techniques such as single-cell RNA-sequencing (scRNA-seq). These tests were carried out on mice on day 14 of embryonic development (E14), and the results revealed that the transcriptional profiles of fibroblasts originating from the dura mater, arachnoid, and pia mater differ significantly [223].

Following the discovery of meningeal-specific markers, such as S100a6 and p75NTR for pia mater, CRYM (μ-crystallin) for a subpopulation of pia mater fibroblasts, and CRABP2 for arachnoid and dura mater in mice, the same markers were sought in humans at the same time of embryonic development. S100a6 and p75NTR were found in pia mater fibroblasts, but CRYM positive cells were evenly distributed throughout the meninges, rather than being confined to a restricted subpopulation as in the mouse model. CRABP2 expression was instead found in broad layers of tissue, a distinctive shape of arachnoid trabeculae traversing the subarachnoid space that is more prominent in higher vertebrates and primates' meninges [223]. The endomeninges, which give rise to the arachnoid and pia mater, arise from both mesoderm and ectoderm, whereas the ectomeninges, which exclusively come from the mesoderm, gives rise to the dura mater and neurocranial bones [183] [184]. Furthermore, the meninges have been demonstrated to produce substances that support healthy neurocranium and brain growth. Ogn is a proteoglycan expressed by the dura mater and arachnoid fibroblasts that regulate the expression of osteoglycine, a bone-forming amino acid [206]. As a result, it is possible that such communication also happens in the other direction, affecting the development of the meninges and the gene expression of the relevant cell populations [194].

Pia mater fibroblasts appear to act as a glue between the brain parenchyma and the meninges themselves, in addition to ensuring proper meninge development. As a result, specific pia mater cell subpopulations, distributed throughout the forebrain, express large amounts of collagen, laminin, proteoglycans, and MMPs, following their specialization. Increased expression of Lamb2, Col12a1, the proteoglycans Ogn and Fmod, and fibronectin is seen in dura mater and arachnoid fibroblasts, on the other hand [206] [223].

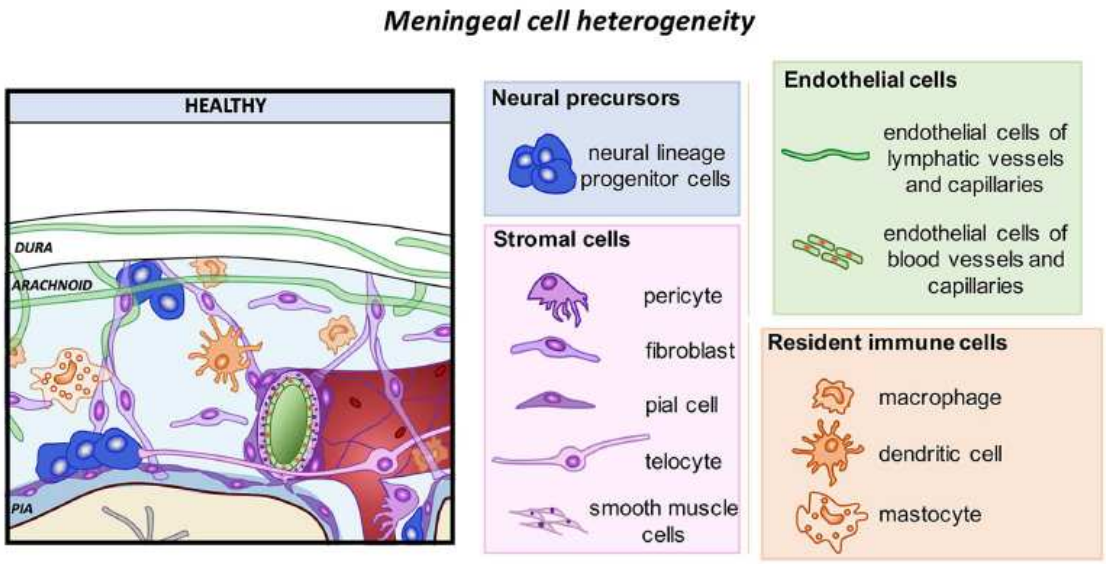

Figure 11: Schematic representation of meningeal cell heterogeneity in healthy conditions (modified from Decimo et al. 2021, [224])

1.10 Regenerative medicine

1.10.1 Induced pluripotent stem cells

The ability to reprogram adult mammalian cells to a stage of pluripotency by overexpressing a small number of embryonic transcription factors (TFs), specifically the Oct4, Sox2, c-Myc, and Klf4 genes, has been established by the production of induced Pluripotent Stem Cells (iPSCs) from somatic cells [125] [61]. This discovery has created an almost limitless opportunity for the creation of individualized therapeutic techniques to repair damaged tissues and organs, as well as to cure degenerative disorders, aging-related diseases, and cancer [225] [226] [227].
The key advantages of cellular reprogramming are that iPSCs can be created from readily available somatic cells, such as skin fibroblasts, and do not cause immunological rejection when implanted in the same patient. Furthermore, unlike traditional embryonic stem cell therapy, the use of iPSCs has no ethical problems due to the death of embryos [61]. Despite these benefits, the procedure of developing iPSCs into other cell types is time-consuming, expensive, and complex, and there are still various questions about it, which prevents its clinical usage [228].
Alternative reprogramming methods, like transdifferentiation and direct reprogramming, have been developed as a result, allowing direct conversion between cell types while avoiding the transition from a pluripotency stage [61].

1.10.2 Transdifferentiation and direct reprogramming

Transdifferentiation is the process of converting one terminally differentiated cell into another by inducing ectopic expression of different TFs or microRNAs that have a particular expression in a certain cell type using adenoviral vectors [229] [230]. The resulting cells are identical to cells formed by iPSC differentiation or their in vivo counterparts. However, these cells may have a low proliferative capacity, phenotypic variety, and senescence, which could make them unsuitable for use in regenerative medicine efforts [231] [232].

The second approach to reprogramming to iPSCs, direct reprogramming mediated by pluripotency factors, involves the conversion of somatic cells into other differentiated cell types without going through the pluripotency stage. Unlike transdifferentiation, however, this method relies on the expression of the same Yamanaka pluripotency factors (Oct4, Sox2, Klf4, and cMyc) for a short period, usually 3 to 6 days. Multipotent progenitor cell populations are created through this method, which can differentiate into specific cell types in the presence of certain stimuli [233] [234] [235].

1.10.3 Small molecules

Small chemical compounds or small molecules (SMs) can also be used to induce transdifferentiation or direct reprogramming (Figure 12). These compounds can occur in a variety of biological processes, including signaling pathways, epigenetic alterations, and metabolic processes, and when used together, they can cause transdifferentiation or reprogramming without the use of exogenous genes. SMs are also permeable to the cell membrane, cheap, non-immunogenic, and simple to make and employ [236] [237] [238] [239] [240]. The use SMs also provides for more control over the biological effects caused, which are quick, often reversible, and highly controlled by changing factors like SM concentration and combination [240]. The Wnt pathway is an example of a signaling system involved in sustaining pluripotency in pluripotent stem cells. TCF3, an inhibitor of transcription binding to the promoter region of pluripotency-related genes, is one of the many factors regulated by this pathway [241] [242]. When the Wnt pathway is activated, TCF3 is phosphorylated and inactivated, permitting transcription of pluripotency-related genes. CHIR99021, a GSK-3 kinase inhibitor, is one of the SMs that can increase Wnt pathway activation. The use of CHIR99021 boosted the effectiveness of converting murine fibroblasts and neural stem cells into iPSCs by 0.2 - 0.4 % [243] [237]. Furthermore, in the presence of only two reprogramming factors, such as Oct4 and Klf4, CHIR99021 can replace Sox2 to promote reprogramming in iPSCs [237]. Using a mixture of eight SMs, including Forskolin, RepSox, SP600125, CHIR99021, Go6983, Y-27632,

ISX9, and I-BET151, researchers were able to generate induced neurons with neuronal features, including the production of specific markers like β-III-tubulin and microtubule-associated protein 2 (Map2). Another combination of SMs, consisting of ISX9, SB431542, Forskolin, and CHIR99021, yielded similarly promising results. The SMs' synergistic effect resulted in primitive cells with a neuron-like shape that expressed β-III-tubulin once more [244]. These findings show that the use of SMs for reprogramming and transdifferentiation has a lot of promise, but more research is needed to figure out which starting somatic cell types and which combinations of SMs will produce the best results to develop new personalized therapeutic strategies for neurodegenerative diseases [244] [245]. Because there are currently no effective pharmaceutical treatments for neurodegenerative diseases, a cell replacement therapy based on neurons generated in vitro could be both novel and effective [246]. Alternative strategies such as transdifferentiation and direct reprogramming, as well as the use of chemical compounds, have been proposed to avoid risks such as immune rejection, high oncogenic potential, and uncertain differentiation fate as a result of the transition from a pluripotency stage to iPSCs [247] [61] [248].

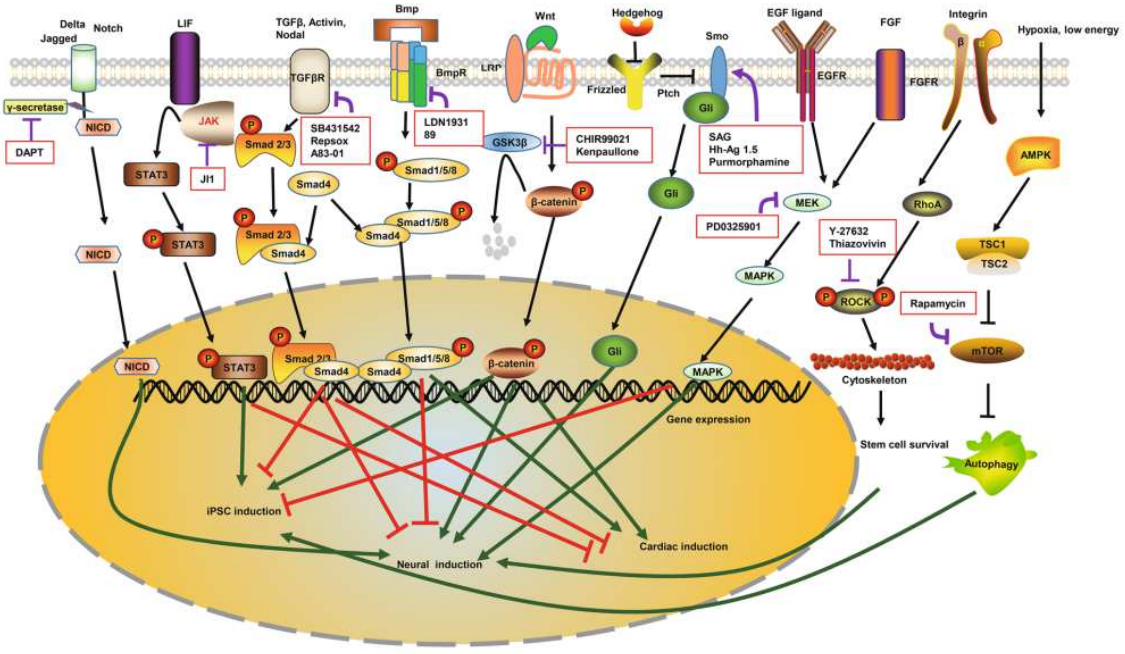

Figure 12: Modification of pathways that promote the formation of iPSCs, cardiac cells, and neurons from somatic cells [240]

2. Aim of the work

Previous reports about fibroblasts strongly indicated the importance of this incredibly adaptable cell type for the study and understanding of a variety of diseases. The availability of fibroblasts allows researchers to look into disease biomarkers, assess the reprogramming ability of mesenchymal cells, and analyze aging and cellular senescence in healthy and pathologic conditions. Fibroblasts, on the other hand, are not all the same. Because of the different embryonic genesis, Colombo et al. [220] suggested that the meninges might contain a distinct fibroblast cell population from the epidermis. DeSisto et al. [223], using scRNA-seq research on rat embryos, corroborated this idea by demonstrating how considerable cellular heterogeneity exists inside the meninges, which is involved in embryonic development and CNS homeostasis. Nonetheless, there is no evidence regarding the characterization and role of meningeal fibroblasts in adult individuals, especially in light of what has recently been highlighted by other authors regarding the existence of stemness niches within the meninges [216] [219] [249].

Starting from this evidence, this work aimed to compare the molecular and cellular properties of fibroblasts from adult human donors' meninges to those of fibroblasts from the same donors' skin, to find the key aspects for this non-neuronal cell, but equally involved in the central nervous system processes. To achieve this result, we observed the cell cultures starting from day 0, to monitor the development of the cells in different aspects. We first observed the frequency of cell escape from the tissue, the cell attachment time, the proliferation rate, and the alignment on culture support. All of these aspects showed that meninges fibroblasts (MFs) and skin fibroblasts (SFs) are two different cell types. Some results gave us that MFs could be a sort of neuronal cells, and for this reason, we decided to try a direct conversion of MFs and SFs (with neural stem cell lines as control) to verify if MFs had the capability to became a neuron, not passing through a stage of pluripotency. We decided to perform a deeper analysis, studying the whole transcriptome, focusing on fibroblast cells only, for a better knowledge of these two cell types. This thesis will be used as a starting point for additional research into fibroblasts from adult meninges and their regenerative potential against the CNS, correlating the clinical evidence and also the neuropathological report. All with the ultimate goal of establishing innovative customized regenerative medicine techniques for the treatment of neuronal degeneration-related pathologies.

This thesis is part of wider research at the Golgi Cenci Foundation's Laboratory of Neuropathology and Neurogenetics in Abbiategrasso (GCF, Milan), which examines human physiological and pathological brain aging on social, neuropsychological, genetic, biochemical, and neuropathological levels. The major goal of

GCF is to collect data needed to estimate the prevalence and course of dementia by following donors throughout their lives, examining their brains after death, and establishing correlations with socio-demographic and clinic neuropathological factors. The isolation of primary cell lines adds to the Brain Bank a tissue that leads to a more depth analysis beyond the histological evidence taking from the donor's brains.

3. Materials and Methods

3.1 Subject recruitment

The population of this study consists of 20 patients, 8 have participated in the InveCe.Ab (Invecchiamento Cerebrale in English: Brain Aging Abbiategrasso, ClinicalTrials.gov, NCT01345110) project, other 12 patients are volunteers from ASP Golgi-Redaelli Geriatric Institute or adult volunteers residing in Abbiategrasso. Brain, cerebellar, and brainstem autopsies were performed at the Abbiategrasso Brain Bank at the time of death (ABB). The male:female ratio is 5:14, 26.3% for male subjects and 73.7% for female subjects. The population's age ranged from 65 to 104 years old at the time of death, with an average age of 82.2 years. All subjects examined had a diagnosis of major neurocognitive disorder.

3.1.1 InveCe.Ab Project

The InveCe.Ab Project is a longitudinal study initiated in 2009 by the Golgi-Cenci Foundation of Abbiategrasso (MI), involving 1321 participants (out of 1644 eligible subjects, with an initial response rate of 80.3%) born between 1935 and 1939 (age range 70-75 years), of Caucasian ethnicity and living in the same geographical area. The project is currently underway. The goal of the study is to obtain a cohort with the greatest homogeneity and least variability to assess the incidence, prevalence, and natural history of dementia, along with its possible risk and protective factors, including behavioral, psychosocial, clinical, and biological variables [250]. Participants are evaluated using a multidimensional approach, through follow-up periods (every 2-3 years after enrollment) in which the same set of parameters is assessed [250]. Clinical data collected during the InveCe.Ab study allows comparison with data collected at neuropathological analysis. The InveCe.Ab participants were asked to donate their brains during the second follow-up, contributes to the establishment of the ABB.

3.1.2 Abbiategrasso Brain Bank

The ABB was established in 2014 to organize an archive of well-characterized, high-quality brain tissue available to the scientific community [251]. As stated before, part of the participants to the InveCe.Ab project has joined the proposal to donate their brains, however the ABB is open to all voluntary donors who want to join (290 InveCe.Ab subjects + 137 volunteers). The donors come from the ASP Golgi-Redaelli Geriatric Institute or are adult volunteers residing in Abbiategrasso or surrounding areas, who have become aware of the ABB project. Adherence to

the donation program requires periodic clinical evaluations (every 10 years under 65 years, every 3 years between 65-75 years, and every 2 years over 75 years) performed by a team, consisting of a neurologist, a geriatrician expert in neurology and three psychologists. If new symptoms appear or there is a rapid progression of cognitive impairment, the time interval between follow-ups should be shortened.
Donor evaluation involves: (1) the administration of a lifestyle questionnaire, including the degree of autonomy (Activities for Daily Living, ADL, and Instrumental ADL, IADL), lifestyle habits, and social factors that may affect cognitive status; (2) the collection of family, medical, and neurological history, with particular attention to any genetic, infectious, toxicological, metabolic, autoimmune, cardiovascular, traumatic, neoplastic, neurological, and degenerative diseases; (3) the collection of clinical examinations previously carried out; (4) the list of pharmacological treatments; (5) the complete neurological examination; (6) the complete neuropsychological examination, which examines the individual cognitive domains; (7) the Center for Epidemiologic Studies Depression Scale (CES-D scale) in case of depression; (8) hematological tests; (9) the determination of APOE and other single nucleotide polymorphisms (SNP); (10) the performance of instrumental tests (electrocardiogram (ECG), quantitative electroencephalography (qEEG)). Once the data collection is completed, a clinical and neurocognitive diagnosis is formulated following the Diagnostic and Statistical Manual of Mental Disorders (DSM-V), and the severity of dementia is classified using the Clinical Dementia Rating (CDR) score.

3.1.3 Ethical aspects of the donation program

Following the Human Research Ethics Committee and the BNE Code of Conduct, the ABB conducts its business by the following ethical standards [252] [253]. The collection procedure has been submitted to and approved by the Ethics Committee of the University of Pavia in the context of the InveCe.Ab program (Guaita et al. 2013). The study procedures conform to the principles outlined in the 1964 Declaration of Helsinki and subsequent amendments. The consent form is complete and easily understood. The choice to participate in the donation program is a personal decision and requires full awareness. If a person is deemed not competent to sign the consent form, authorization is granted by the legal guardian or next of kin (NOKs). Those who participate in the donation program are guaranteed anonymity, through the assignment of an individual numerical code. Inclusion and exclusion criteria for brain donation are reported in Table 1. The study is conducted under the supervision of the Federazione Alzheimer Italia.

Table 1: Criteria for brain donation

INCLUSION CRITERIA	EXCLUSION CRITERIA
All individuals aged 18 and above	People who blatantly refuse donation
People living within the territory of Abbiategrasso	People who live outside the Lombardy region
Volunteers who give consent on their own, or for those unable to decide for one's fate, NOKs' permission.	Discrepancies between the potential donor and NOKs wishes regarding brain donation
Death by a natural cause	Subacute encephalitis of <2 years to exclude the possibility of a prion disease
	Death caused by homicide or suicide, with the need for a coroner's report

3.2 Brain tissue handling

3.2.1 Time of death and brain removal

Time of death. Potential donors and NOKs who agree to participate in the brain donation program are given all the information on who to contact and what to say in the event of death outside of the brain bank's hospital. In the event of a late-night death, the entire process of brain removal will take place the next morning. Because of a lack of people, deaths that occur during a big holiday or on weekends are the most difficult to address. The brains of these donors are at risk of an extended postmortem time (PMT). For death to be confirmed, Italian law states that cardiac activity must cease for a period longer than 20 minutes. The recording of a flat electrocardiogram of at least 20 minutes (tanatogram) allows to perform the autopsy within 24 hours of death (DPR 285/90 art. 8; Law 578 Dec 29, 1993), ensuring better preservation of tissue quality.

Brain removal. The body is placed on a table for autopsy. Measurements of anthropometry are taken. At the widest area of the head, the circumference of the skull is measured. The anteroposterior diameter (APD) is determined by measuring from the nasion to the inion, while the transverse diameter (TD) is determined by measuring from one ear to the other. Using the formula CI = TD/APD x 100, the cephalic index is determined.

Before accessing the contents of the cranial box, a sample of temporalis muscle is removed from both sides during the autopsy, with one side being preserved in 4% formaldehyde and the other being frozen (see section 3.2.4). A V-cut is used to

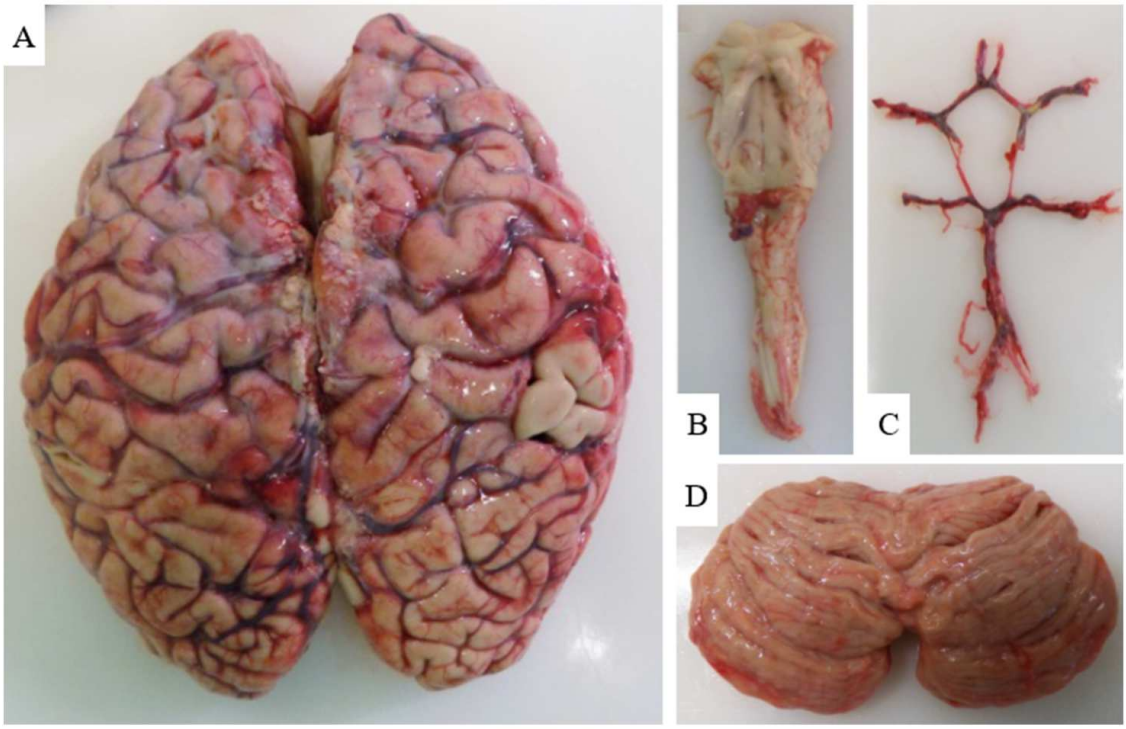

Figure 13: Pictures of the dissected parts. (A) Brain, (B) Brainstem, (C) Willis circle, (D) Cerebellum

cut the skull with an electrical saw. The meninges are sliced and the skull cap is removed. Two dura mater samples are collected using the same preservation techniques. CSF is collected from the third ventricle, appearance, color, turbidity, and pH are analyzed and then CSF is stored at -80 °C. The brain (Figure 13 A), cerebellum (Figure 13 D), and brainstem (Figure 13 B) block are all removed. The Gasser's ganglia on both sides are harvested, one preserved in 4% formaldehyde and the other frozen; the olfactory bulbs and optic nerves are harvested using the same preservation methods; and finally, the pituitary gland is reached and harvested by fracturing the sella turcica, which is fixed in 4% formaldehyde. The entire brain is examined macroscopically for vascular changes and macroscopic abnormalities, as well as weight and transverse and anteroposterior diameter.

The brain is then separated from the cerebellum and brainstem, and each is weighed separately. The three structures are placed on ice at 4 °C for 2-4 hours to allow the tissue to solidify in preparation for dissection. The Willis circle (Figure 13C), is isolated from the brain, and anatomic variations, lesions, or stenosis of the vessels are looked for under a microscope. Finally, the cranial convexity yields 1-2 leptomeningeal specimens ranging in size from 2-4 cm^2 [254] [253].

3.2.2 Brain dissection

A cut on the sagittal plane through the corpus callosum separates the two cerebellar hemispheres. Each hemisphere is cut separately into anteroposterior coronal sections of about 1 cm thickness, numbered from the frontal to the occipital pole (Figure 14 A). The area crossing between the optic chiasm and the mammillary bodies, as well as the area 1 cm posterior to the crossing one, going through the mammillary bodies, serve as reference points for the coronal plane cut (Red dotted line in Figure 14 B). By alternating the two techniques between adjacent portions, dissected sections are fixed or frozen. The frontal, temporal, and cingulate lobes, as well as the basal ganglia, Meynert basal nucleus, amygdala, thalamus, hippocampus, entorhinal cortex, occipitotemporal gyrus, and parietal and occipital lobes, should be fixed. The slices are laid out on waxed paper all in the same direction, with the upper face visible, named, and numbered, alternating one slice for fixation and one slice for freezing to perform qualitative (histological) and quantitative (biochemical-genetic) analyses respectively (Figure 14 C-D).

3.2.3 Brainstem and cerebellum dissection

The cerebellum is dissected by first cutting in the sagittal plane to split the two hemispheres at the level of the vermis, and then cutting in the sagittal plane to obtain 4 sections from each hemisphere (Figure 15 A-B). The slices are laid out on waxed paper, named and numbered, alternating one slice for fixation and one slice for freezing.
The brainstem is cut in axial rostrocaudal sections, a spot between the superior colliculi of the rostral midbrain to obtain two half layers, exposing the substantia nigra (SN), followed by transverse cuts of the half layers to obtain roughly 10 sections of 1 cm each. The superior margin of the fourth ventricle at the level of the rostral pons, to expose the locus coeruleus (LC), and the inferior margin of the fourth ventricle at the level of the medulla oblongata region inferior to the acoustic striae, to include the dorsal motor nucleus of the vagus (DMNV), are the landmarks during transverse cutting (Figure 15 C-D).

3.2.4 Cryopreservation and fixation

Once the slices have been cut, they are placed on metal support and 'frozen' for about 4 minutes in liquid nitrogen, and then placed in plastic bags sealed with an identification label and stored at -80°C. Instead, the slices to be fixed are placed in special bio-cassettes if they are small and medium-sized or wrapped in gauze if they are large, both types of slices are then placed in formalin solution (Sigma Aldrich,

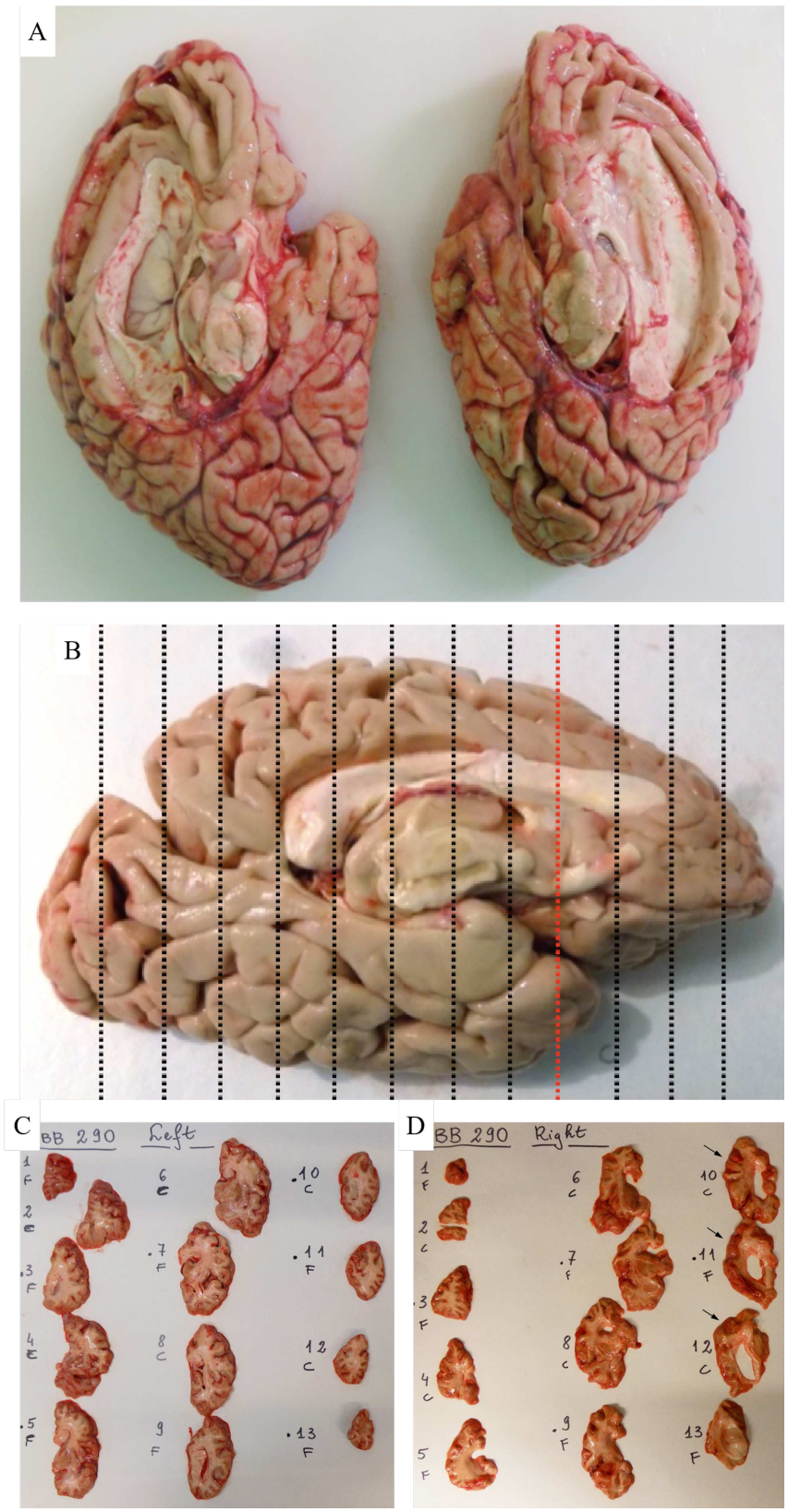

Figure 14: Pictures of brain dissection: (A) First dissection of the brain in the two hemispheres, left and right. (B) Plan for the coronal sectioning, starting from the area crossing between the optic chiasm and the mammillary bodies (red dotted line). (C-D) Slices laid out on waxed paper, with the indication of slice number and if the slice will be cryopreserved – C – or fixed – F -

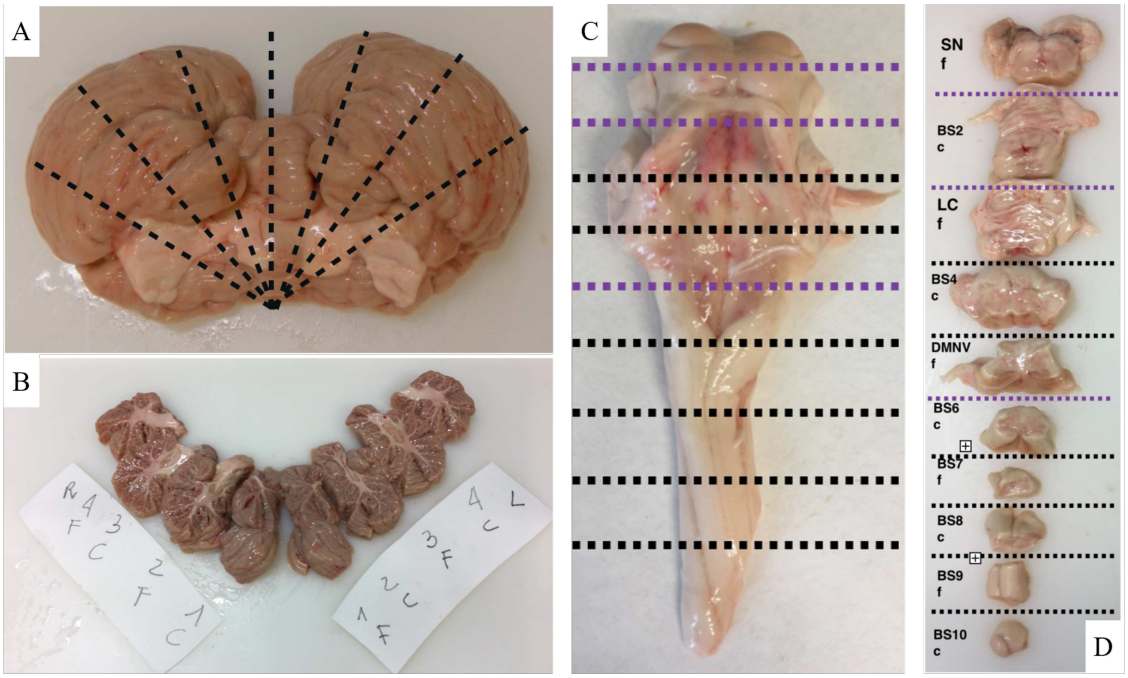

Figure 15: Pictures of the cerebellum and brainstem dissection: (A) Dissection of the cerebellum in 8 slices, starting from the vermis (central line). (B) Slices laid out on waxed paper, with the indication of slice number and if the slice will be cryopreserved – C – or fixed – F. (C) Dissection of the brainstem in 10 slices (D) Slices laid out on waxed paper, with the indication of slice content (SN: substantia nigra, BS: brainstem, LC: locus coeruleus, DMNV: dorsal motor nucleus of the vagus) and if the slice will be cryopreserved – C – or fixed – F-

Italy) at 4°C. Afterward, the fixed brain autopsy samples will be processed to obtain the histological slide to be observed under the light microscope.
The solution permeates through the tissues reaching the inner layers at a rate of about 1 mm per hour. Within two days the initial solution is replaced with fresh formalin maintained at 4°C. After about 8/10 days the samples are transferred into 1x PBS with sodium azide as a preservative (1x PBS + 0,02% NaN_3) to wash them and remove fixative excess.

3.2.5 Dehydration, inclusion, and cutting

Small samples will be dehydrated in an automated manner using a processor (ATP1000, Histo-Line laboratories, Italy) following the techniques indicated in Table 2. The biggest samples will be dehydrated manually using the same technique indicated in Table 2. To eliminate water from the tissue and prepare it for the inclusion of hydrophobic kerosene, steps in alcohol and xylene are required. This will enable the tissue to be immersed in liquid kerosene, which will subsequently solidify in a mold at room temperature (RT). Once the paraffin mold is obtained, the sample will be cut with the microtome into 5-8 μm sections. The slide microtome (Leitz 1400) is used for medium and large pieces, and the rotary microtome (ARM3600, Histo-Line Laboratories, Italy) is used for small pieces. Cut sections are placed in a solution of Chromalin (5g gelatin per 1l H_2Od, Sigma Aldrich, Italy) at 60°C that allows for slice distension and adherence to the slide. Slides are dried in an oven at 36°C overnight (ON).

3.3 Histological staining and immunohistochemistry

Paraffin sections are stripped of hydrophobic paraffin to react with aqueous dye solutions and expose target antigens that allow antibody binding. We then proceed with deparaffinization and rehydration according to the following protocol:
- Xylene I (10 min)
- Xylene II (10 min)
- Ethyl alcohol 100% (5 min)
- Ethyl alcohol 90% (5 min)
- Ethyl alcohol 80% (5 min)
- Ethyl alcohol 70% (5 min)
- H2Od (5 min)

Table 2: Abbiategrasso Brain Bank tissue processing protocol

PROCESS	SOLUTION	DURATION	
		MACRO SAMPLES	MICRO SAMPLES
Fixation	10% buffered formalin	8 days at 4°C	8 days at 4°C
Washing	Phosphate buffer	2-15 days at RT	2-15 days at RT
Washing	H2O wash	2-3 hrs tap water	2-3 hrs tap water
Dehydration	Ethyl alcohol 70%	24 hrs	8 hrs
Dehydration	Ethyl alcohol 80%	24 hrs	4 hrs
Dehydration	Ethyl alcohol 90%	60 (over the WE)	4 hrs
Dehydration	Ethyl alcohol95%	12 hrs	4 hrs
Dehydration	Ethyl alcohol95%	12 hrs	4 hrs
Dehydration	Ethyl alcohol 100%	6 hrs	4 hrs
Dehydration	Ethyl alcohol 100%	6 hrs	4 hrs
Clearing	Xylene I	12 hrs	10 hrs
Clearing	Xylene II	12 hrs	10 hrs
Infiltration	Paraffin I	12 hrs	10 hrs
Infiltration	Paraffin II	12 hrs	10 hrs
Embedding	Paraffin wax	-	-

3.3.1 Histological staining

Stains allow the morphology of colorless tissues to be distinguished, enhance the contrast between different components, and highlight structures of interest depending on the type of dye; they also allow the detection of prevalent cell types and patterns and structural abnormalities.

Basic staining in the microscopic study of tissues and routine histopathological examinations:

- Hematoxylin and Eosin (H&E), Hematoxylin is a basic dye that stains in blue-purple the acidic structures such as nucleus (DNA) and RNA-containing organelles (nucleolus and Nissl bodies), allowing to distinguish cell type and the relationship between nucleus and cytoplasm. Eosin, being an acidic dye, stains in pink the basic components of the cell including cytoplasmic organelles and the collagen fibers of the extracellular matrix. It provides a comprehensive and detailed view of the of tissue sample allowing the determination of the basic morphology.

Nerve Tissue-Specific Staining:

- Cresyl violet (Nissl) is a basic dye that interacts with the acidic components of the cell (DNA and RNA), highlighting dark purple-blue Nissl nuclei and bodies. It is used to determine the cytoarchitecture of the cerebral cortex, differentiating the different cortical layers and detecting possible neuronal loss.
- Luxol Fast Blue (LFB) stains myelin blue allowing the identification of myelinated fibers present mainly in the white matter and less in the gray matter. Using the LFB staining it is possible to evaluate demyelination as decreasing intensity in the staining due to lower density of myelinated fibers. Counterstaining with Cresyl violet highlights the neurons and allows contextualization of the tissue.
- Gallyas is a stain that uses silver and gold salts with high specificity for neurofibrillary degeneration, neuritic plaques, and neurofilaments (neuropil threads); it stains these structures in black while the nuclei are counterstained in red with Nuclear Fast Red.

3.3.2 Immunohistochemistry reactions

Immunohistochemistry reactions (IHC) exploit antigen-antibody interactions to highlight the presence of specific target structures. The antigen-antibody interaction will be revealed by a polyclonal secondary antibody directed against the primary antibody and conjugated to a catalyst enzyme, peroxidase (HRP), which reacts with a chromogen (Diaminobenzidine, DAB) (DAKO, USA). The DAB in the presence of an oxidizing agent (H_2O_2) precipitates forming a colored product visible under a light microscope. In Table 3 the list of the primary and secondary antibodies.

Table 3: Primary and secondary antibodies for IHC

PRIMARY ANTIBODY	SUPPLIER	HOST	DILUTION	NOTE
Anti-βamyloid (4G8)	BioLegend	Mouse	1:1000	It recognizes abnormally processed β-amyloid isoforms and its precursors.
Anti-phospho TAU (AT8)	ThermoScientific	Mouse	1:200	It recognizes an epitope of phosphorylated Tau
Anti-α-SYN (KM51)	Novocastra	Mouse	1:500	It marks α-SYN
Anti-phospho TDP-43 (pS409/410-2)	CosmoBio	Rabbit	1:4000	It marks phosphorylated TDP-43
Anti-NeuN (A60)	Chemicon	Mouse	1:1000	It marks the nucleus of all neuronal cells
Anti-GFAP	Dako	Rabbit	1:1000	It marks astrocytes

SECONDARY ANTIBODY	SUPPLIER	HOST	DILUTION
EnVision+System-HRP	Dako	Anti-mouse	1:2
EnVision+System-HRP	Dako	Anti-rabbit	1:2

3.3.3 Mounting

At the end of each staining or IHC protocol, the slides should be dehydrated in an increasing scale of alcohols (from 70% to 100%) according to a reverse protocol to the one used in section 3.3 and then covered. They are removed from the xylene under a hood and a few drops of the DPX mount are added to cover the slice. Finally, the slides are covered with a coverslip and left to dry under the hood. We will then proceed with the vision and evaluation of the preparations under a light microscope (RX Series Researching biological microscope, South Optics, China).

3.3.4 Routine neuropathological analysis

To analyze the preparations, histological staining and IHC reactions are subsequently performed. To execute routine neuropathological analysis, a standard protocol is used to analyze specific brain areas with specific dyes and antibodies (Table 4) (Poloni et al. 2020). Subsequently, based on the analysis of the preparations, the neuropathological diagnosis will be performed. The standard procedures described above are performed on all donor's brains to draw up, through histological staining and IHC techniques, a detailed neuropathological report which it is possible to classify the different brains according to the pathology involved. Once classified, the brain included in the ABB, it is possible to perform specific and detailed studies on well-selected cases.

3.4 Cellular isolation from the skin and meningeal tissue

3.4.1 Skin fragment dissection

1-2 skin fragments were taken from the subject using a punch and were stored in a complete medium of Dulbecco's modified Eagle's medium (DMEM) (Carlo Erba, Italy) at a high glucose concentration containing 20% fetal bovine serum (FBS) (Carlo Erba, Italy), 2mM L-glutamine (Carlo Erba, Italy), 10 mg/mL streptomycin (Carlo Erba, Italy), 100 U/mL penicillin (Carlo Erba, Italy), and 1X nonessential amino acids (NEAA) (Carlo Erba, Italy) until processed. Skin fragments were placed in a 10-cm-diameter Petri dish and the tissue was fragmented into smaller than 1 mm pieces with a surgical scissor.

Table 4: List of IHC staining and reactions performed on different brain, brainstem, and cerebellum areas

REGION	H&E	NISSL	LFB	GALLYAS	4G8	AT8	α-SYN	TDP-43	NeuN	GFAP
BRAINSTEM										
Medulla- DMNV	x					x	x			
Pons - Locus Coeruleus	x					x	x			
Midbrain - Substantia Nigra	x				x	x	x			
CEREBELLUM										
Cerebellar cortex and Dentate nucleus	x	x	x		x					
CEREBRUM										
Middle frontal gyrus	x	x	x		x	x	x			
Basal Ganglia + nucleus of Maynert	x	x	x		x				x	x
Cingulate, anterior	x	x	x		x		x		x	x
Amygdala	x					x	x	x	x	x
Thalamus and Subthalamic nucleus	x					x				
Superior and middle temporal gyri	x	x	x	x	x	x	x		x	x
Hippocampus and Entorhinal cortex	x	x	x	x	x	x	x	x	x	x
Inferior parietal lobule	x	x	x	x	x	x	x			
Occipital cortex	x		x		x	x	x			
Olfactory bulb	x						x			

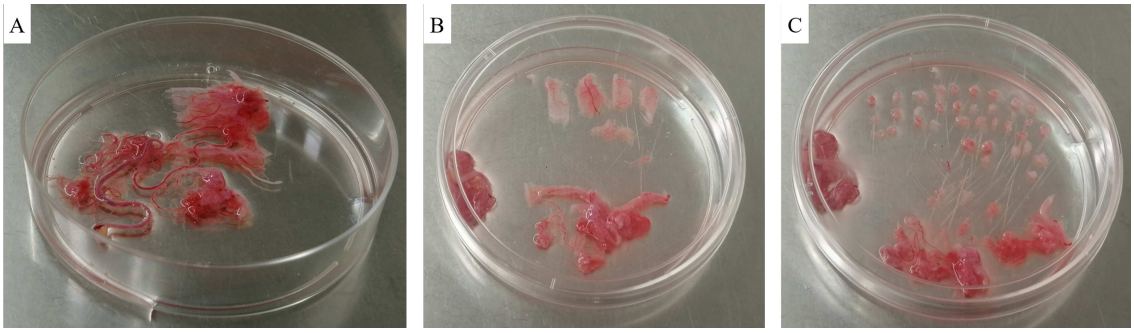

Figure 16: Pictures of meningeal fragment dissection. (A) Meningeal explant after washing with 1X PBS. (B)Vessel removal from the meningeal explant and isolation of meningeal tissue. (C) Meningeal tissue fragmentation in 2-3 mm pieces

3.4.2 Meningeal fragment dissection

1-2 meningeal fragments of approximately 2-4 cm2 were collected during brain explantation. These were preserved in a complete medium composed of DMEM (Carlo Erba, Italy) at high glucose concentration containing 20% FBS (Carlo Erba, Italy), 2mM L-glutamine (Carlo Erba, Italy), 10 mg/mL streptomycin (Carlo Erba, Italy), 100 U/mL penicillin (Carlo Erba, Italy), and 1X NEAA (Carlo Erba, Italy) until processed. To culture the explant, the meningeal fragments were placed in a 10-cm-diameter Petri dish and washed twice with 1X PBS (Carlo Erba, Italy) to remove any residual blood (Figure 16 A). Subsequently, the tissue was separated from the blood vessel (Figure 16 B) and fragmented into small pieces of approximately 2-3 mm using a surgical scalpel (Figure 16 C).

3.4.3 Preparation of cell cultures

Skin and meningeal fragments were transferred within 6-well plates previously treated with 0.5% gelatin for 1 hour (Figure 17). Fragments were cultured in a complete medium composed of DMEM (Carlo Erba, Italy) at high glucose concentration containing 20% FBS (Carlo Erba, Italy), 2mM L-glutamine (Carlo Erba, Italy), 10 mg/mL streptomycin (Carlo Erba, Italy), 100 U/mL penicillin (Carlo Erba, Italy), and 1X NEAA (Carlo Erba, Italy) with a final addition of 250 ng/ml amphotericin B (Sigma Aldrich, Italy). The plates were then placed in a 5% CO_2 incubator at 37°C. The culture medium was changed every 3 to 4 days. Once 70% confluence was reached, fibroblasts from meninges (MFs) and fibroblasts from the skin (SFs) were treated with trypsin 1X (EuroClone, Italy) to promote their detachment and displacement into the T75 flask. When cells reached 100% confluence, they were frozen in FBS with 10% dimethyl sulfoxide (DMSO) (Sigma Aldrich, Italy) inside cryovials at -80°C for 24 hours, and then in liquid nitrogen. Cells with a passage of no more than 4 were employed in the following experiments.

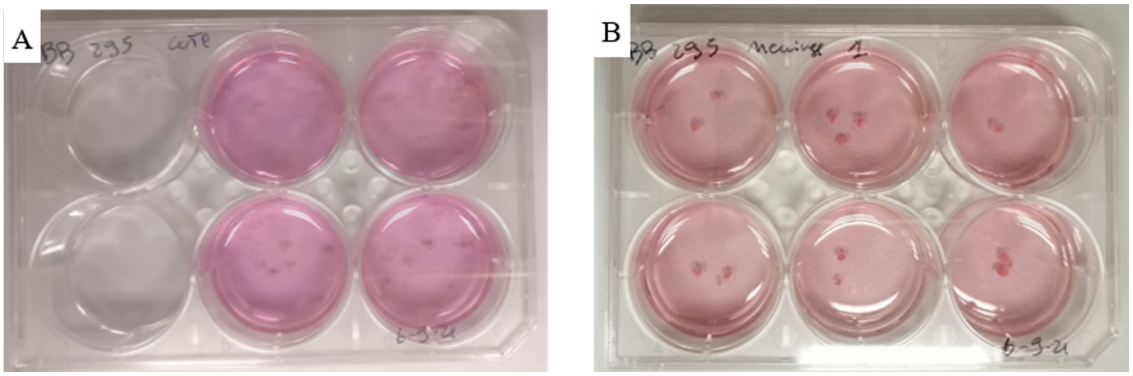

Figure 17: Pictures of skin and meningeal fragment plating. (A) Skin fragment and (B) meningeal fragment

3.5 Fibroblast characterization

3.5.1 MTT assay

The MTT assay (Sigma Aldrich, Italy) was used to determine the rate of proliferation of MFs and SFs. The MTT assay is a colorimetric test that measures cell metabolic activity as a function of the generation of purple-colored formazan crystals, which form when MTT (3-(4,5-dimethylthiazol-2-yl)-2,5-diphenyltetrazolium) molecules are cleaved by cells. Cell growth is analyzed by an increase in cellular activity and, as a result, crystal formation. $5x10^3$ cells were plated in a 96-well plate and five observation times were identified at day 1, day 4, day 7, day 10, and day 14. The culture medium was removed and the cells were cultured in a 37°C incubator with 5% CO_2 for 4 hours with a 5 mg/ml MTT solution (Sigma Aldrich, Italy) in FBS-free complete medium. The MTT solution was withdrawn from the wells after 4 hours and replaced with a 4 mM HCl solution containing 0.1 percent Nonidet P-40 (Sigma Aldrich, Italy) in isopropanol (i.e., the MTT solvent, Sigma Aldrich, Italy). The plate was then incubated for 15 minutes under agitation. Subsequently, the absorbance was read using a spectrophotometer (EnSight PerkinElmer, USA) at 570 nm. The results obtained at the various times were normalized on the results obtained at day 1.

3.5.2 Analysis of cell adhesion

After the detachment process in the culture plate, cells were observed for 24 hours at 2 hours timepoints for the first 8 hours (T0, T2, T4, T6, T8) and after 24 hours from the starts (T24). The cells were carefully evaluated and counted. The percentage was computed by dividing total cells and attached cells by 1 image of each timepoint.

3.5.3 Analysis of cell directionality

Cell directionality waw measured using the ImageJ Directionality plugin (NIH, USA, https://imagej.nih.gov). Both phase contrast images and immunofluorescence images were used to settle the directionality graph (Martella et al. 2017).

3.5.4 MACS separation using magnetic microspheres associated with anti- fibroblast antibodies

To obtain specific fibroblast cell cultures and to eliminate possible contamination of other cell types after culturing explants from skin and meninges, separation was performed using Anti-Fibroblasts MicroBeads (Miltenyi Biotec, Germany) and Magnetic Activated Cell Sorting (MACS) (Miltenyi Biotec, Germany). This procedure, through the use of magnetic microbeads bound to anti-fibroblast antibodies, allows the separation of fibroblasts, which will bind to the microbeads, from the other cell types (not bound to the microbeads). Fibroblasts will then be magnetically retained in the column while other cell types will not. Approximately $10x10^6$ cells were centrifuged at 300 g for 10 minutes. The resulting pellet was resuspended in 80 µl of a buffer containing 1X PBS (Sigma Aldrich, Italy), 0.5% bovine serum albumin (BSA, Sigma Aldrich, Italy), 2 mM EDTA (Invitrogen, USA), and 20 µl of Anti-Fibroblast MicroBeads (Miltenyi Biotec, Germany), and incubated at RT for 30 minutes. The cells were wash with 1-2 ml with the buffer containing 1X PBS (Sigma Aldrich, Italy), 0.5% bovine serum albumin (BSA, Sigma Aldrich, Italy), 2 mM EDTA (Invitrogen, USA) and centrifuged again at 300 g for 10 min. The supernatant was removed and the pellet was resuspended in the buffer containing 1X PBS (Sigma Aldrich, Italy), 0.5% BSA (Sigma Aldrich, Italy), and 2 mM EDTA (Invitrogen, USA). Cells were then resuspended and transferred inside an LS column and placed inside a magnetic separator (Miltenyi Biotec, Germany). Sequential additions of the same volume of previously reported buffer inside the column allowed the collection of eluates containing negative cells to Anti-Fibroblast MicroBeads (Miltenyi Biotec, Germany). Finally, the column was removed from the magnetic separator and placed in a new tube, filled with 5 ml of buffer, and antibody-positive fibroblasts were collected using a plunger. Cell number and viability were analyzed using the Trypan Blue exclusion method (Sigma Aldrich, Italy) and a TC20 automatic cell counter (BioRad, Italy).

3.5.5 Total RNA Extraction

Total RNA was extracted using TRIzol Reagent (Sigma Aldrich, Italy). The pellet of SFs and MFs was resuspended in 1 ml TRIzol and incubated for 5 minutes at

RT. Next, 200 μl of chloroform was added and centrifuged at 12000 g for 15 minutes at 4°C. Three distinct phases were formed: RNA (upper transparent phase), DNA (middle white ring), and protein (lower pink phase). The harvested RNA was placed in a new eppendorf and 500 μl of isopropanol (Sigma Aldrich, Italy) was added to ensure RNA precipitation. After incubation for 10 min at RT, the samples were centrifuged at 12000 g for 10 minutes at 4°C. Subsequently, the obtained pellet was resuspended in 1 ml of 75% ethanol (Sigma Aldrich, Italy) and centrifuged again at 7600 g for 5 minutes at 4°C. The pellet was dried by evaporating and resuspended in UltraPure distilled water (Thermo Fisher Scientific, USA). Quantification of the extracted RNA was performed using the NanoDrop™ One/OneC Microvolume UV-Vis spectrophotometer (Thermo Fisher Scientific, USA). The quality and integrity of the extracted RNA were assessed based on the RNA Integrity Number (RIN) using the Bioanalyzer 2100 (RNA 6000 Nano Kit, Agilent, Germany).

3.5.6 Retrotranscription and cDNA synthesis

500 ng of RNA was reverse transcribed using the iScript™ cDNA Synthesis Kit (BioRad, Italy). Four μL of 5x iScript Reaction Mix, 1μL of iScript Reverse Transcriptase, and UltraPure distilled water (Thermo Fisher Scientific, USA) were added to RNA to reach a total volume of 20 μL. The reaction mix was incubated for 5 minutes at 25°C, for 30 minutes at 42°C, and 5 minutes at 85°C. The cDNA samples were stored at -20°C.

3.5.7 qPCR

Quantitative PCR amplification was performed using SYBR Green Master Mix (Bio-Rad, Italy). Each reaction mixture was composed of 7.5 μl of SYBR Green Master Mix 2x (BioRad, Italy), 0.5 μl of primer forward, 0.5 μl of primer reverse, 1 μl of cDNA, and 5.5 µl of UltraPure distilled water (Thermo Fisher Scientific, USA). Primers with a starting concentration of 100 µM, were diluted at 1:10 (Table 5) in UltraPure distilled water (Thermo Fisher Scientific, USA). The reaction was performed using the CFX Connect™ Real-Time PCR Detection System (BioRad, Italy). The protocol consists of initial denaturation for 3 minutes at 95°C; 40 cycles of:15 seconds at 95°C, 45 seconds at 60°C.

Cycle threshold (Ct) values were automatically recorded for each replicate qPCR reaction, and mean Ct values were normalized against those determined for GAPDH. Fold-expression differences were determined using the 2-$\Delta\Delta$Ct method.

Table 5: List of primer sequences

PRIMER	FORWARD SEQUENCE	REVERSE SEQUENCE	ASSAY
GAPDH	ATGGAAATCCCATCACCAT	CGCCCACTTGATTTTGG	Housekeeping
VIM	CTTCAGAGGAAGCCGA	ATTCCACTTTGCGTTCAAGG	Fibroblasts characterization
FN1	CCATAAAGGGCAACCAAGAG	ACCTCGGTGTTGTAAGGTGG	Fibroblasts characterization
SERPINH1	GAGTAGAATCGTGTCGCGG	TTTCATTCTGGGTCGCTG	Fibroblasts characterization
NES	GAAACAGCCATAGGGCAA	TGGTTTTCCAGTCTTCAGTGA	Fibroblasts characterization Direct differentiation in generic neuron
TUBB3	CAGATGTTCGATGCCAAGAA	GGGATCCACTCCACGAAGTA	Fibroblasts characterization Direct differentiation in generic neuron
MAP2	AGGGCTGGTAGGTTATCT	TGTCTGCCTTTGCATC	Fibroblasts characterization Direct differentiation in generic neuron
TNFSF18	TCTGAACCTCCTTGCGTGAA	GTTTGCATTGGGAGCCACTT	RNAseq platform technical validation
NPY4R	TCTGGGTCATTGCCTGTC	TATCCGCCAGGAACTCCAGA	RNAseq platform technical validation
AhR	GGTCCAGTCTAATGCACG	GCAGGAAAAGGGTTGC	Pathway analysis RNAseq platform technical validation
ADCY1	GTGGGGAAACTGAGGCTCG	GAAGGTGAGGCTGAAGAGCA	Pathway analysis RNAseq platform technical validation
ADCY5	CAGACAGGTCCTGGAGGAGA	CTGGAAAGCCTGTCTGGG	Pathway analysis RNAseq platform technical validation
ADCY6	CTGTGGGCCTCTCTG	TTTGCTACCACCCCATCC	Pathway analysis RNAseq platform technical validation
ARNT	ACTACTGCCAACCCCGAAAT	CTCTGGACAATGGCTCCTCC	Pathway analysis RNAseq platform technical validation
PDE3B	GAGACCGTCGTTGCCTTGTA	ACCTCCAGAATTTTGATAATGAGGC	Pathway analysis RNAseq platform technical validation
PDE4B	GGGATGACTAAGGCAGAGAG	GCGGAGGGAACGGTCTCTTA	Pathway analysis RNAseq platform technical validation
ADM	AATGAATGCTGAGACCCG	TGACACGCCGTGAGAAATCA	Pathway analysis RNAseq platform technical validation

3.5.8 Immunofluorescence assay

SFs and MFs were cultured in 24-well plates over a coverslip for at least 5 days. The culture medium was removed and the cells were fixed with 4% paraformaldehyde (PFA, Sigma Aldrich, Italy) for 20 minutes at RT. Subsequently, cells were permeabilized with 0.3% Triton X-100 in 1X PBS (Sigma Aldrich, Italy). The cells were then incubated for 1 hour with 1X PBS (Sigma Aldrich, Italy) with 5% normal goat serum (NGS; Carlo Erba, Italy). Primary antibodies were then added to the same solution (Table 6), and slides were incubated ON at 4°C. Subsequently, cells were washed with 1X PBS (Sigma Aldrich, Italy) and incubated for 1 hour with secondary antibodies (Table 6) at RT. An additional wash with 1X PBS (Sigma Aldrich, Italy) was then performed. Slides were then removed from the wells and mounted on glass slides with a solution containing DAPI (4',6-diamidino-2-phenylindole, a fluorescent dye capable of binding adenine- and thymine-rich DNA sequences; Sigma Aldrich, Italy), dried and nail-polished. Analysis was performed using an Axio Imager 2 fluorescence microscope (Zeiss, Germany) equipped with an Axiocam Mrm camera (Zeiss, Germany).

3.6 Preparation of libraries for RNA-Seq

3.6.1 Ribosomal RNA depletion

Ribosomal RNA (rRNA) was depleted using the RiboCop rRNA Depletion Kit V1.2 (Lexogen, Austria). The RNA depletion process consists of an initial step of hybridization of denatured RNA fragments, an intermediate step of rRNA depletion, and a final step of purification.

Five hundred ng of total RNA was diluted in 26 µl of RNase-free water (Invitrogen, USA). Next, 4 µl of hybridization solution and 5 µl of a mix containing rRNA fragments probes were added. Next, RNA denaturation was performed by placing the solution in a thermomixer (Eppendorf, Germany) at 75°C for 5 minutes while shake at 1250 rpm. After 5 minutes the temperature of the thermomixer was reduced to 60°C, and the incubation process was extended for another 30 minutes. For the rRNA depletion step, the depletion beads were washed. 30 µl of depletion solution containing the beads was added to the hybridized RNA, and subsequently, the sample was placed in a thermomixer at 60°C for 15 minutes while shaking at 1250 rpm. Next, the solution was placed on a magnetic rack to isolate the rRNA bound to the beads and 60 µl of supernatant containing the depleted rRNA was collected. The final purification step was conducted by adding 24 µl of the solution containing magnetic purification beads and 108 µl of purification solution to this 60

Table 6: Primary and secondary antibodies used for immunofluorescence analysis of MFs and SFs

PRIMARY ANTIBODY	SUPPLIER	HOST	DILUTION	ASSAY
Fibronectin	Abcam, UK	Rabbit	1:300	Fibroblasts characterization
HSP 47 (Serpin H1)	Santa Cruz Biotechnology Inc., Germany	Mouse	1:250	Fibroblasts characterization
Nestin	Abcam, UK	Mouse	1:200	Fibroblasts characterization Direct differentiation in generic neuron
β-III-Tubulin	Abcam, UK	Rabbit	1:1000	Fibroblasts characterization Direct differentiation in generic neuron
Map2	Thermo Fisher Scientific, USA	Mouse	1:200	Direct differentiation in generic neuron

SECONDARY ANTIBODY	SUPPLIER	HOST	DILUTION	ASSAY
Anti - Rabbit 488	Sigma Aldrich, Italy	Rabbit	1:400	Fibroblasts characterization Direct differentiation in generic neuron
Anti - Mouse 488	Sigma Aldrich, Italy	Mouse	1:400	Fibroblasts characterization Direct differentiation in generic neuron
Anti - Mouse 594	Sigma Aldrich, Italy	Mouse	1:400	Fibroblasts characterization Direct differentiation in generic neuron
Anti - Rabbit 594	Sigma Aldrich, Italy	Rabbit	1:400	Fibroblasts characterization Direct differentiation in generic neuron

µl. RNA was then washed with 80% ethanol solution twice.
Upon completion, the quality of total rRNA depletion was assessed using the Bioanalyzer 2100 (RNA 6000 Pico Kit, Agilent, Germany).

3.6.2 Preparation of RNA sequencing libraries

Libraries for RNA-Seq were prepared using the CORALL Total RNA-Seq Library Prep Kit (Lexogen, Austria) from the depleted RNA samples. The first step was to incubate the RNA samples with primers and retrotranscriptase to obtain cDNA by a retrotranscription process. The samples were then placed in a thermocycler using the following protocol: 10 minutes at 25°C; 40 minutes at 37°C; 10 minutes at 42°C. Next, purification was performed using magnetic beads, binding the cDNA fragments, and wash with ethanol. Following purification, cDNA samples were incubated at 37°C for 30 minutes with a Linker Oligo solution (Lexogen, Austria) consisting of primers capable of marking the 3' end of cDNA fragments. Samples were then purified again using magnetic beads and transferred to a plate for the amplification reaction. The exact number of cycles for PCR was calculated by performing qPCR on the previously purified samples and taking into account the number of cycles required to obtain 50% of the maximum fluorescence. The protocol consists of initial denaturation for 30 seconds at 98°C; 35 cycles of: 10 seconds at 98°C, 20 seconds at 65°C, 30 seconds at 72°C; final extension for 60 seconds at 72°C. Finally, the library was purified using magnetic beads and ethanol.
The quality of the libraries was then analyzed using the Tape Station (D1000 High sensitivity Kit, Agilent, Germany) and quantified with Qubit™ dsDNA HS Assay Kit (Invitrogen, USA). Sequencing was performed using a NextSeq 500 Sequencer (Illumina, USA).

3.7 Bioinformatic data analysis

FastQ files were generated via Illumina bcl2fastq2 starting from raw sequencing reads produced by Illumina NextSeq sequencer (Version 2.17.1.14-
http://support.illumina.com/downloads/bcl-2fastq-conversion-software-v217.html). Gene and transcript intensities were computed using STAR/RSEM software using Gencode Release 27 (GRCh38) as a reference, using the "stranded" option. Differential expression analysis for mRNA was performed using R package DESeq.2. Coding and non-coding genes were considered differentially expressed and retained for further analysis with $|\log2(MFs/SFs)| \geq 1$ and a False Discovery Rate ≤ 0.1.

3.8 Pathways Data Analysis and Gene Ontology

Pathway analysis was performed using KEGG pathway analysis (Kyoto Encyclopedia of Genes and Genomes http://www.genome.ad.jp/KEGG), WikiPathways analysis, and Gene Ontologies of differentially expressed coding genes via enrichR web tool (Kuleshov et al. 2016). The R software was used to generate Dotplot graphs (with the ggplot2 library) and GOChord graphs (with the GOplot library).

3.9 Direct differentiation to generic neuron

To assess the differentiation capacity and the presence of any differences between cell populations of MFs and SFs, a standard differentiation protocol towards generic neurons was applied. The same protocol was also applied to Neural Stem Cells (NSCs) already available in our laboratory, derived from reprogrammed and differentiated human healthy peripheral cells (Fantini et al. 2019). NSCs were used as a control.

3.9.1 Preparation of culture substrate

We used 6-well and 24-well plates, treated with a 20 µg/ml solution of poly-L-ornithine (Sigma Aldrich, Italy). Inside the wells of the 24-well plates, coverslips were placed for immunofluorescence analysis. Plates with poly-L-ornithine were incubated for 1 hour at 37°C and then treated with a 10 μg/ml laminin solution (Thermo Fisher Scientific, USA) for 2 hours at 37°C. The excess solution was removed and 1X PBS (Carlo Erba, Italy) was placed inside the wells until further use.

3.9.2 Cell differentiation

MFs, SFs, and NSCs were placed in their corresponding plates at a concentration of 2.5-5 x 104 cells/cm^2 and incubated for 7 days with StemPro NSC SFM medium (Thermo Fisher Scientific, USA) (Table 7) to ensure their survival and stability.
The medium was replaced every 2-3 days. After 7 days, cells were incubated for an additional 14 days with the neural differentiation medium (Table 8), replaced every 2-3 days.

Table 7: Composition of StemPro NSC SFM medium (Thermo Fischer Scientific, USA) with the addition of Pen/Strep 1% (Carlo Erba, Italy)

COMPONENT	SUPPLIER	FINAL CONCENTRATION	VOLUME
D-MEM/F-12	Thermo Fisher Scientific, USA	1X	96ml
GlutaMAX-I-Supplement	Thermo Fisher Scientific, USA	2 mM	1ml
bFGF (stock at 100 µg/ml)	Thermo Fisher Scientific, USA	20 ng/ml	20 µl
EGF (stock at 100 µg/ml)	Thermo Fisher Scientific, USA	20 ng/ml	20 µl
StemPro Neural Supplement	Thermo Fisher Scientific, USA	2%	2ml
Pen/Strep	Carlo Erba, Italy	1%	1ml

Table 8: Composition of the neural differentiation medium with the addition of Pen/Strep 1% (Carlo Erba, Italy)

COMPONENT	SUPPLIER	FINAL CONCENTRATION	VOLUME
Neurobasal Medium	Thermo Fisher Scientific, USA	1X	96ml
B-27 Serum-free Supplement	Thermo Fisher Scientific, USA	0,02	2ml
GlutaMAX-I-Supllement	Thermo Fisher Scientific, USA	2 mM	1ml
Pen/Strep	Carlo Erba, Italy	0,01	1ml

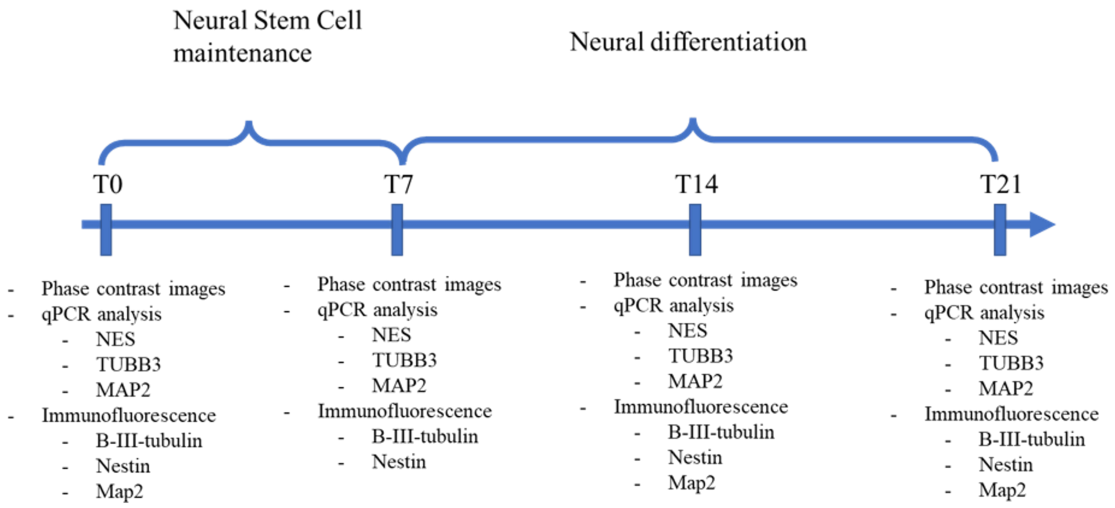

Figure 18: Time intervals of the differentiation protocol and relative analysis for each timepoint. T0, T7, T14, and T21 refer to the number of days from the starting protocol

3.9.3 Characterization of cell lines at different stages of differentiation

Cells characterization was performed at T0, T7, T14, and T21 as timepoints for phase-contrast images, qPCR, and immunofluorescence images. Phase-contrast images were taken using EVOS XL Core Cell Imaging System microscope (Thermo Fisher Scientific, USA), qPCR of NES, TUBB3, and MAP2 genes was performed as previously reported (see section 3.5.7, table 5 for primer sequences), immunofluorescence images of Nestin, β-III-tubulin, and MAP2 was performed as previously specified (see section 3.5.8, table 6 for antibody), using an Axio Imager 2 fluorescence microscope (Zeiss, Germany) equipped with an Axiocam Mrm camera (Zeiss, Germany) (Figure 18).

3.10 Statistical Analysis

All parameters and results are shown as mean values $\pm$ standard deviation (SD). Statistical analyses were conducted using GraphPad Prism (version 7, GraphPad software), adopting a one-way analysis of variance (one-way ANOVA), followed by the Newman-Keuls multiple comparison test. Data with p-values < 0.05 were considered statistically significant.

4. Results

4.1 Brain characterization

4.1.1 Clinical Diagnosis and Neuropathological Report

For this project, ABB's last twenty brains were considered. When the clinical diagnosis and the neuropathological report are compared, the clinical diagnosis differs as expected. When a clinical diagnosis of a Major-NCD is made, it will be attributed to a variety of factors, including various stages of Alzheimer's disease, TAU pathology, other precipitated proteins, such as TDP-43, and possibly vascular damage (Table 9).

4.1.2 Brain immunohistochemical in a NOLD and high AD cases

The histological analysis of the brain led to confirm or not the clinical diagnosis of the brain. Figure 19 shows a NOLD brain section and a high AD. 4G8 positivity is present in both samples, more marked in the high AD brain, with the presence of amyloid plaque, diffusely distributed in the parenchyma (Figure 19 B). The NOLD brain presents some amyloid plaque, probably due to the donor's age (80), resulting in a low form of AD, without any clinical evidence of AD (Figure 19 A). AT8 immunoreactivity identifies tangles, threads, and plaque in the high AD brain in the frontal lobe (Figure 19 D), while the NOLD brain lacks specific marking for AT8 (Figure 19 C).

Table 9: Generalities (progression number, sex and age), clinical diagnosis and neuropathological report of the 20 recruited donors

n.	Sex	Age	Clinical Diagnosis	Neuropathological Report
1	F	80	Major-NCD due to LBD (BPSD)	Intermediate AD, Neocortical/limbic LTS (Beach IV), limbic TDP, HS
2	F	104	Major-NCD due to multiple etiologies (probably mixed pathology)	TAU pathology (PART-ARTAG), HS
3	M	83	Major-NCD due to LBD (BPSD)	Severe limbic LTS, intermediate AD, Moderate SVD, severe CAA-capCAA, HS
4	F	82	Major-NCD due to multiple etiologies (AD-VaD)	Intermediate AD pathology, Moderate SVD
5	F	76	Major Frontotemporal NCD (nfPPA BPSD)	TDP (type A), ILBD, moderate SVD, low AD, HS
6	F	80	NOLD (death due to cancer with widespread metastatic diffusion)	moderate SVD, CAA, low AD, limbic encephalitis
7	F	65	major Frontotemporal NCD (bvFTD BPSD)	TDP (type A)
8	F	89	Major-NCD due to AD (BPSD)	high AD, limbic TDP, mod SVD
9	M	75	Major-NCD due to bvAD (frontal variant - BPSD)	High AD pathology, limbic LTS (Beach IIb), limbic TDP, HS, mod. CAA
10	F	79	Mild-NCD due to vascular disorder	MSA (OPCA pattern), low AD, mild SVD, small transitional meningioma
11	M	78	Major-NCD due to AD	int AD, limbic TDP, limbic LTS (Beach IIb), mild SVD, mCAA, HS
12	M	84	Major-NCD due to multiple etiologies	VaD, limbic LTS (Beach IIb), limbic TAU path (PART), amy TDP, no AD
13	F	84	Major-NCD due to multiple etiologies	mod SVD, int AD
14	M	85	in progress	in progress
15	F	85	in progress	in progress
16	F	81	Mild-NCD due to vascular pathology (VCI)	mod SVD, low AD, HS
17	F	84	in progress	in progress
18	F	85	in progress	in progress
19	M	81	in progress	in progress
20	M	80	in progress	in progress

NCD: neurocognitive disorder; LBD: Lewy body dementia; BPSD: Behavioral and psychological symptoms of dementia; AD: Alzheimer's disease; HS: Hippocampal Sclerosis; VaD: vascular dementia; NOLD: physiological aging; nfPPA: primary progressive nonfluent aphasia; SVD: small vessel disease; LTS: Lewy synucleopathy; HS: hippocampal sclerosis; CAA: cerebral amyloid angiopathy; capCAA: capillary CAA; TDP: variant fronto-temporal dementia (FTD)

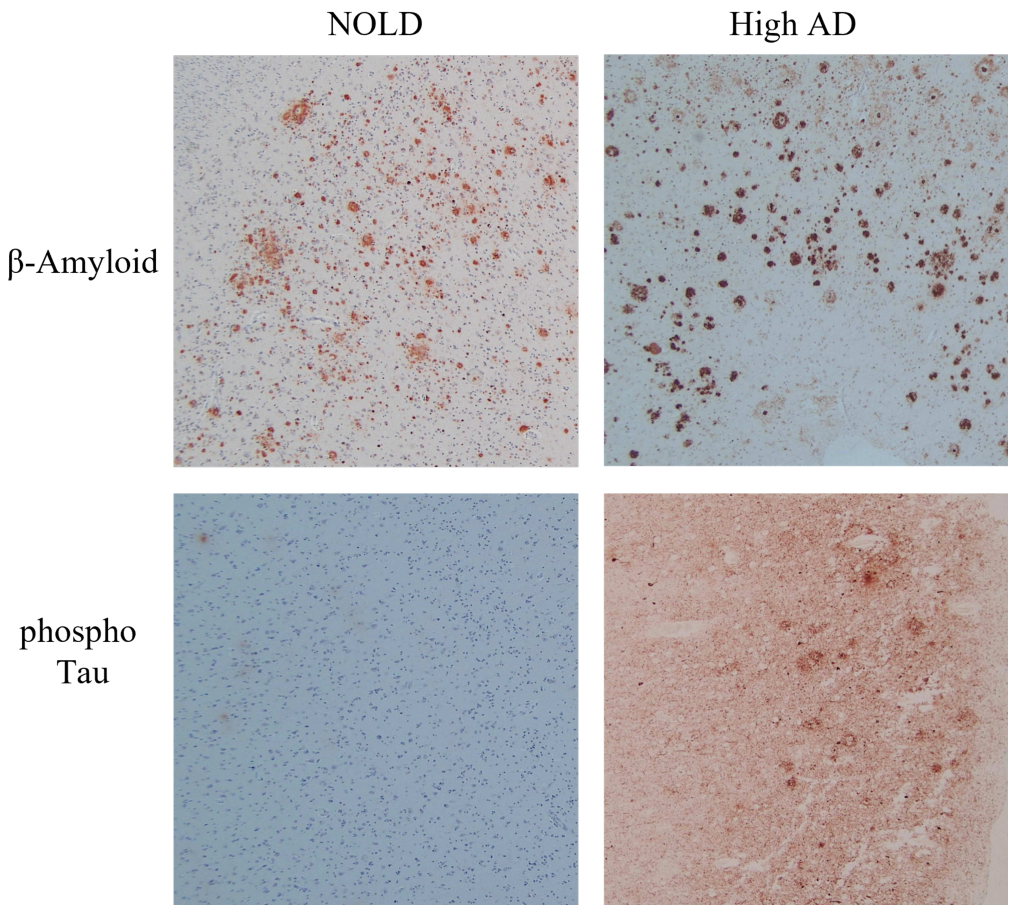

Figure 19: Histological images of two different cases from the ABB. (A) and (C) images from a NOLD donors, and (B) and (D) from a high AD donor. (A) Inferior parietal lobule marked with anti β-Amyloid antibody (4G8) at 4x magnification; (B) Inferior parietal lobule marked with anti β-Amyloid antibody (4G8) at 4x magnification; (C) Middle frontal gyrus marked with anti phospho Tau (AT8) at 4x magnification; (D) Middle frontal gyrus marked with anti phospho Tau (AT8) at 4x magnification

4.2 Fibroblasts characterization

4.2.1 Isolated cells and timing of cell appearance following the tissue fragment dissection show a premature appearance of MFs and a higher isolation rate

From the 20 patients examined in this work, 19 MFs and 13 SFs were obtained (see section 3.4). The first data of MFs and SFs analyzed was the appearance of cells in culture after plating the tissue fragments obtained from both meninges and skin. Cultures were checked daily until 10-20 cells appeared.

Table 10 shows the time elapsed, in terms of days, from the explant to the release of 10-20 fibroblasts from the tissue fragments in culture. Figure 20 shows in the x-axis the number of days elapsed since explantation, while the y-axis shows the number

of explants with the same time. The columns of different colors refer to the two cell types examined: grey columns for SFs and black columns for MFs. From these data, it is possible to assume that MFs tend to spill earlier from tissue fragments in culture than SFs. Leakage of MFs occurs between 7 and 14 days, whereas leakage of SFs occurs between 12 and 22 days.

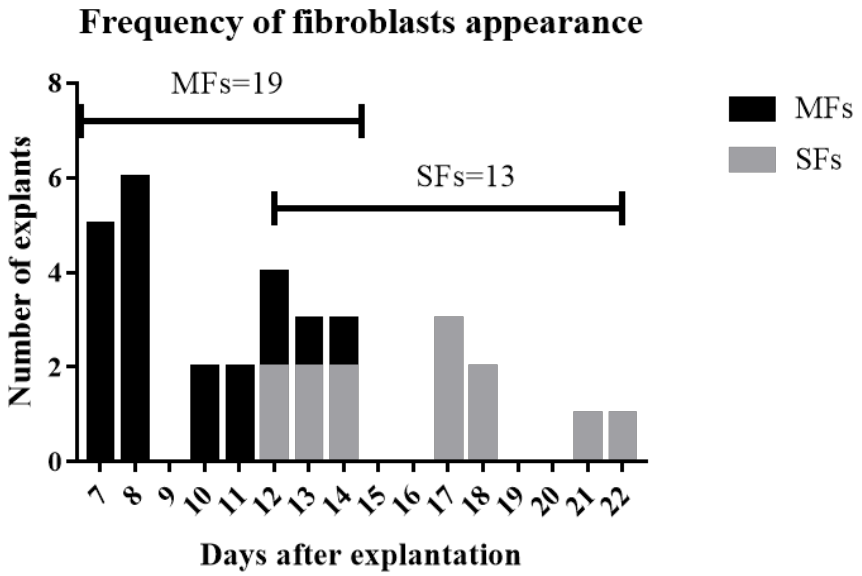

Figure 20: Daily frequency of cell appearance (Y-axis) since the day of explantation (x-axis). Grey columns indicate MFs; Black columns indicate SFs. MFs appear between 7- and 14-days post explantation; as for SFs, cell appearance occurs between 12- and 22-days post explantation

Table 10: Generalities (progression number, sex and age), list of isolated cells for each case and indication of days elapsed until the appearance of 10-20 cells from meningeal and skin explants, respectively

				Isolated Fibroblasts			
n.	**Sex**	**Age**	**Process date**	**Meningeal fibroblasts (MFs)**	**Days of appearance**	**Skin fibroblasts (SFs)**	**Days of appearance**
1	F	80	15/01/2018	MFs	8	/	/
2	F	104	09/04/2018	MFs	8	SFs	12
3	M	83	15/04/2018	MFs	12	SFs	17
4	F	82	17/05/2018	MFs	8	SFs	21
5	F	76	14/08/2018	MFs	13	SFs	13
6	F	80	16/11/2018	MFs	10	SFs	18
7	F	65	14/01/2019	MFs	11	/	/
8	F	89	04/03/2019	MFs	11	SFs	17
9	M	75	18/03/2019	MFs	14	SFs	22
10	F	79	29/04/2019	MFs	10	/	
11	M	78	21/10/2019	MFs	7	SFs	18
12	M	84	13/11/2019	MFs	12	/	
13	F	84	06/12/2019	MFs	7	SFs	12
14	M	85	11/06/2020	/		SFs	17
15	F	85	31/08/2020	MFs	7	SFs	14
16	F	81	06/12/2020	MFs	7	/	
17	F	84	09/12/2020	MFs	8	/	
18	F	85	25/03/2021	MFs	8	SFs	13
19	M	81	03/06/2021	MFs	8	/	
20	M	80	06/09/2021	MFs	7	SFs	14
Total				19/20		13/20	

4.2.2 SFs have a more rapidly time of attachment than MFs

The qualitative observation of both MFs and SFs, allowed us to observe that the two cell lines present a different time of adhesion to the culture plate. The analysis was performed by phase-contrast microscopy at 10X magnification (EVOS XL Core

Cell Imaging System microscope, Thermo Fisher Scientific, USA) at different time points, T0, T2, T4, T6 T8 and T24 in terms of hours elapsed after detachment and replating. Cells were manually counted separating adherent cells (with a flat shape) and the suspended cells (with a round shape) (Figure 21).

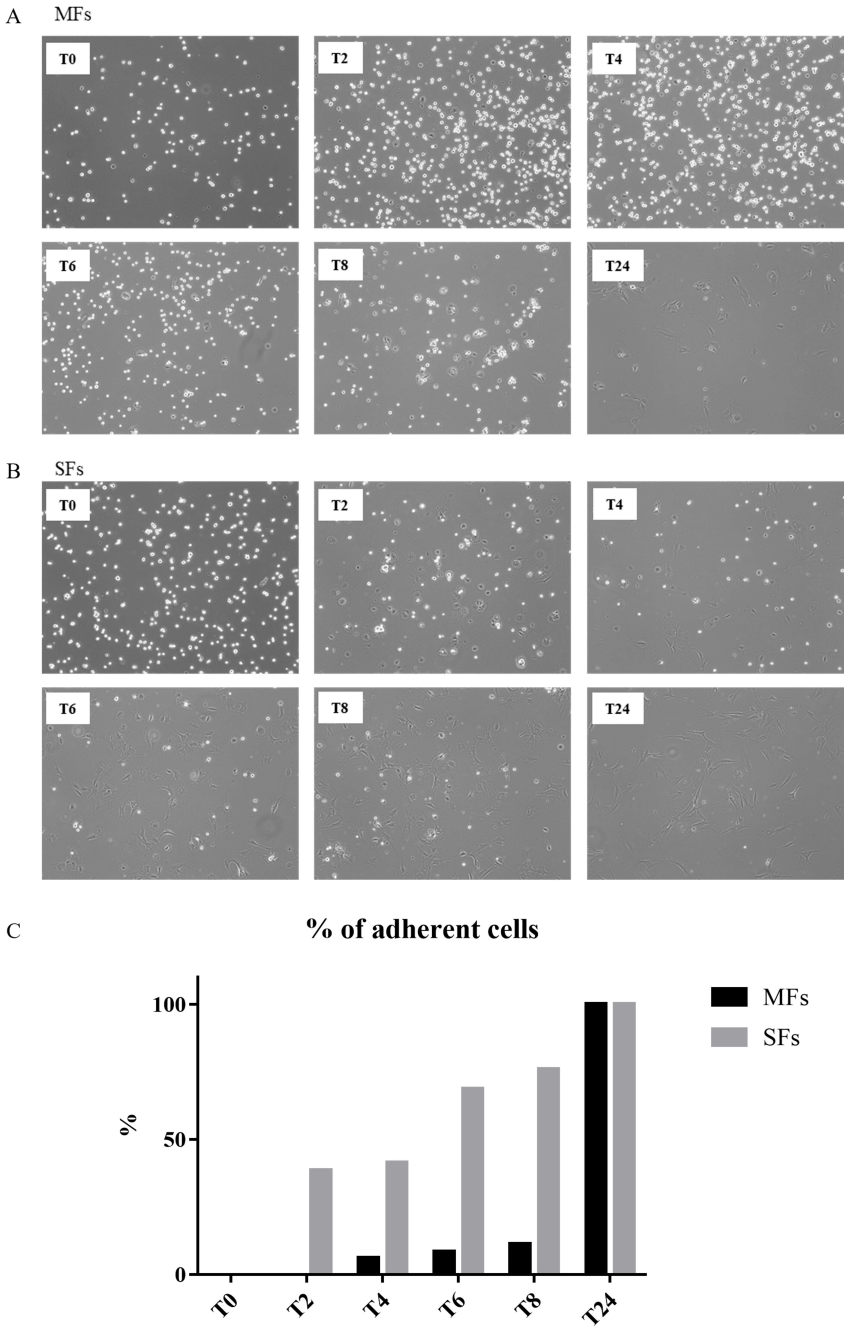

Figure 21: Time attachment of MFs and SFs. (A) MFs phase-contrast images at T0, T2, T4, T6, T8, and T24, in terms of hours. (B) SFs phase-contrast images at T0, T2, T4, T6, T8, and T24, in terms of hours. (C) Percentage of adherent cells. The x-axis represents the time points, while the y-axis represents the percentage of adherent cells. The percentage was calculated of 1 field of both MFs and SFs culture plates

4.2.3 SFs have a higher metabolic activity

The metabolic activity of MFs and SFs was measured using the MTT assay. The growth curves of the cell lines are shown in Figure 22 on days 4, 7, 10, and 14. (Section 3.5.1). From day 4 (T4) to day 14 (T14), it is feasible to observe how SFs proliferate more than MFs, which, despite their early appearance in culture (Figure 20), tend to retain a lower and steady proliferation rate (Figure 22).

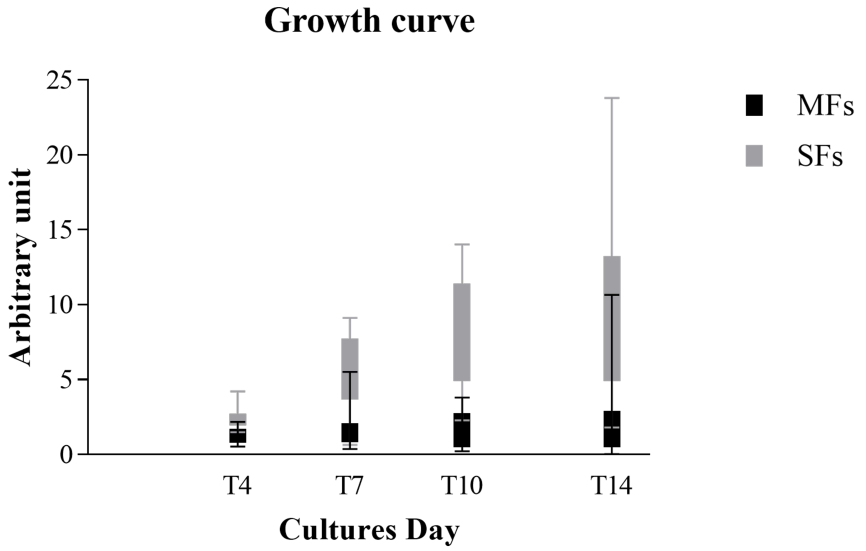

Figure 22: Cell metabolic activity was evaluated using the MTT test. The x-axis represents the number of days the analysis was conducted (Cultures Day), while the y-axis represents the proliferation rate in arbitrary units. The observed results were adjusted on day 0. The mean and standard deviation (SD) are used to express the results. During the 14-day monitoring period, the rate of proliferation of SFs increases. Results are shown as median ± SD

4.2.4 SFs have a preferential growth direction

A different growth pattern related to the orientation of cells in space was observed. This difference was quantified to exclude its possible stochastic nature. The analysis was conducted by analyzing the preferential growth direction of MFs and SFs observed upon reaching 100% confluence. The analysis was performed using both phase-contrast images at 10X magnification (EVOS XL Core Cell Imaging System microscope, Thermo Fisher Scientific, USA) and immunofluorescence images of β-III-tubulin labeling, acquired with the fluorescence microscopy at 40X magnification (Axio Imager 2 microscope with Axiocam Mrm camera, Zeiss, Germany) (Figure 23). The directionality histograms were obtained using the ImageJ Directionality plugin (NIH, USA, https://imagej.nih.gov). The directionality histograms display the preferred direction of growth as degrees of angle on the x-axis and the number of events

on the y-axis. The angles are presented in accordance with the normal mathematical definition, which states that the amplitude of the angle increases in a counterclockwise manner starting at 0° in the East direction.
In the case of a preferential growth direction, the interpolating function of these graphs is a Gaussian curve with a distinct peak when we compared a large number of cells in culture with the same orientation. In particular, when it comes to MFs (Figure 23 C-D), there is no discernible peak at any given orientation, whereas a preferential growth direction is present in cultures of SFs, as evidenced by the formation of distinguishable peaks at about +60° (Figure 23 D) and about -60° (Figure 23 H).
The difference in gene expression of VIM (Figure 23 L) could be explained by the different embryonic origin of the tissues they belong to. Skin derives from mesoderm [132], while meninges derive from elements of head mesenchyme and neural crest [183] [184]. This difference could be explained also using the difference in terms of cell organization and microtubule compositions [255].

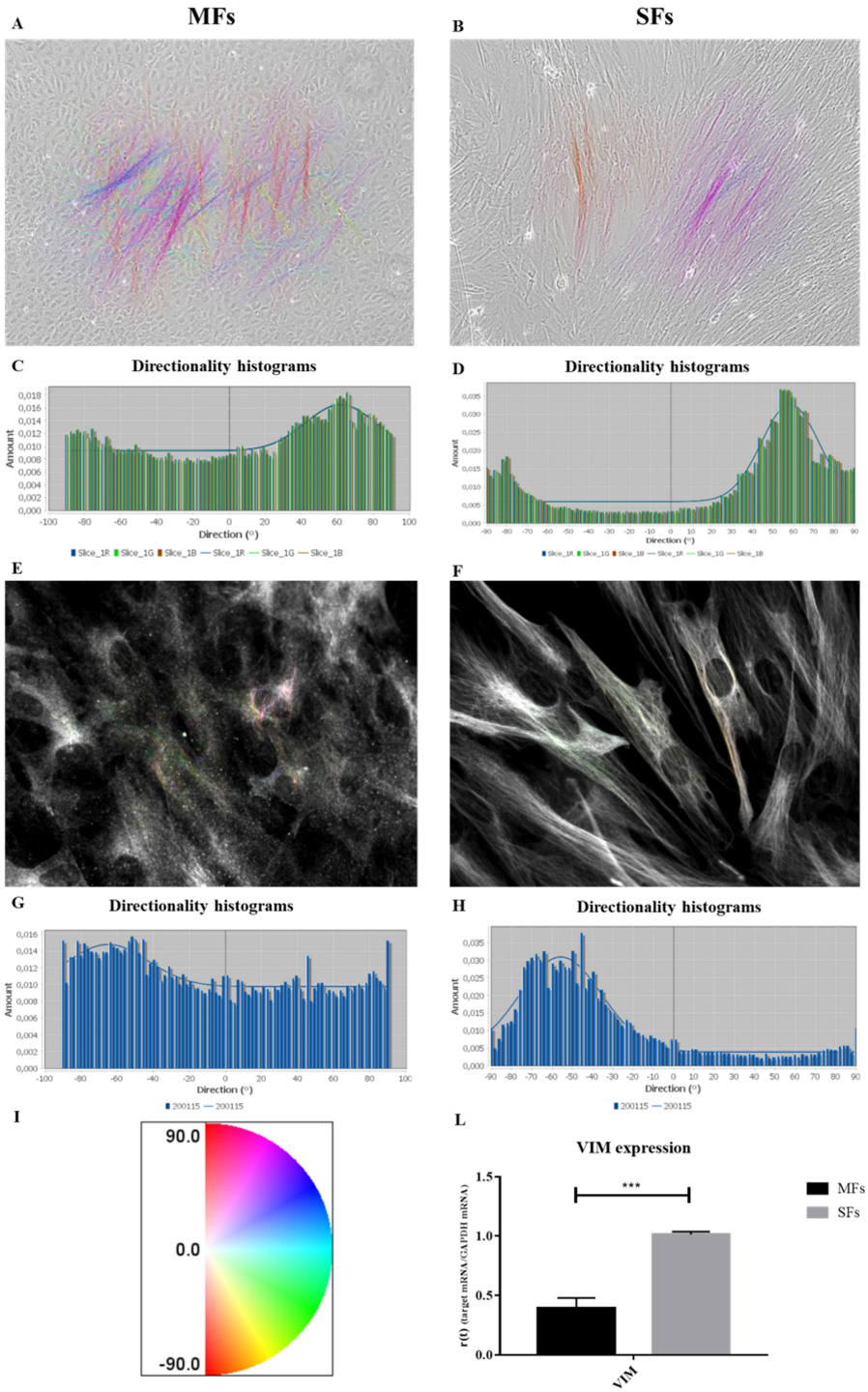

Figure 23: Grow direction analysis. Orientation maps were obtained using phase-contrast images at 10X magnification (A for MFs – B for SFs) and immunofluorescence images of β-III-tubulin labeling using microscopy at 40X magnification (F for MFs – G for SFs) and directionality histograms related to MFs (C, G) and SFs (D, H). Maps and histograms were obtained using the Directionality plugin from ImageJ (NIH, USA, https://imagej.nih.gov). (I) The rainbow indicates the correspondence of gamma color of orientation maps (A, B, E, F). (L) Histograms of the VIM expression using qPCR. Results are shown as mean ± SD. VIM resulted in a statistically significant difference ($p<0.001$) using paired t-test

4.2.5 MFs exhibit increased expression of nestin compared with SFs

The gene expression of the FN1, NES, SERPINH1, and TUBB3 genes, which encode for fibronectin a meninges marker; nestin, a marker for neural stem cell; serpin H1 which is a protein found in the endoplasmic reticulum (ER) and a fibroblast marker; β-III-tubulin a marker of neurons, were evaluated to characterize the cell lines. The expression of all previously mentioned markers was assessed based on earlier research extracting and defining MFs [254].
The characterization was handled by analyzing gene expression through qPCR (Figure 24) and protein expression through immunofluorescence staining (Figure 25 and Figure 26).

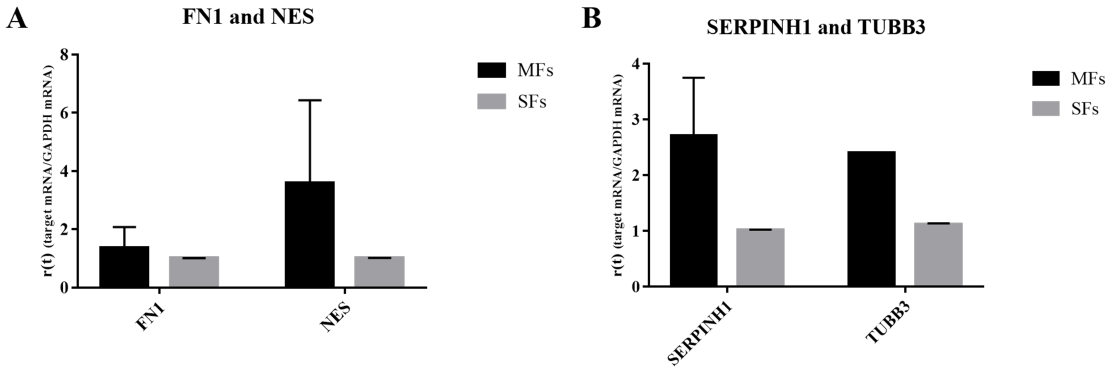

Figure 24: qPCR analysis of fibroblasts markers and neuronal markers. (A) Gene expression of FN1 and NES in MF and SFs. (B) Gene expression of SERPINH1 and TUBB3 in MF and SFs. Results are shown as mean ± SD

The qPCR analysis (Figure 24) showed that gene expression related to NES, TUBB3, SERPINH1 and FN1 is different between the two cell lines. All genes considered are up-regulated in MFs, with the exception of FN1, which is similar between the two cell lines.

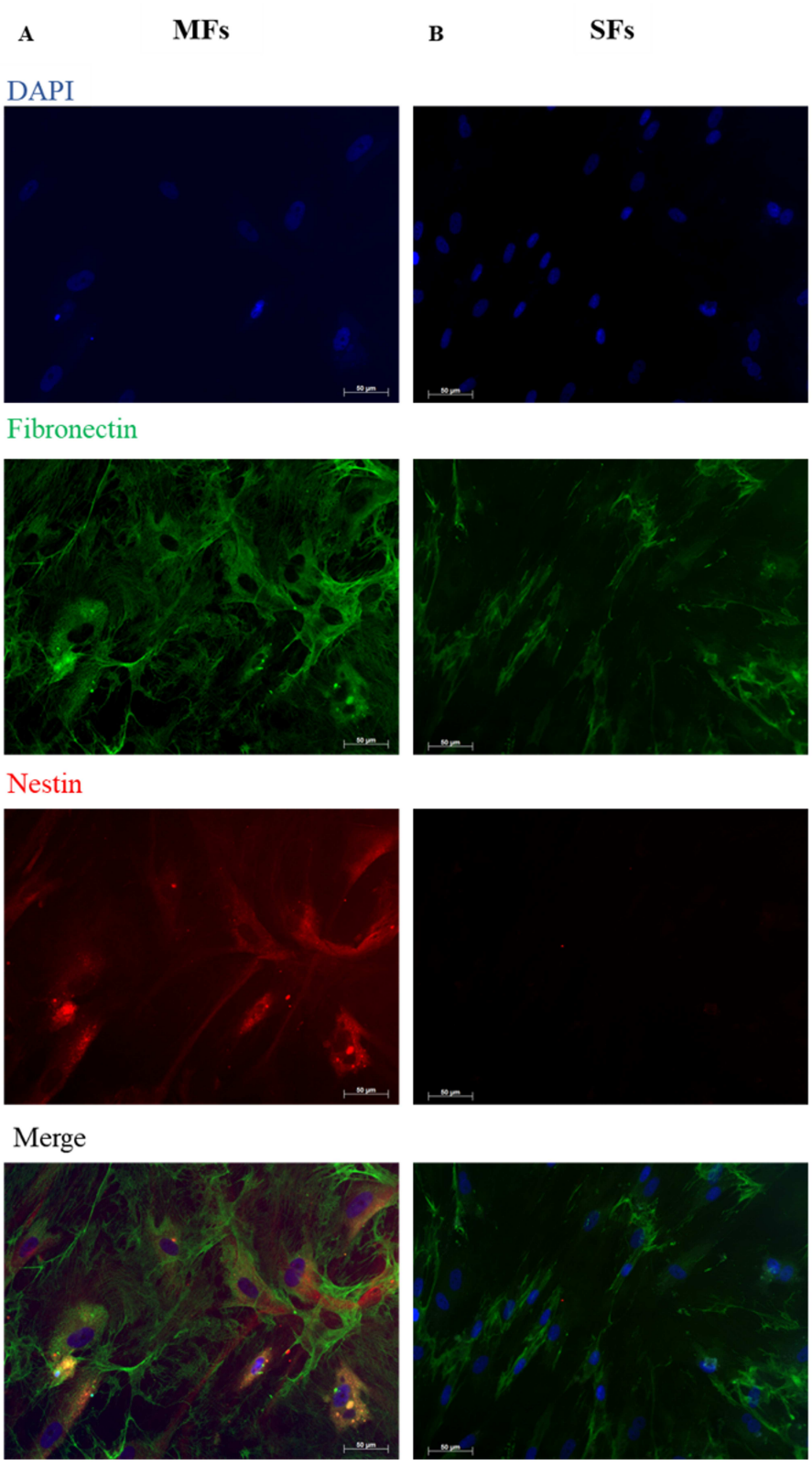

Figure 25: Immunofluorescence images of MFs (A) and SFs (B) obtained using Axio Imager 2 microscope with Axiocam Mrm camera (Zeiss, Germany) at 40X magnification. In green the fibronectin marking and in red the nestin marking. In blue the DAPI used for staining nuclei

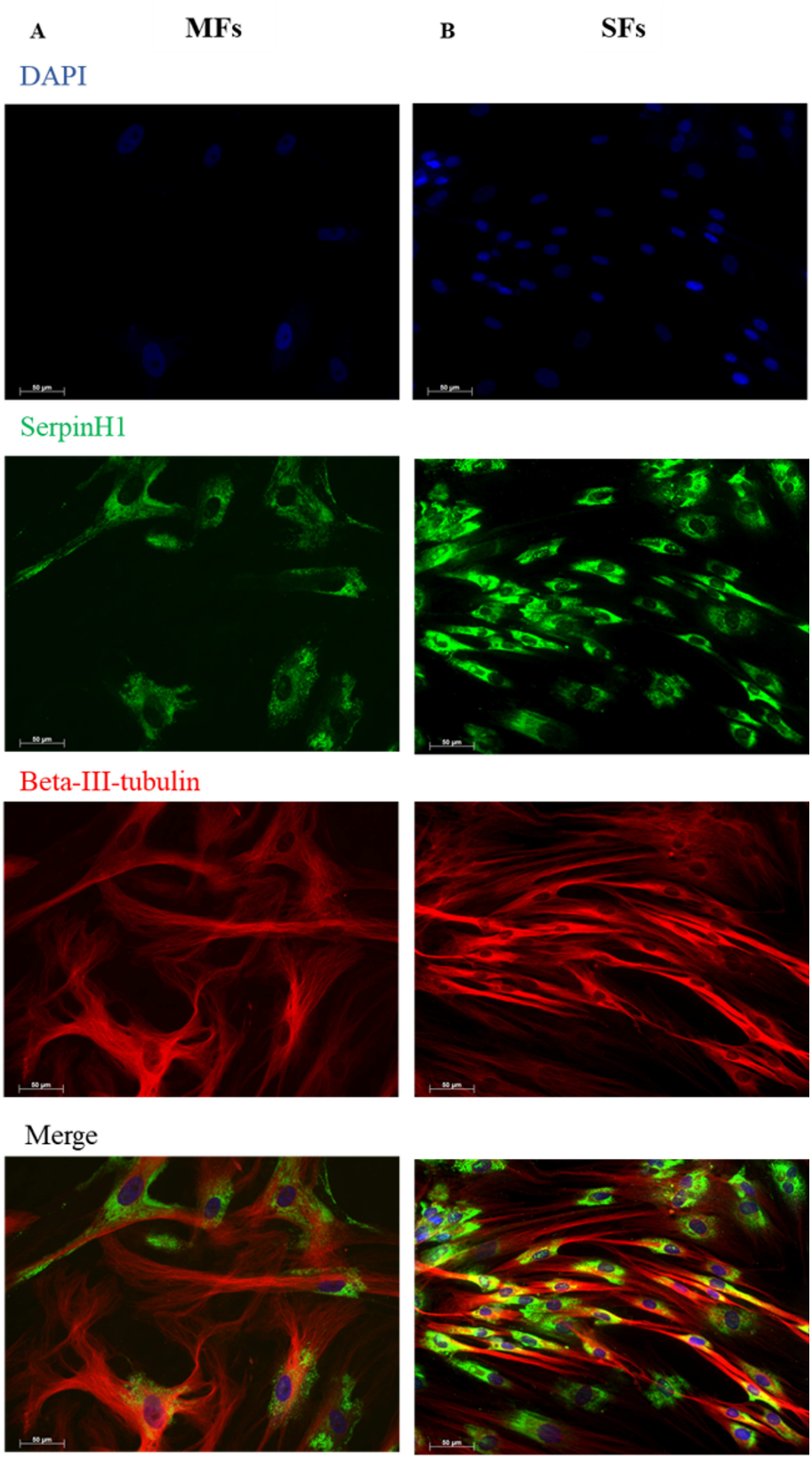

Figure 26: Immunofluorescence images of MFs (A) and SFs (B) obtained using Axio Imager 2 microscope with Axiocam Mrm camera (Zeiss, Germany) at 40X magnification. In green the marking with serpin H1 and in red the marking with β-III-tubulin. In blue the DAPI used for staining nuclei

Figure 25 and figure 26 show the results of the immunofluorescence analysis related to the genes investigated by qPCR. The immunofluorescence data confirms the gene expression data. This finding could indicate the presence of nestin-positive cells that can differentiate into neurons in response to foreign inputs.

4.3 Nestin positive cells in MFs are not sufficient for a direct differentiation in neurons

To test the role of nestin in MFs, it was established to differentiate both MFs and SFs in neurons derived from the NOLD cell line. To perform this protocol, as a positive control it has been used a cell line from yet available in our lab, the neural stem cells (NSCs). A first qualitative analysis was obtained using phase-contrast images during the 21 days, at T0, T7, T14, and T21.
It was analyzed the gene expression of NES, MAP2, and TUBB3 as neuronal markers: NES for the early stage of differentiation, starting from T0; MAP2 for the late stage of differentiation, and TUBB3, which is present in all stages of differentiation, with an increment over the 21 days. The expression of the relative proteins nestin, Map2, and β-III-tubulin was observed by immunofluorescence at T0, T7, T14, and T21 of the differentiation protocol.

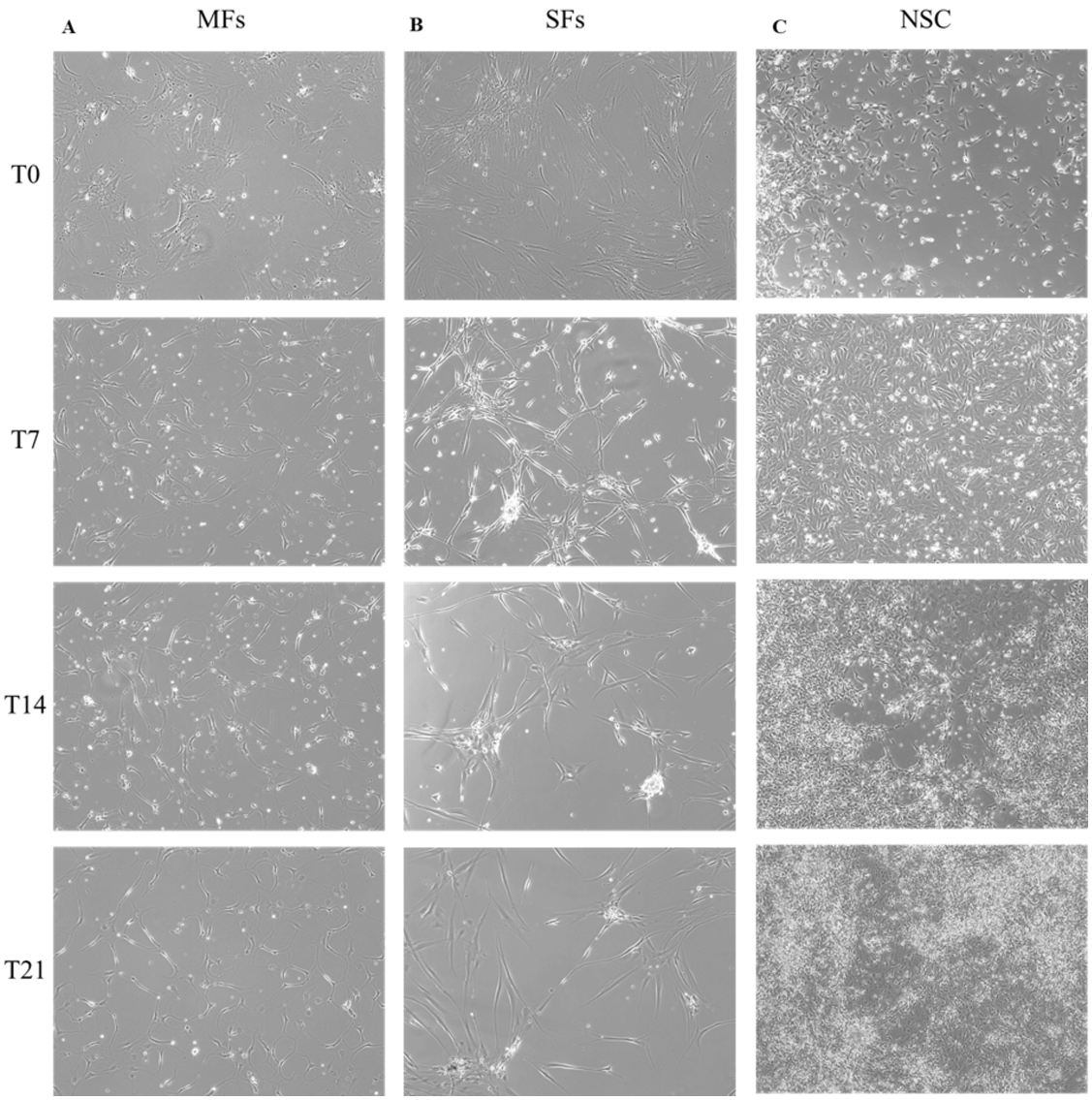

Figure 27: Phase contrast microscopy images of MFs, SFs, and NSCs at different times of the differentiation protocol (T0, T7, T14, T21) obtained using an EVOS XL Core Cell Imaging System microscope (Thermo Fisher Scientific, USA)

Based on phase-contrast images, the MFs have a branching morphology, while the SFs become thinner, elongated, and polarized. NSCs are the smallest of the three types of cells, and they grow throughout the differentiation process. It is tough to tell if there was a significant shift in morphology (Figure 27).

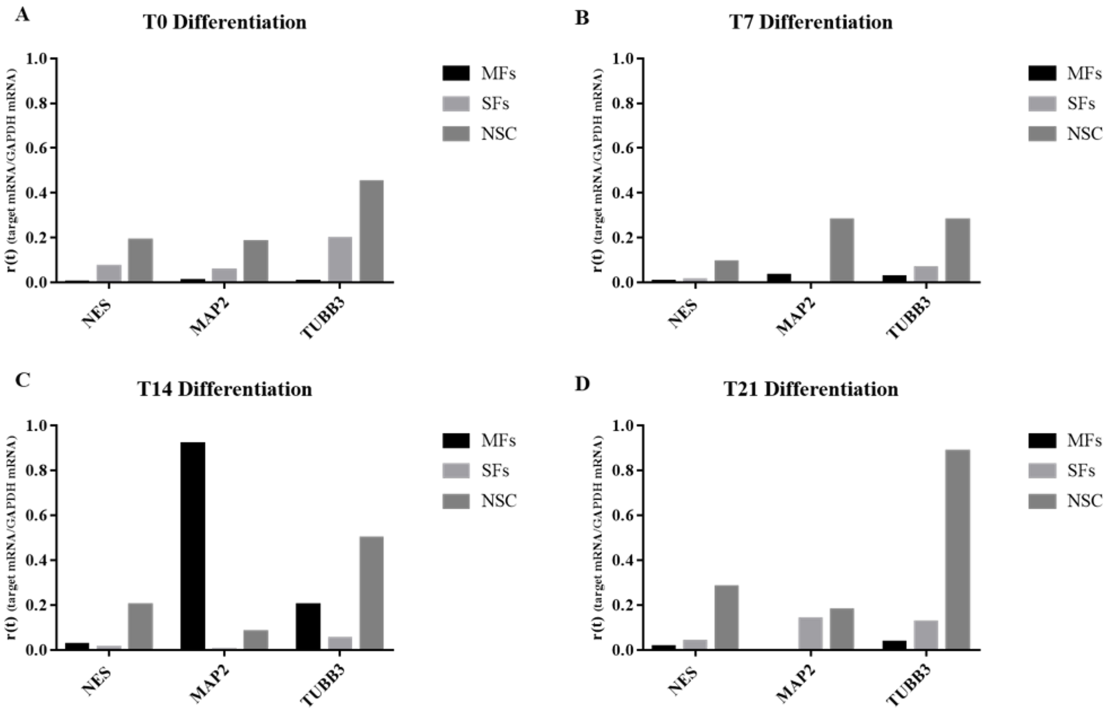

Figure 28: Gene expression analysis by qPCR of NES, MAP2, and TUBB3 in MFs, SFs, and NSCs

The expression varies between cell lines and between the differentiation days. NSCs were able to differentiate into neurons in general, with significant expression of all genes examined throughout the experiment. The neuronal marker MAP2 was not expressed by the MFs and SFs as much as its expression in NSCs. MAP2 expression in MFs and SFs was quite low (Figure 28 D). During the last 14 days of differentiation, NSCs showed an increase in NES levels. Regarding TUBB3, a neuron-specific marker, an increase was observed in MFs at day 14 and in NSCs at day 21 (Figure 28 C-D).

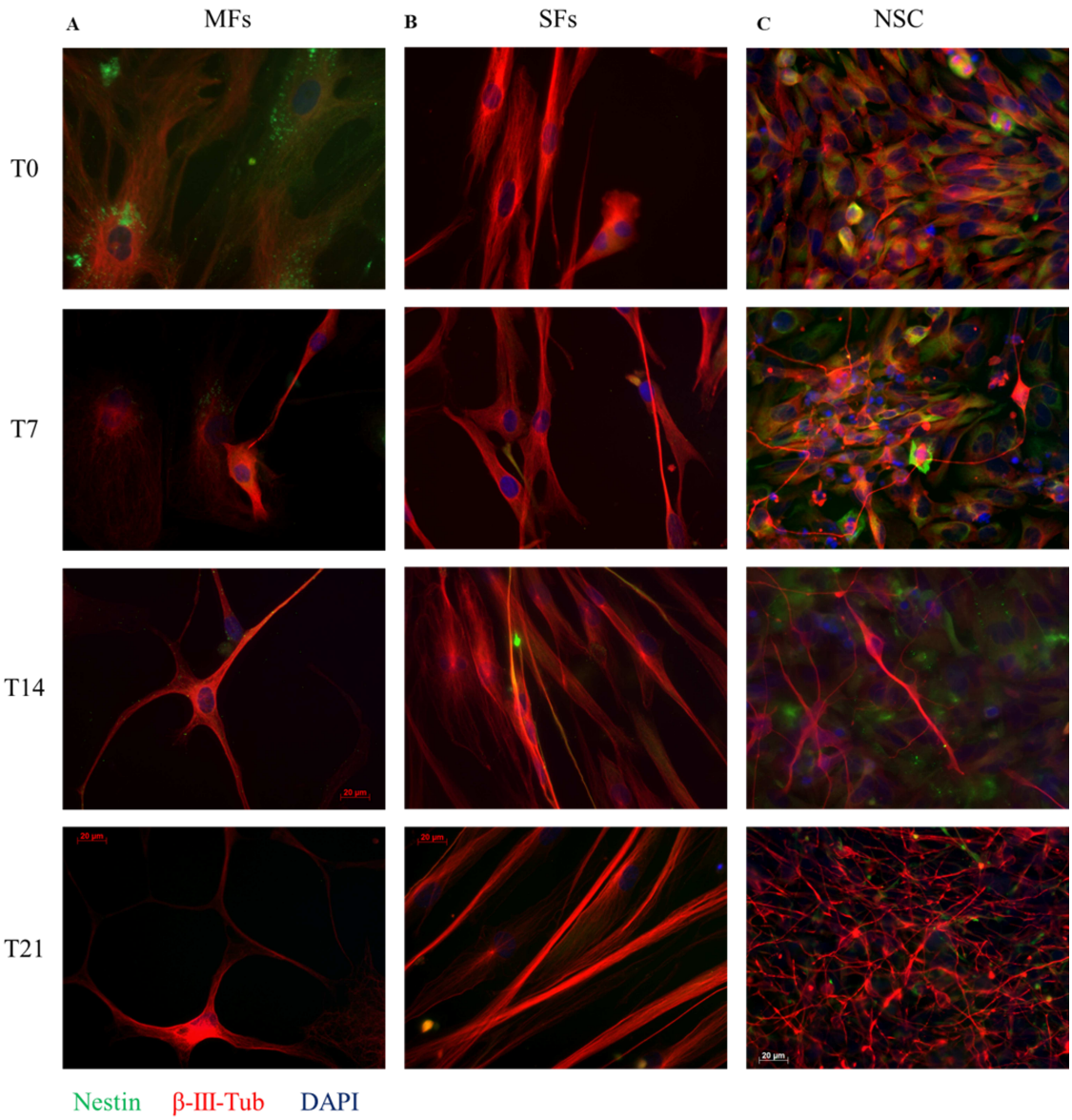

Figure 29: Immunofluorescence images of MFs, SFs, and NSCs at different times of the differentiation protocol (T0, T7, T14, T21) obtained using the Axio Imager 2 microscope with Axiocam Mrm camera (Zeiss, Germany) at 40X magnification. In green the nestin staining and in red the β-III-tubulin one. In blue the DAPI used for staining the cell nuclei

Levels of nestin, a marker of stemness, remained low in MFs and SFs although its expression at day 0 was higher in MFs than in the SFs (Figure 29). For NSCs, an increase in nestin levels was observed during the last 14 days of differentiation (Figure 29). The β-III-tubulin expression seems to be similar during the entire protocol in all cell lines.

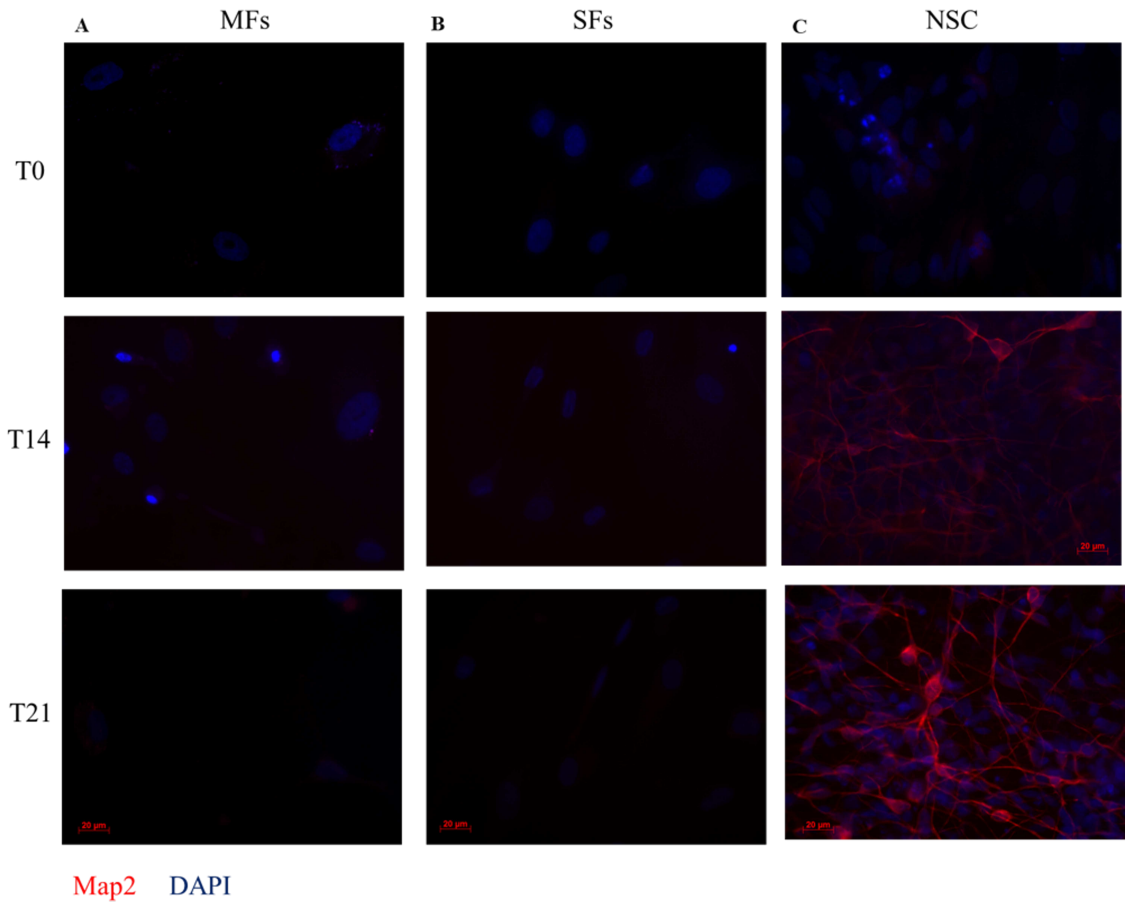

Figure 30: Immunofluorescence images of MFs, SFs and NSCs at different times of the differentiation protocol (T0, T14, T21) obtained using Axio Imager 2 microscope with Axiocam Mrm camera (Zeiss, Germany) at 40X magnification. In red the staining of Map2. In blue is the DAPI used for staining the cell nuclei. Day 0 of the protocol was not considered because Map2 expression is specific for proliferating cells and is not detectable at early stage

The expression of MAP2, used in different works for identifying the terminal neuronal differentiation, is not present at T0 in none of the cell lines considered. The presence of MAP2 was first observed at T14 only in the NSCs, and indicate that the differentiation protocol was successful only for this cell line. MFs and SFs do not MAP2 present in none of the timepoints (Figure 30).

4.4 Different transcriptomic profile of MFs compared with SFs

4.4.1 Principal Component Analysis (PCA) and heatmap show a marked different between the two cell lines

To investigate the differences in gene expression and molecular pathways of 6 couple of MFs and SFs, deriving from 6 brain donors, a transcriptome analysis of the two cell populations (MFs and SFs) was performed using Anti-Fibroblasts MicroBeads (Miltenyi Biotec, Germany) and Magnetic Activated Cell Sorting (MACS) (Miltenyi Biotec, Germany) to assure a pure cell population made of fibroblasts. After transcriptomic analysis, a series of de-regulated genes, subject to ≥ 1 (up-regulated) or ≤ 1 (down-regulated) deregulation in terms of |Log2FC|, were identified within MFs derived from the 6 cell lines. PCA obtained using all differentially expressed genes (DEGs) dataset in MFs compared to SFs shows different expression profiles (Figure 31 A). The volcano plots show the most significant DEGs in MFs compared to SFs, confirming the different degrees of alteration in the two sample types (Figure 31 B). A total of 1145 DEGs were identified in MFs, 591 messenger RNA (mRNA), and 554 noncoding RNAs (Table 11). The two genes that showed larger deregulation in MFs compared to SFs in terms of |Log2FC| were taken into consideration among

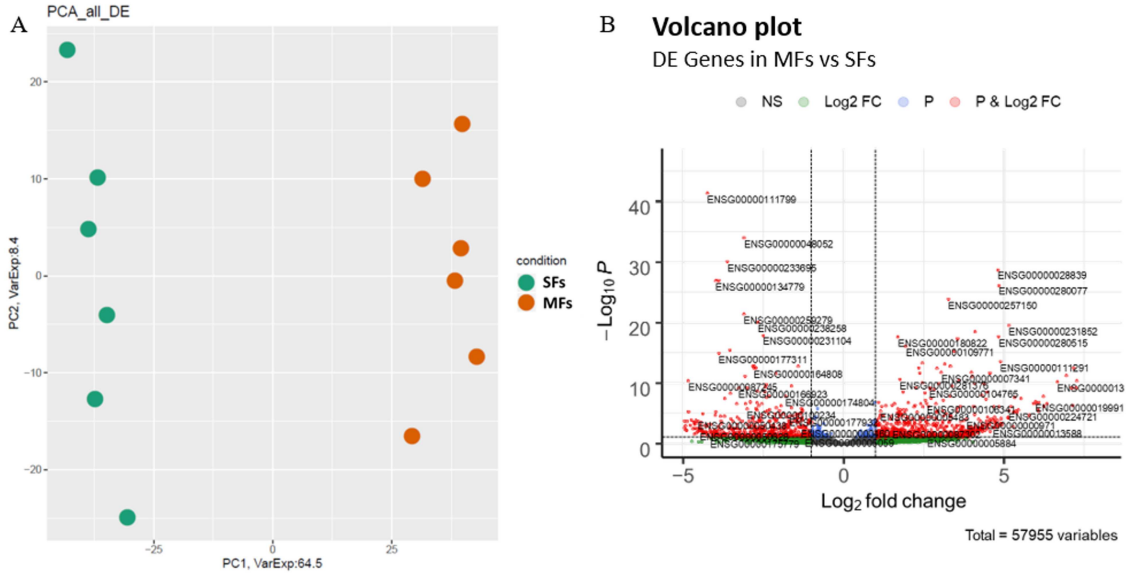

Figure 31: Expression profiles of DEGs within the two cell populations. (A) PCA of DEGs. The dots of different colors indicate the two cell populations (SFs in green and MFs in red). (B) Volcano plot of DEGs between MFs and SFs. Gene ID of the most deregulated transcripts is reported, red dots represent differentially expressed genes based on p-value and Fold Change. Only genes with $|\log2(\text{MFs}/\text{SFs})| \geq 1$ and a False Discovery Rate (FDR) ≤ 0.1 were considered as differentially expressed

Table 11: Number of the statistically significant differentially expressed mRNAs and lncRNAs in MFs compared to SFs, in terms of up-regulated transcripts, down-regulated transcripts, and total deregulated transcripts. Transcripts were considered as differentially expressed when $|\log2(MFs/SFs)| \geq 1$ and an FDR ≤ 0.1

	MFs	
	mRNAs	ncRNAs
Up-Regulated	303	305
Down-Regulated	288	249
Total	591	554
	1145	

the DEGs identified: qPCR was used to examine the expression of NPY4R, the most up-regulated gene, and TNFSF18, the most down-regulated gene. Because the expression of NPY4R is higher in MFs, whereas the expression of TNFSF18 is higher in SFs, the results obtained by qPCR confirmed what was observed by the bioinformatic analysis of the data (Figure 32). NPY4R is a G-protein-coupled receptor (GPCR) that binds the neuropeptide Y (NPY), which has neuroprotective properties [256]. TNFSF18, on the other hand, codes for the cytokine TNFSF18, which is implicated in immune response modulation [257] [258] [259].

4.4.2 Pathway analysis of deregulated transcripts

Deregulated transcripts, with $|\log2(MFs/SFs)| \geq 1$ fold change, subjected to pathways-related analyses using the EnrichR web tool [260]. Deregulated pathways were identified using the KEGG 2019 tools (http://www.genome.ad.jp/KEGG) and Wikipathways (https://www.wikipathways.org/) (Figure 33 and figure 34). In particular the

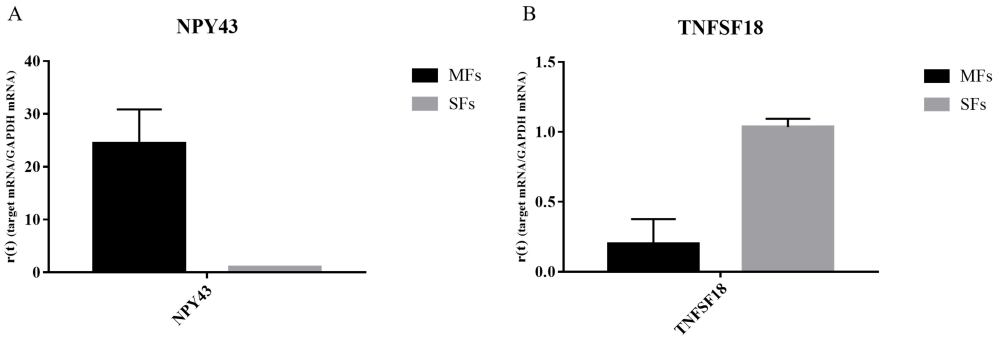

Figure 32: Expression analysis of NPY43 and TNFSF18 in MFs and SFs. Results are shown as mean ± SD

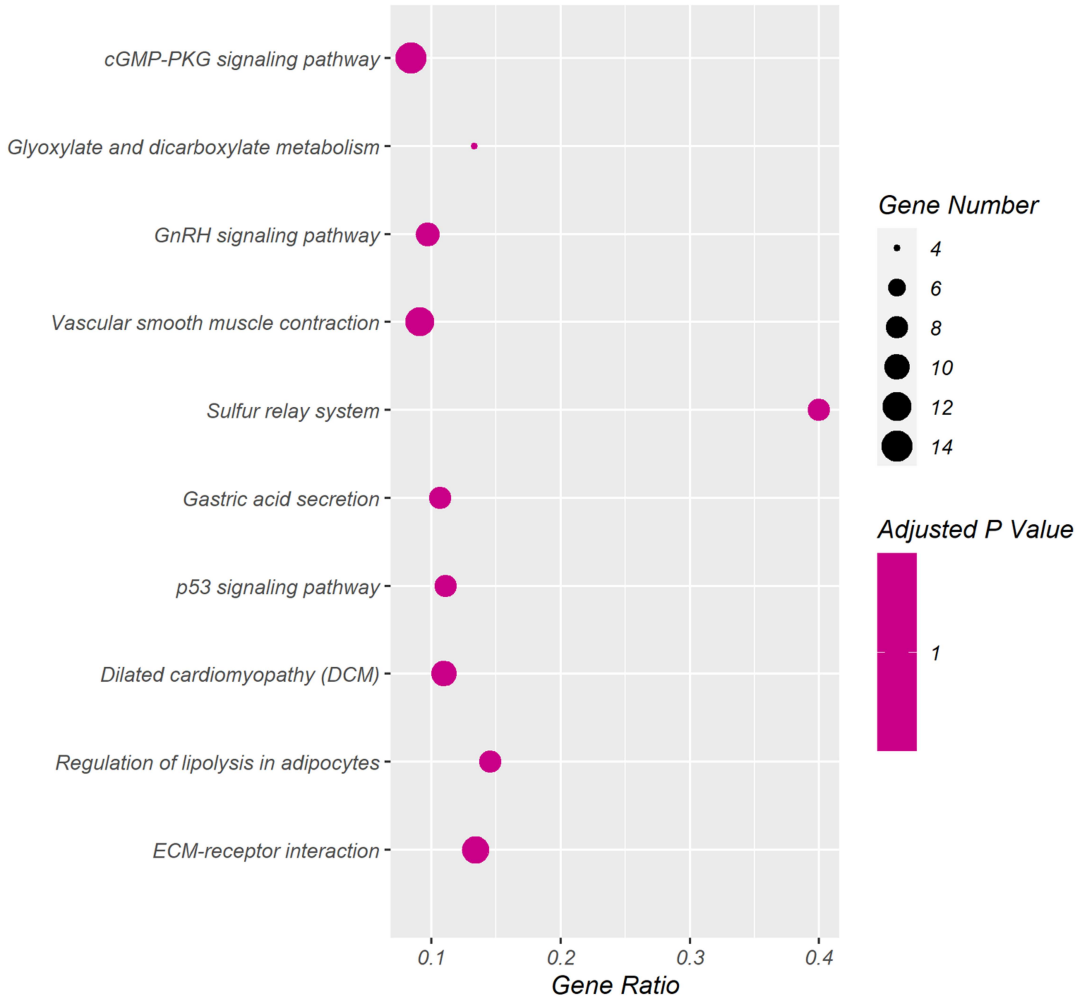

Figure 33: Dot plot of the top 10 deregulated pathways in MFs according to KEGG analysis. The y-axis indicates the names of the pathways; the x-axis represents the Rich factor, which is the value indicating the ratio between the number of differentially expressed genes in a given pathway and the total number of genes within the same pathway. The size of the dots represents the number of different genes and the color indicates the adjusted p-value

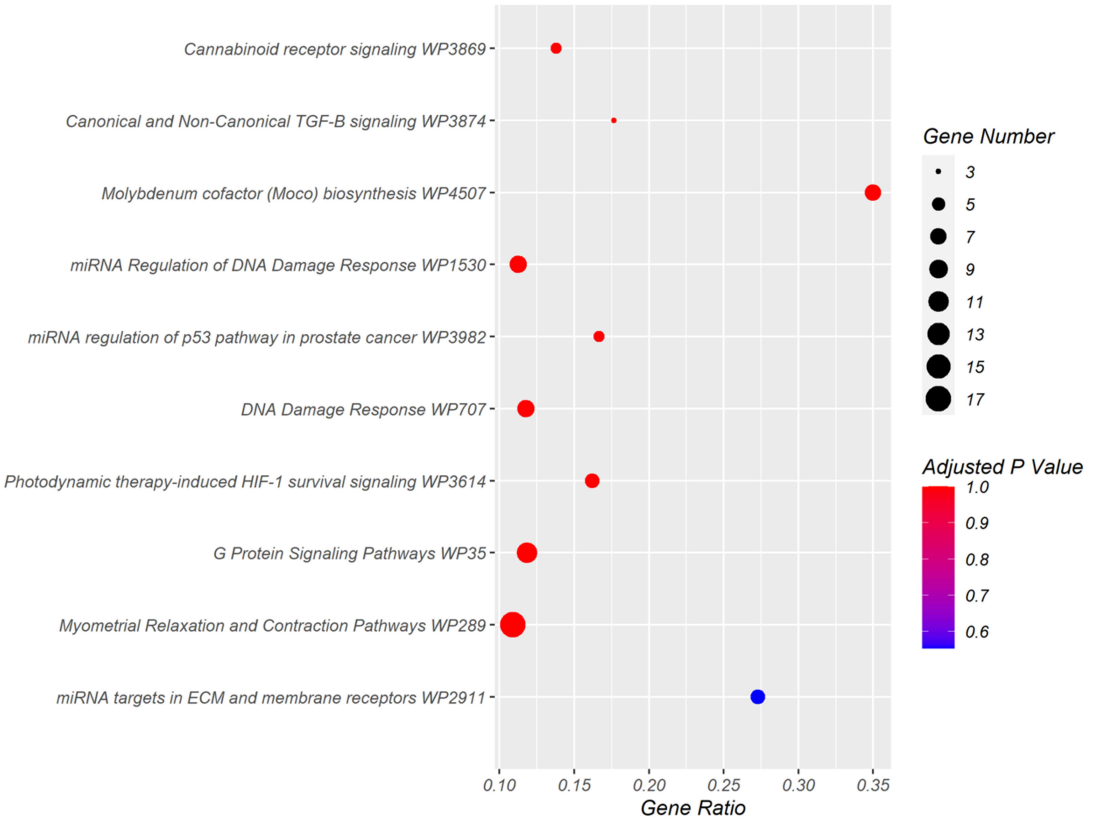

Figure 34: Dot plot of the top 10 deregulated pathways in MFs according to Wikipathways analysis. The y-axis indicates the names of the pathways; the x-axis indicates the rich factor, that is the ratio between the number of differentially expressed genes in a given pathway and the total number of genes within the same pathway. The size of the dots represents the number of different genes and the color indicates the adjusted p-value

ECM-receptor interaction results deregulated with the involvement of 11 coding genes. The genes resulting downregulated in this pathway are two types of integrin α (ITGA4 and ITGA1), three types of collagens α (COL6A1, COL6A2, and COL6A3), gene that encode for Thrombospondin-1, an adhesive glycoprotein that mediates cell-to-cell and cell-to-matrix interactions (THBS1), and gene that encode for tenascin, an extracellular matrix protein implicated in guidance of migrating neurons (TNC). These genes, correlated to the ECM, are also correlated to the previously result about the cell migration, cell growth, and orientation.

4.4.3 Gene Ontology enrichment analysis

Expression profiles of deregulated genes related to MFs were subjected to analysis by Gene Ontology (GO) enrichment analysis. Through these analyses, it was possible to define their roles based on biological processes, cellular components, and molecular function (Figure 35). The first 10 GO terms were considered for each category. About biological processes (Figure 35 A), it can be seen that there is a

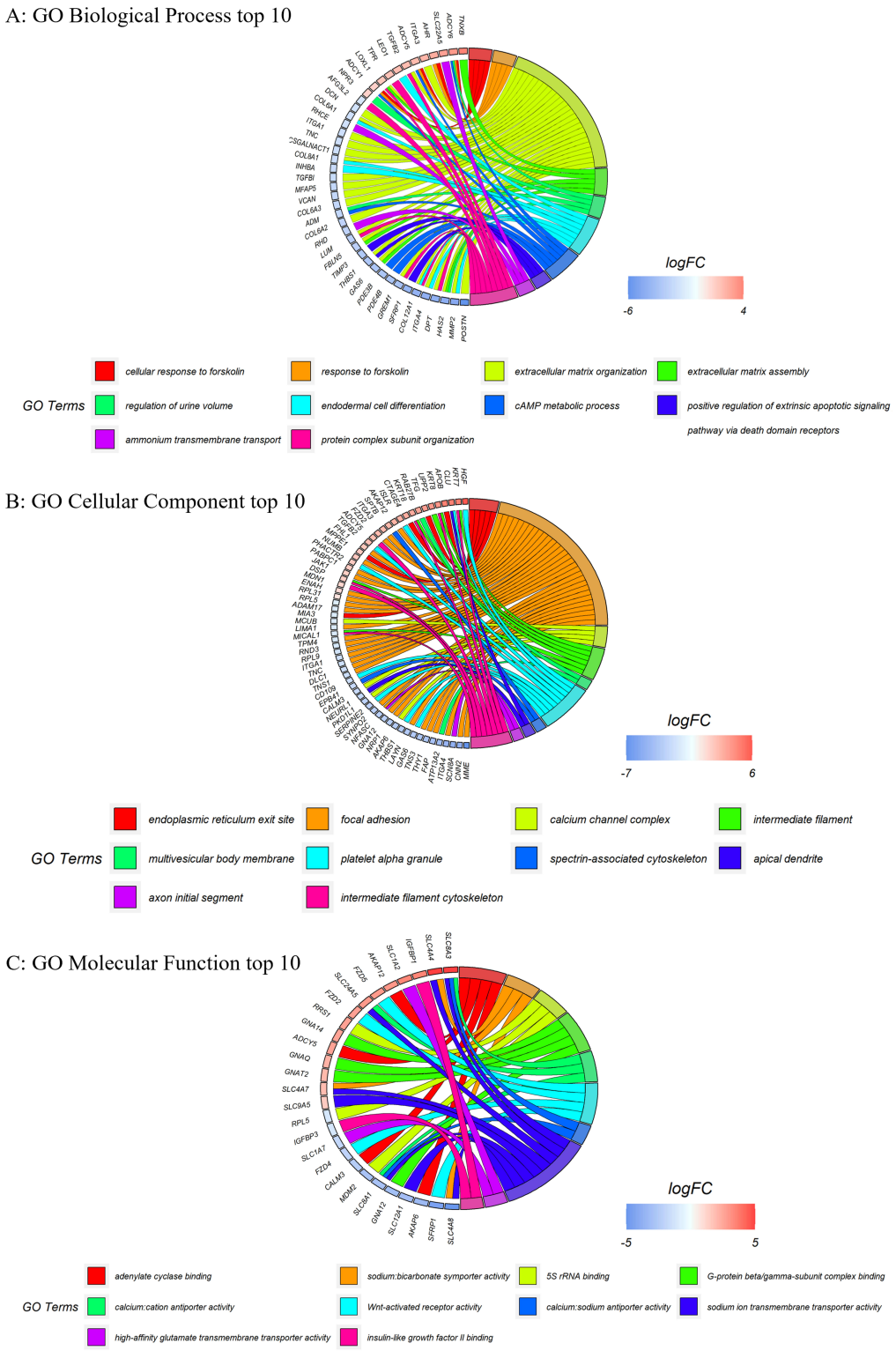

Figure 35: GO analysis of deregulated genes in MFs. The first 10 GO terms for A) biological process, B) cellular component, and C) molecular function are shown. Colors refer to different pathways related to deregulated genes. Down-regulated genes are shown in blue and up-regulated genes in red

majority of down-regulated genes, in particular for the genes involved in the extracellular matrix organization and assembly (Yellow and green in figure 35 A). A minor part of genes deregulated are up-regulated, and they are involved in two correlated processes: cellular response to forskolin and response to forskolin (Red and orange in Figure 35 A), with another process, entire down-regulated, strictly correlated to the above-mentioned process, the cAMP metabolic process (Light blue in Figure 35 A). Regarding the cellular components, the majority of deregulations concern the components involved in focal adhesion, a sub-cellular structure that mechanically link the ECM to cells (Orange in Figure 35 B). About molecular functions, a more deregulated process resulting in adenylate cyclase binding, strictly connected to the cAMP metabolic process and also for the forskolin responses (Red in Figure 35 C).

4.4.4 Analysis of pathways related to forskolin response and cAMP metabolism

Considering the deregulated biological process, the attention goes to the cAMP because of the results of the unique paper previously published by Colombo and colleagues [220]. The authors demonstrated that MFs and SFs react differently to exposure to cAMP and astroglial conditioned medium. The expression of genes involved in the biological processes of cAMP metabolism and response to forskolin were analyzed using qPCR. The pathway inherent to the cellular response to forskolin (Figure 36 A) includes the involvement of three genes (ADCY1, ADCY5, and ADCY6) encoding for three different isoforms of adenylate cyclase whose expression is increased in MFs (Figure 36 C). Within the same pathway, we also find the up-regulation of AHR in MFs, encoding for the aryl hydrocarbon receptor AhR, which heterodimerizes with ARNT (AHR-nuclear translocator). Regarding the pathway related to cAMP metabolism (Figure 36 B), involvement of ADCY1, ADCY5, ADCY6, PDE3B, PDE4B, and ADM was observed. In MFs, ADCY1, ADCY5, and ADCY6 are up-regulated whereas PDE3B, PDE4B, and ADM are down-regulated (Figure 36 C). PDE3B and PDE4B encode for two different phosphodiesterase isoforms involved in cAMP hydrolysis whereas ADM for adrenomedullin, a peptide with neuroprotective function involved in the cAMP synthesis.

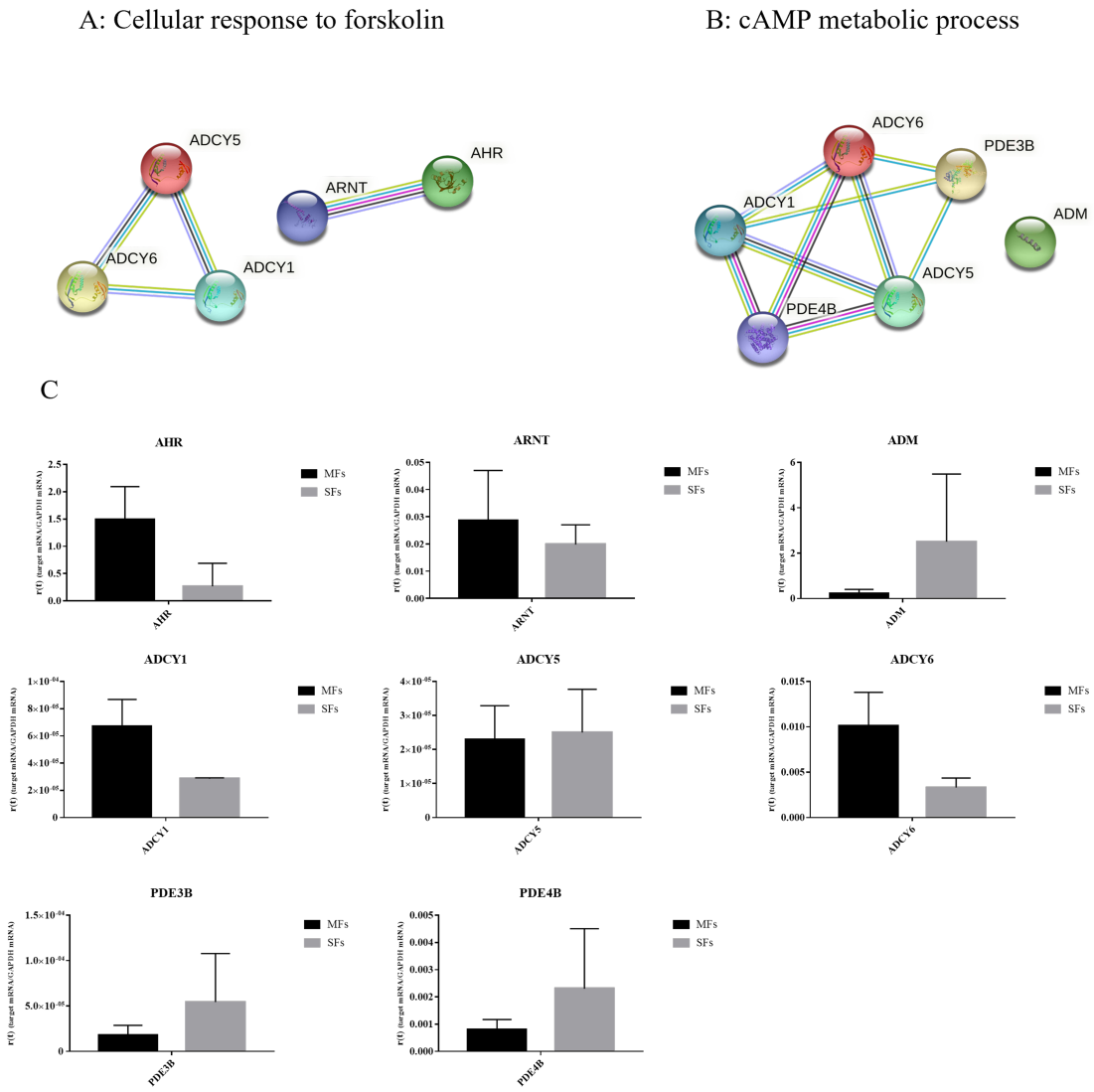

Figure 36: Protein-protein interaction networks obtained by String (https://string-db.org) related to the (A) processes of cellular response to forskolin and (B) cAMP metabolism. In (C) validation by qPCR of gene expression in fibroblasts from MFs versus SFs of the genes involved in both pathways analyzed. Specifically, ADCY1, ADCY5, ADCY6, and AHR for cellular response processes to forskolin and ADCY1, ADCY5, ADCY6, PDE3B, PDE4B, and ADM for cAMP metabolism. Gene expression of ARNT was also evaluated. Results are shown as mean ± SD

5. Discussion

The brain is the most complex and tough organ in the human body. Its complex anatomy, distinct roles, and complex disorders, such as Alzheimer's diseases, Parkinson's diseases, behavioral and psychological symptoms of dementia, and vessel diseases, present us with several unanswered doubts and questions, but they also open the way to several discoveries. In vivo brain examination became possible to evaluate morphological brain abnormalities such as brain atrophy, vascular damage, and fiber loss in the long pathways and white matter. The ability and the possibility to examine a human brain after death is a valuable chance to learn more about the mechanisms underlying brain aging and related diseases, which are still poorly understood. This evidence, combined with the detection of biomarkers such as β-amyloid and normal and phosphorylated tau proteins in the CSF, and the use of liquid biopsy to assess brain conditions, provided a massive amount of data, to make the correct and final diagnosis. The ability to produce a versatile tissue by isolating primary cells, such as fibroblasts from meninges, can be added to the vast amount of existing data obtained through neuropathology and biomarkers analysis, to obtain a useful tool for future studies.

Fibroblasts are the most common and abundant cell type in the body's connective tissues, and their primary function is to secrete ECM components that keep the tissues healthy [131] [261] [128]. SFs serve an important function in regulating skin morphogenesis in the embryo, and they also contribute to skin homeostasis in adults. During tissue repair processes, adult SFs can also develop into a contractile phenotype known as the myofibroblast. As a result, the creation of ECM components increases, making the reaction to tissue damage more effective [144]. The functions of SFs are aided by the dynamic interactions with other cell populations through direct cell-cell communications, interactions with the ECM, and the secretion of soluble factors such as growth factors and cytokines [262] [261] [263] [264] [152]. MFs, on the other hand, are essential for the generation of ECM components that maintain homeostasis not only in the meninges but also in the CNS. Glial limiting membrane proteins are mostly produced by MFs [265] [194], and their production of retinoic acid is important for cortical neurogenesis and cerebrovascular development [213] [215] [266] [267]. Within the meninges, several populations of fibroblasts, as well as neural stem cells, have been discovered. All of this evidence suggests that this tissue is critical for the proper development of the CNS as well as the possibility of adult brain parenchyma cellular regeneration [219] [223] [249]. Based on what has been reported, it is clear that an extensive understanding of the meninges and the cell types that populate them is required to assess the use of new regenerative medicine strategies for the treatment of neurodegenerative diseases and other disorders characterized

by neuronal death.

Our preliminary findings are based on the observations of cells in vitro, to monitor more in-depth the new cells, the MFs. Many are the difference found between the two cell types, MFs and SFs. First, the cell appearance following explantation from meningeal fragments revealed that the appearance of 10-20 MFs occurs on average after 9 days, which is consistent with previous findings [254], while the appearance of SFs from cultured skin occurs on average after 17 days, more days respect to the previously reported data, which states that SFs shed from cultured skin pieces between 7 and 14 days following explantation [268] [269]. The discrepancy in the appearance of SFs cells from previous data is most likely related to the timing of the punching procedure, which normally is performed in live individuals, whereas on the brain donors the skin biopsy is performed after death. Death, and hence circulatory arrest, probably has a greater impact on cell viability and, as a result, tissue exit in SFs than in MFs, which respect the timing of cellular exit.

The qualitative analysis of cells in normal culture conditions allows us to observe the differences in cell adhesion times. We analyzed the number of attached cells during the first 24 hours post-detachment and we found that SFs adhere more rapidly to the plasticware than MFs. This difference could be explained by the expression of different ECM proteins, that after the RNA-seq analysis was found to be deregulated in MFs. In particular, in MFs we reported the upregulation of coding genes ITGA3 and the downregulation of ITGA1 and ITGA4, which codes for different types of integrin α, and the downregulation of three different types of collagens α, COL6A1, COL6A2, and COL6A3, which act as cell-binding proteins. The first step in a cascade of cell–biomaterial interactions is cell attachment, which is critical for cellular activities like cell guidance, proliferation, and differentiation [270]. Cell proliferation can only happen on a substrate for numerous adhering cells. As a result, cell-surface interactions are critical for understanding cell behavior and for controlling and quantifying cell activity [271]. Integrins control multiple steps in signaling pathways that regulate activities as cytoskeletal architecture, cell proliferation, differentiation, apoptosis, and migration in their capacity to act as adhesion receptors. Integrins generate biochemical signals important for cell development, function, and survival in most cell types when they adhere [272]. This different expression of integrins genes probably explains in part the distinct capacity of cell adhesion.

To extend the characterization of the two cell lines under consideration, MFs and SFs, we analyzed the metabolic activity and the cell proliferation. Our observations revealed that the growth rates of MFs and SFs diverge. Starting from a similar metabolic activity in the first 4 days, the observation diverges during the other 10 days in a significant manner, with an increase of the metabolic activity of SFs.

The result is directly connected with our previous observation, as cell adhesion also influences cell growth. Moreover, the old age of donors is crucial to reduce the in vitro development rate of SFs [273], thus it is possible that the advanced age of the individuals in this study had a similar effect on the MFs that we looked at. Therefore, the patients' age may have influenced the proliferation rate of both cell types under investigation, resulting in a higher decline in MFs than SFs. However, to confirm the actual decrease in proliferation rate, the same investigation should be performed using SFs and MFs obtained from young people.

The direction of fibroblasts once they have reached 100% confluence suggests another distinction between MFs and SFs. SFs revealed an intrinsic capacity of the organization on a classical culture plate, without any kind of modification. With the image analysis, it has been possible to quantify the grade of the alignment of the cells, finding a preferential orientation of SFs, the orientation that is missing in MFs. This could be due to the intrinsic nature of SFs, which are critical for transferring the elasticity and tensile strength that are characteristic of the skin, in particular during wound healing processes. These tasks need cell-cell interactions such as FAK-dependent focal adhesions and cell density-induced cytoskeleton remodeling processes involving microtubules, intermediate filaments, and actin filaments. As a result, what we observed appears to support the findings of the literature [255] [274].

According to published researches, we analyzed FN1, TUBB3, NES, and SERPINH1, the genes encoding fibronectin, β -III-tubulin, nestin, and serpin H1 [275] [254]. Both MFs and SFs equally express these markers, except for NES expression, which is higher in MFs, with a neat difference in the immunofluorescence analysis. Nestin is a neural stem cell marker that rises in expression as new neurons and glial elements are synthesized to treat various brain pathological situations such as ischemia and inflammation [276]. NES expression in MFs may show how this cell group contributes to CNS homeostasis in adults, not just during neurodevelopment. Furthermore, we can not exclude that the production of nestin allows MFs to differentiate into neurons in the presence of injury to the brain parenchyma to carry out a repair process, similar to how SFs differentiate into myofibroblasts during wound healing [144].

We then differentiated both MFs and SFs into generic neurons to see if and how differences in NES expression between these two cell types influenced the expression of differentiation markers such β -III-tubulin and Map2 at various stages of differentiation (Day 0, 7, 14, and 21). The same generic neuron development method was applied to NSCs, which served as controls. During differentiation, nestin expression should decrease in favor of the greater expression of neuronal markers (Map2). Nestin decreases appropriately over 21 days, but only NSCs express map2. The

NSCs differentiated successfully in generic neurons, expressing the map2 differentiated neuronal marker, as expected. In NSCs, the expression of Map2, a protein involved in the formation of microtubules [277], enhances gradually, on the other hand in MFs and SFs, Map2 expression is moderate and stable. In MFs, a change in cellular morphology resembling that of a neuronal cell did not correspond to the reduced expression of the investigated neuronal markers, nor the protein levels measured by immunofluorescence. β-III-tubulin, a neuron-specific marker, increases in NSCs throughout 21 days. However, as previously stated by the literature, it was also found in MFs on day 0 [254], and its increased expression in NSCs could indicate differentiation, but not in MFs.

A more detailed description of the differences between MFs and SFs emerged by the gene expression studies and whole transcriptome analysis. We concentrated on the genes and functional pathways that were more deregulated in MFs than in SFs. RNA-sequencing analysis results in a large number of deregulated genes (1145 genes), both coding, and non-coding, confirming all the differences previously reported and, underling more in-depth that MFs and SFs are two very different cell types.

One of the most up-regulated genes in MFs is NPY4R, a gene encoding for a receptor subtype for neuropeptide Y (NPY), peptide YY, and pancreatic polypeptide PP. Because of the interactions between the CNS and the meninges, its increased expression in this cell type could indicate an enhanced concentration of ligands, particularly NPY, in the brain parenchyma. NPY has a neuroprotective function, and high levels of NPY have been detected in neurons and plasma of people suffering from various neurodegenerative disorders [256]. Donor subjects with neurological diseases and neurocognitive disorders such as Alzheimer's disease, Parkinson's disease, and behavioral and psychological symptoms of dementia may have increased in ligands. More investigation about NPY in the plasma and the brain analyzed are required. TNFSF18, a particular ligand of the TNFRSF18 receptor belonging to the Tumor Necrosis Factor (TNF) receptor family, was shown to be down-regulated in MFs. The ligand-receptor contact is capable of inducing an intracellular signaling cascade capable of influencing several aspects of the immune system components such as T-cell response regulation and proliferation [257] [258] [259]. The lower expression of TNFSF18 in MFs compared to SFs led us to believe, based on previous findings on the meningeal immune compartment [278], that MFs could be involved in immune response modulation.

In terms of functional pathways and according to Colombo and colleagues the dysregulation of cAMP-dependent pathways has acquired a lot of attention [220]. AHR, ADCY1, ADCY5, and ADCY6 genes are deregulated in gene expression studies and are involved in biological processes related to the response to forskolin.

Forskolin is a diterpene derived from Plectranthus barbatus that can activate adenylate cyclase and elevate cAMP levels [279]. The aryl hydrocarbon receptor AhR heterodimerizes with ARNT (AHR-nuclear translocator) and translocate within the nucleus to serve as a transcription factor for genes involved in immunological control, cell proliferation, differentiation, and retinoic acid metabolism [280]. ADCY1, ADCY5, and ADCY6 are adenylate cyclase genes that code for distinct isoforms of the enzyme. These genes have been linked to behavioral abnormalities, intellectual deficiencies, and greater susceptibility to stress, implying that they are important for healthy CNS homeostasis [281] [245] [282]. Increased susceptibility to cAMP, as well as increased susceptibility to forskolin, could be indicated by the upregulation of genes associated with cellular response to forskolin in MFs compared to SFs. Because forskolin, along with other MSs, is used to stimulate direct reprogramming processes and transdifferentiation of fibroblasts into neurons, this evidence, combined with the high expression of nestin, could indicate an inclination for reprogramming of this cell type [220] [245] [283].

The cAMP metabolism pathway is the second most deregulated one in MFs. ADCY1, ADCY5, and ADCY6 were found to be up-regulated, while PDE3B, PDE4B, and ADM were found to be downregulated. PDE3B and PDE4B are two isoforms of phosphodiesterase, which are enzymes involved in cAMP hydrolysis [284] [285]. Exogenous treatment of cAMP analogs (8-Br-cAMP) has been found to improve the reprogramming efficiency of fibroblasts into iPSCs, highlighting the relevance of cAMP signaling for MFs [286]. A down-regulation of PDE3B and PDE4B and an up-regulation of ADCY1, ADCY5, and ADCY6 could further highlight how MFs have a great reprogramming potential. The last gene studied was ADM, which encodes for a peptide called adrenomedullin, which is found in the adrenal medulla, in the heart, and the brain. ADM protects neurons, increases cAMP synthesis, and mediates correct neuron proliferation and morphological development via interacting with cytoskeletal components like microtubules [287] [288] [289]. A knock-out of ADM at the neuronal level results in an increase in the volume of the infarcted area and aggravation of brain damage in mouse models of ischemia with infarct induction [290], but a knock-out of the same gene in endothelial cells results in a reduction in the volume of the infarcted area and subsequent brain damage [291]. Given the contradictory nature of the literature, our evidence about ADM down-regulation in MFs needs additional examination.

In conclusion, our results highlighted that MFs and SFs have distinct appearances in culture, shape, proliferation, protein marker expression, and transcriptome profile, indicating that they are two distinct cell types. Furthermore, the discovery of nestin expression and the up-regulation of pathways involved in the cellular response to forskolin and cAMP metabolism in MFs paves the way for more research into MF's

ability to differentiate into mature neurons, which could lead to new personalized treatments for neurodegenerative diseases. Finally, new findings of the presence of stem cell niches within the meninges demonstrate how to study the meninges and the cells that reside there might yield unexpected outcomes, considerably enlarging the horizons of regenerative medicine.

Bibliography

(1) Beard, J. R.; Officer, A.; de Carvalho, I. A.; Sadana, R.; Pot, A. M.; Michel, J. P.; Lloyd-Sherlock, P.; Epping-Jordan, J. E.; Peeters, G.; Mahanani, W. R.; Thiyagarajan, J. A.; Chatterji, S. The World report on ageing and health: a policy framework for healthy ageing. *Lancet* **2016**, *387*, 2145–2154.

(2) Nations, U.; of Economic, D.; Affairs, S.; Division, P. World Population Ageing 2019: Highlights.

(3) Rose, M.; Flatt, T.; Graves Jr, J.; Greer, L. F.; Martínez, D.; Matos, M.; Mueller, L.; Shmookler Reis, R.; Shahrestani, P. What is Aging? *Frontiers in Genetics* **2012**, *3*, 134.

(4) López-Otín, C.; Blasco, M. A.; Partridge, L.; Serrano, M.; Kroemer, G. The hallmarks of aging. *Cell* **2013**, *153*, 1194–1217.

(5) Fragala, M. S. In *Exercise for Aging Adults: A Guide for Practitioners*; Springer International Publishing: Cham, 2015, pp 1–11.

(6) Piedrafita, G.; Keller, M. A.; Ralser, M. The Impact of Non-Enzymatic Reactions and Enzyme Promiscuity on Cellular Metabolism during (Oxidative) Stress Conditions. *Biomolecules* **2015**, *5*, 2101–2122.

(7) Johnson, I. P. Age-related neurodegenerative disease research needs aging models. *Front Aging Neurosci* **2015**, *7*, 168.

(8) Hou, Y.; Dan, X.; Babbar, M.; Wei, Y.; Hasselbalch, S. G.; Croteau, D. L.; Bohr, V. A. Ageing as a risk factor for neurodegenerative disease. *Nat Rev Neurol* **2019**, *15*, 565–581.

(9) Chow, H. M.; Herrup, K. Genomic integrity and the ageing brain. *Nat Rev Neurosci* **2015**, *16*, 672–684.

(10) Moskalev, A. A.; Shaposhnikov, M. V.; Plyusnina, E. N.; Zhavoronkov, A.; Budovsky, A.; Yanai, H.; Fraifeld, V. E. The role of DNA damage and repair in aging through the prism of Koch-like criteria. *Ageing Res Rev* **2013**, *12*, 661–684.

(11) Hoeijmakers, J. H. DNA damage, aging, and cancer. *N Engl J Med* **2009**, *361*, 1475–1485.

(12) Lord, C. J.; Ashworth, A. The DNA damage response and cancer therapy. *Nature* **2012**, *481*, 287–294.

(13) Niedernhofer, L. J.; Gurkar, A. U.; Wang, Y.; Vijg, J.; Hoeijmakers, J. H. J.; Robbins, P. D. Nuclear Genomic Instability and Aging. *Annu Rev Biochem* **2018**, *87*, 295–322.

(14) Jeppesen, D. K.; Bohr, V. A.; Stevnsner, T. DNA repair deficiency in neurodegeneration. *Prog Neurobiol* **2011**, *94*, 166–200.

(15) McKinnon, P. J. Maintaining genome stability in the nervous system. *Nat Neurosci* **2013**, *16*, 1523–1529.

(16) Fang, E. F.; Lautrup, S.; Hou, Y.; Demarest, T. G.; Croteau, D. L.; Mattson, M. P.; Bohr, V. A. NAD(+) in Aging: Molecular Mechanisms and Translational Implications. *Trends Mol Med* **2017**, *23*, 899–916.

(17) Blackburn, E. H.; Greider, C. W.; Szostak, J. W. Telomeres and telomerase: the path from maize, Tetrahymena and yeast to human cancer and aging. *Nat Med* **2006**, *12*, 1133–1138.

(18) Robin, J. D.; Ludlow, A. T.; Batten, K.; Magdinier, F.; Stadler, G.; Wagner, K. R.; Shay, J. W.; Wright, W. E. Telomere position effect: regulation of gene expression with progressive telomere shortening over long distances. *Genes Dev* **2014**, *28*, 2464–2476.

(19) Stroik, S.; Kurtz, K.; Hendrickson, E. A. CtIP is essential for telomere replication. *Nucleic Acids Res* **2019**, *47*, 8927–8940.

(20) Hayflick, L.; Moorhead, P. S. The serial cultivation of human diploid cell strains. *Experimental Cell Research* **1961**, *25*, 585–621.

(21) Fraga, M. F.; Esteller, M. Epigenetics and aging: the targets and the marks. *Trends Genet* **2007**, *23*, 413–418.

(22) Talens, R. P.; Christensen, K.; Putter, H.; Willemsen, G.; Christiansen, L.; Kremer, D.; Suchiman, H. E.; Slagboom, P. E.; Boomsma, D. I.; Heijmans, B. T. Epigenetic variation during the adult lifespan: cross-sectional and longitudinal data on monozygotic twin pairs. *Aging Cell* **2012**, *11*, 694–703.

(23) Han, S.; Brunet, A. Histone methylation makes its mark on longevity. *Trends Cell Biol* **2012**, *22*, 42–49.

(24) Ito, T.; Teo, Y. V.; Evans, S. A.; Neretti, N.; Sedivy, J. M. Regulation of Cellular Senescence by Polycomb Chromatin Modifiers through Distinct DNA Damage- and Histone Methylation-Dependent Pathways. *Cell Rep* **2018**, *22*, 3480–3492.

(25) Mizushima, N.; Levine, B.; Cuervo, A. M.; Klionsky, D. J. Autophagy fights disease through cellular self-digestion. *Nature* **2008**, *451*, 1069–1075.

(26) Hartl, F. U.; Bracher, A.; Hayer-Hartl, M. Molecular chaperones in protein folding and proteostasis. *Nature* **2011**, *475*, 324–332.

(27) Koga, H.; Martinez-Vicente, M.; Arias, E.; Kaushik, S.; Sulzer, D.; Cuervo, A. M. Constitutive upregulation of chaperone-mediated autophagy in Huntington's disease. *J Neurosci* **2011**, *31*, 18492–18505.

(28) Tanaka, K.; Matsuda, N. Proteostasis and neurodegeneration: the roles of proteasomal degradation and autophagy. *Biochim Biophys Acta* **2014**, *1843*, 197–204.

(29) Powers, E. T.; Morimoto, R. I.; Dillin, A.; Kelly, J. W.; Balch, W. E. Biological and chemical approaches to diseases of proteostasis deficiency. *Annu Rev Biochem* **2009**, *78*, 959–991.

(30) Kenyon, C. J. The genetics of ageing. *Nature* **2010**, *464*, 504–512.

(31) Fontana, L.; Partridge, L.; Longo, V. D. Extending healthy life span–from yeast to humans. *Science* **2010**, *328*, 321–326.

(32) Barzilai, N.; Huffman, D. M.; Muzumdar, R. H.; Bartke, A. The critical role of metabolic pathways in aging. *Diabetes* **2012**, *61*, 1315–1322.

(33) Green, D. R.; Galluzzi, L.; Kroemer, G. Mitochondria and the autophagy-inflammation-cell death axis in organismal aging. *Science* **2011**, *333*, 1109–1112.

(34) Vermulst, M.; Wanagat, J.; Kujoth, G. C.; Bielas, J. H.; Rabinovitch, P. S.; Prolla, T. A.; Loeb, L. A. DNA deletions and clonal mutations drive premature aging in mitochondrial mutator mice. *Nat Genet* **2008**, *40*, 392–394.

(35) Sun, N.; Youle, R. J.; Finkel, T. The Mitochondrial Basis of Aging. *Mol Cell* **2016**, *61*, 654–666.

(36) Bar-Ziv, R.; Bolas, T.; Dillin, A. Systemic effects of mitochondrial stress. *EMBO Rep* **2020**, *21*, e50094.

(37) Johri, A.; Beal, M. F. Mitochondrial dysfunction in neurodegenerative diseases. *J Pharmacol Exp Ther* **2012**, *342*, 619–630.

(38) Keogh, M. J.; Chinnery, P. F. Mitochondrial DNA mutations in neurodegeneration. *Biochim Biophys Acta* **2015**, *1847*, 1401–1411.

(39) Bodnar, A. G.; Ouellette, M.; Frolkis, M.; Holt, S. E.; Chiu, C. P.; Morin, G. B.; Harley, C. B.; Shay, J. W.; Lichtsteiner, S.; Wright, W. E. Extension of life-span by introduction of telomerase into normal human cells. *Science* **1998**, *279*, 349–352.

(40) Coppé, J. P.; Desprez, P. Y.; Krtolica, A.; Campisi, J. The senescence-associated secretory phenotype: the dark side of tumor suppression. *Annu Rev Pathol* **2010**, *5*, 99–118.

(41) Basisty, N.; Kale, A.; Patel, S.; Campisi, J.; Schilling, B. The power of proteomics to monitor senescence-associated secretory phenotypes and beyond: toward clinical applications. *Expert Rev Proteomics* **2020**, *17*, 297–308.

(42) Cao Dinh, H.; Njemini, R.; Onyema, O. O.; Beyer, I.; Liberman, K.; De Dobbeleer, L.; Renmans, W.; Vander Meeren, S.; Jochmans, K.; Delaere, A.; Knoop, V.; Bautmans, I. Strength Endurance Training but Not Intensive Strength Training Reduces Senescence-Prone T Cells in Peripheral Blood in Community-Dwelling Elderly Women. *J Gerontol A Biol Sci Med Sci* **2019**, *74*, 1870–1878.

(43) Li, L.; Ngo, H. T. T.; Hwang, E.; Wei, X.; Liu, Y.; Liu, J.; Yi, T. H. Conditioned Medium from Human Adipose-Derived Mesenchymal Stem Cell Culture Prevents UVB-Induced Skin Aging in Human Keratinocytes and Dermal Fibroblasts. *Int J Mol Sci* **2019**, *21*, DOI: 10.3390/ijms21010049.

(44) Ma, T.; Fu, B.; Yang, X.; Xiao, Y.; Pan, M. Adipose mesenchymal stem cell-derived exosomes promote cell proliferation, migration, and inhibit cell apoptosis via Wnt/β-catenin signaling in cutaneous wound healing. *J Cell Biochem* **2019**, *120*, 10847–10854.

(45) Sotiropoulou, P. A.; Blanpain, C. Development and homeostasis of the skin epidermis. *Cold Spring Harb Perspect Biol* **2012**, *4*, a008383.

(46) Castilho, R. M.; Squarize, C. H.; Chodosh, L. A.; Williams, B. O.; Gutkind, J. S. mTOR mediates Wnt-induced epidermal stem cell exhaustion and aging. *Cell Stem Cell* **2009**, *5*, 279–289.

(47) Russell, S. J.; Kahn, C. R. Endocrine regulation of ageing. *Nat Rev Mol Cell Biol* **2007**, *8*, 681–691.

(48) Laplante, M.; Sabatini, D. M. mTOR signaling in growth control and disease. *Cell* **2012**, *149*, 274–293.

(49) Rando, T. A.; Chang, H. Y. Aging, rejuvenation, and epigenetic reprogramming: resetting the aging clock. *Cell* **2012**, *148*, 46–57.

(50) Zhang, G.; Li, J.; Purkayastha, S.; Tang, Y.; Zhang, H.; Yin, Y.; Li, B.; Liu, G.; Cai, D. Hypothalamic programming of systemic ageing involving IKK-β, NF-κB and GnRH. *Nature* **2013**, *497*, 211–216.

(51) Alexander, G. E.; Ryan, L.; Bowers, D.; Foster, T. C.; Bizon, J. L.; Geldmacher, D. S.; Glisky, E. L. Characterizing cognitive aging in humans with links to animal models. *Front Aging Neurosci* **2012**, *4*, 21.

(52) Dykiert, D.; Der, G.; Starr, J. M.; Deary, I. J. Age differences in intra-individual variability in simple and choice reaction time: systematic review and meta-analysis. *PLoS One* **2012**, *7*, e45759.

(53) Levin, O.; Fujiyama, H.; Boisgontier, M. P.; Swinnen, S. P.; Summers, J. J. Aging and motor inhibition: a converging perspective provided by brain stimulation and imaging approaches. *Neurosci Biobehav Rev* **2014**, *43*, 100–117.

(54) Mattson, M. P. Pathways towards and away from Alzheimer's disease. *Nature* **2004**, *430*, 631–639.

(55) Kalia, L. V.; Lang, A. E. Parkinson's disease. *Lancet* **2015**, *386*, 896–912.

(56) Scheltens, P.; Blennow, K.; Breteler, M. M.; de Strooper, B.; Frisoni, G. B.; Salloway, S.; der Flier, W. M. Alzheimer's disease. *Lancet* **2016**, *388*, 505–517.

(57) Aarsland, D.; Creese, B.; Politis, M.; Chaudhuri, K. R.; Ffytche, D. H.; Weintraub, D.; Ballard, C. Cognitive decline in Parkinson disease. *Nat Rev Neurol* **2017**, *13*, 217–231.

(58) Rocca, W. A.; Petersen, R. C.; Knopman, D. S.; Hebert, L. E.; Evans, D. A.; Hall, K. S.; Gao, S.; Unverzagt, F. W.; Langa, K. M.; Larson, E. B.; White, L. R. Trends in the incidence and prevalence of Alzheimer's disease, dementia, and cognitive impairment in the United States. *Alzheimers Dement* **2011**, *7*, 80–93.

(59) Schrijvers, E. M.; Verhaaren, B. F.; Koudstaal, P. J.; Hofman, A.; Ikram, M. A.; Breteler, M. M. Is dementia incidence declining?: Trends in dementia incidence since 1990 in the Rotterdam Study. *Neurology* **2012**, *78*, 1456–1463.

(60) Norton, S.; Matthews, F. E.; Barnes, D. E.; Yaffe, K.; Brayne, C. Potential for primary prevention of Alzheimer's disease: an analysis of population-based data. *Lancet Neurol* **2014**, *13*, 788–794.

(61) Lopez-Leon, M.; C. Reggiani, P.; Claudia, B. H.; Rodolfo, G. G. Regenerative Medicine for the Aging Brain. *Enliven: Journal of Stem Cell Research and Regenerative Medicine* **2014**, *01*, 1–9.

(62) Gaillard, A.; Jaber, M. Rewiring the brain with cell transplantation in Parkinson's disease. *Trends Neurosci* **2011**, *34*, 124–133.

(63) Grothe, M.; Heinsen, H.; Teipel, S. J. Atrophy of the cholinergic basal forebrain over the adult age range and in early stages of Alzheimer's disease. *Biological Psychiatry* **2012**, *71*, 805–813.

(64) Mattson, M. P.; Arumugam, T. V. Hallmarks of Brain Aging: Adaptive and Pathological Modification by Metabolic States. *Cell metabolism* **2018**, *27*, 1176–1199.

(65) Oschwald, J.; Guye, S.; Liem, F.; Rast, P.; Willis, S.; Röcke, C.; Jäncke, L.; Martin, M.; Mérillat, S. Brain structure and cognitive ability in healthy aging: A review on longitudinal correlated change. *Reviews in the Neurosciences* **2019**, *31*, 1–57.

(66) Elobeid, A.; Libard, S.; Leino, M.; Popova, S. N.; Alafuzoff, I. Altered Proteins in the Aging Brain. *J Neuropathol Exp Neurol* **2016**, *75*, 316–325.

(67) Galloway, P. G.; Perry, G.; Gambetti, P. Hirano body filaments contain actin and actin-associated proteins. *J Neuropathol Exp Neurol* **1987**, *46*, 185–199.

(68) Maciver, S. K.; Harrington, C. R. Two actin binding proteins, actin depolymerizing factor and cofilin, are associated with Hirano bodies. *Neuroreport* **1995**, *6*, 1985–1988.

(69) Abbott, R. D.; Nelson, J. S.; Ross, G. W.; Uyehara-Lock, J. H.; Tanner, C. M.; Masaki, K. H.; Launer, L. J.; White, L. R.; Petrovitch, H. Marinesco bodies and substantia nigra neuron density in Parkinson's disease. *Neuropathol Appl Neurobiol* **2017**, *43*, 621–630.

(70) Moreno-García, A.; Kun, A.; Calero, O.; Medina, M.; Calero, M. An Overview of the Role of Lipofuscin in Age-Related Neurodegeneration. *Front Neurosci* **2018**, *12*, 464.

(71) Cao, X.; Jin, X.; Liu, B. The involvement of stress granules in aging and aging-associated diseases. *Aging Cell* **2020**, *19*, e13136.

(72) Wyss-Coray, T. Ageing, neurodegeneration and brain rejuvenation. *Nature* **2016**, *539*, 180–186.

(73) Blennow, K.; Brody, D. L.; Kochanek, P. M.; Levin, H.; McKee, A.; Ribbers, G. M.; Yaffe, K.; Zetterberg, H. Traumatic brain injuries. *Nature Reviews Disease Primers* **2016**, *2*, 1–19.

(74) Krishnamurthi, R. V. et al. Global and regional burden of first-ever ischaemic and haemorrhagic stroke during 1990-2010: findings from the Global Burden of Disease Study 2010. *Lancet Glob Health* **2013**, *1*, e259–81.

(75) Yew, K. S.; Cheng, E. M. Diagnosis of acute stroke. *Am Fam Physician* **2015**, *91*, 528–536.

(76) Moskowitz, M. A.; Lo, E. H.; Iadecola, C. The science of stroke: mechanisms in search of treatments. *Neuron* **2010**, *67*, 181–198.

(77) Weinstein, P. R.; Hong, S.; Sharp, F. R. Molecular identification of the ischemic penumbra. *Stroke* **2004**, *35*, 2666–2670.

(78) Bekris, L. M.; Yu, C. E.; Bird, T. D.; Tsuang, D. W. Genetics of Alzheimer disease. *J Geriatr Psychiatry Neurol* **2010**, *23*, 213–227.

(79) Liu, C. C.; Kanekiyo, T.; Xu, H.; Bu, G. In *Nat Rev Neurol*, 2013, pp 106–118.

(80) Crews, L.; Masliah, E. Molecular mechanisms of neurodegeneration in Alzheimer's disease. *Hum Mol Genet* **2010**, *19*, R12–20.

(81) Bloom, G. S. Amyloid-β and tau: the trigger and bullet in Alzheimer disease pathogenesis. *JAMA Neurol* **2014**, *71*, 505–508.

(82) Wang, X.; Ao, Q.; Tian, X.; Fan, J.; Tong, H.; Hou, W.; Bai, S. Gelatin-Based Hydrogels for Organ 3D Bioprinting. *Polymers 2017, Vol. 9, Page 401* **2017**, *9*, 401.

(83) Flanary, B. E.; Sammons, N. W.; Nguyen, C.; Walker, D.; Streit, W. J. Evidence that aging and amyloid promote microglial cell senescence. *Rejuvenation Res* **2007**, *10*, 61–74.

(84) Poewe, W.; Seppi, K.; Tanner, C. M.; Halliday, G. M.; Brundin, P.; Volkmann, J.; Schrag, A. E.; Lang, A. E. Parkinson disease. *Nat Rev Dis Primers* **2017**, *3*, 17013.

(85) Melki, R. Role of Different Alpha-Synuclein Strains in Synucleinopathies, Similarities with other Neurodegenerative Diseases. *J Parkinsons Dis* **2015**, *5*, 217–227.

(86) Rocha, E. M.; De Miranda, B.; Sanders, L. H. Alpha-synuclein: Pathology, mitochondrial dysfunction and neuroinflammation in Parkinson's disease. *Neurobiol Dis* **2018**, *109*, 249–257.

(87) Baker, D. J.; Petersen, R. C. Cellular senescence in brain aging and neurodegenerative diseases: evidence and perspectives. *J Clin Invest* **2018**, *128*, 1208–1216.

(88) Hardiman, O.; van den Berg, L. H.; Kiernan, M. C. Clinical diagnosis and management of amyotrophic lateral sclerosis. *Nat Rev Neurol* **2011**, *7*, 639–649.

(89) Shaw, C. E.; Al-Chalabi, A.; Leigh, N. Progress in the pathogenesis of amyotrophic lateral sclerosis. *Curr Neurol Neurosci Rep* **2001**, *1*, 69–76.

(90) Vance, C. et al. Mutations in FUS, an RNA processing protein, cause familial amyotrophic lateral sclerosis type 6. *Science* **2009**, *323*, 1208–1211.

(91) Kwiatkowski T. J., J. et al. Mutations in the FUS/TLS gene on chromosome 16 cause familial amyotrophic lateral sclerosis. *Science* **2009**, *323*, 1205–1208.

(92) Hardiman, O.; Al-Chalabi, A.; Chio, A.; Corr, E. M.; Logroscino, G.; Robberecht, W.; Shaw, P. J.; Simmons, Z.; van den Berg, L. H. Amyotrophic lateral sclerosis. *Nat Rev Dis Primers* **2017**, *3*, 17071.

(93) MacDonald, M. E. et al. A novel gene containing a trinucleotide repeat that is expanded and unstable on Huntington's disease chromosomes. *Cell* **1993**, *72*, 971–983.

(94) Bates, G. P.; Dorsey, R.; Gusella, J. F.; Hayden, M. R.; Kay, C.; Leavitt, B. R.; Nance, M.; Ross, C. A.; Scahill, R. I.; Wetzel, R.; Wild, E. J.; Tabrizi, S. J. Huntington disease. *Nat Rev Dis Primers* **2015**, *1*, 15005.

(95) Machiela, E.; Jeloka, R.; Caron, N. S.; Mehta, S.; Schmidt, M. E.; Baddeley, H. J. E.; Tom, C. M.; Polturi, N.; Xie, Y.; Mattis, V. B.; Hayden, M. R.; Southwell, A. L. The Interaction of Aging and Cellular Stress Contributes to Pathogenesis in Mouse and Human Huntington Disease Neurons. *Front Aging Neurosci* **2020**, *12*, 524369.

(96) Marrie, R. A.; Yu, N.; Blanchard, J.; Leung, S.; Elliott, L. The rising prevalence and changing age distribution of multiple sclerosis in Manitoba. *Neurology* **2010**, *74*, 465–471.

(97) Trapp, B. D.; Nave, K. A. Multiple sclerosis: an immune or neurodegenerative disorder? *Annu Rev Neurosci* **2008**, *31*, 247–269.

(98) Scalfari, A.; Neuhaus, A.; Daumer, M.; Ebers, G. C.; Muraro, P. A. Age and disability accumulation in multiple sclerosis. *Neurology* **2011**, *77*, 1246–1252.

(99) Gilgun-Sherki, Y.; Melamed, E.; Offen, D. The role of oxidative stress in the pathogenesis of multiple sclerosis: the need for effective antioxidant therapy. *J Neurol* **2004**, *251*, 261–268.

(100) Mahad, D. J.; Ziabreva, I.; Campbell, G.; Lax, N.; White, K.; Hanson, P. S.; Lassmann, H.; Turnbull, D. M. Mitochondrial changes within axons in multiple sclerosis. *Brain* **2009**, *132*, 1161–1174.

(101) Haider, L.; Fischer, M. T.; Frischer, J. M.; Bauer, J.; Höftberger, R.; Botond, G.; Esterbauer, H.; Binder, C. J.; Witztum, J. L.; Lassmann, H. Oxidative damage in multiple sclerosis lesions. *Brain* **2011**, *134*, 1914–1924.

(102) Elkjaer, M. L.; Frisch, T.; Reynolds, R.; Kacprowski, T.; Burton, M.; Kruse, T. A.; Thomassen, M.; Baumbach, J.; Illes, Z. Molecular signature of different lesion types in the brain white matter of patients with progressive multiple sclerosis. *Acta Neuropathol Commun* **2019**, *7*, 205.

(103) Tamburrino, A.; Decressac, M. Aged and Diseased Neurons Get Lost in Transport. *Trends Neurosci* **2016**, *39*, 199–201.

(104) García-Prat, L.; Martínez-Vicente, M.; Perdiguero, E.; Ortet, L.; Rodríguez-Ubreva, J.; Rebollo, E.; Ruiz-Bonilla, V.; Gutarra, S.; Ballestar, E.; Serrano, A. L.; Sandri, M.; Muñoz-Cánoves, P. Autophagy maintains stemness by preventing senescence. *Nature* **2016**, *529*, 37–42.

(105) Yanai, H.; Fraifeld, V. E. The role of cellular senescence in aging through the prism of Koch-like criteria. *Ageing Res Rev* **2018**, *41*, 18–33.

(106) McHugh, D.; Gil, J. Senescence and aging: Causes, consequences, and therapeutic avenues. *J Cell Biol* **2018**, *217*, 65–77.

(107) Demidenko, Z. N.; Blagosklonny, M. V. Growth stimulation leads to cellular senescence when the cell cycle is blocked. *Cell Cycle* **2008**, *7*, 3355–3361.

(108) Gray-Schopfer, V. C.; Cheong, S. C.; Chong, H.; Chow, J.; Moss, T.; Abdel-Malek, Z. A.; Marais, R.; Wynford-Thomas, D.; Bennett, D. C. Cellular senescence in naevi and immortalisation in melanoma: a role for p16? *Br J Cancer* **2006**, *95*, 496–505.

(109) Song, S.; Tchkonia, T.; Jiang, J.; Kirkland, J. L.; Sun, Y. Targeting Senescent Cells for a Healthier Aging: Challenges and Opportunities. *Adv Sci (Weinh)* **2020**, *7*, 2002611.

(110) Gosselin, D.; Rivest, S. Getting Too Old Too Quickly for Their Job: Senescent Glial Cells Promote Neurodegeneration. *Neuron* **2018**, *100*, 777–779.

(111) Campisi, J.; d'Adda di Fagagna, F. Cellular senescence: when bad things happen to good cells. *Nat Rev Mol Cell Biol* **2007**, *8*, 729–740.

(112) Banimohamad-Shotorbani, B.; Kahroba, H.; Sadeghzadeh, H.; Wilson D. M., 3.; Maadi, H.; Samadi, N.; Hejazi, M. S.; Farajpour, H.; Onari, B. N.; Sadeghi, M. R. DNA damage repair response in mesenchymal stromal cells: From cellular senescence and aging to apoptosis and differentiation ability. *Ageing Res Rev* **2020**, *62*, 101125.

(113) He, S.; Sharpless, N. E. Senescence in Health and Disease. *Cell* **2017**, *169*, 1000–1011.

(114) Musi, N.; Valentine, J. M.; Sickora, K. R.; Baeuerle, E.; Thompson, C. S.; Shen, Q.; Orr, M. E. Tau protein aggregation is associated with cellular senescence in the brain. *Aging Cell* **2018**, *17*, e12840.

(115) Saez-Atienzar, S.; Masliah, E. Cellular senescence and Alzheimer disease: the egg and the chicken scenario. *Nat Rev Neurosci* **2020**, *21*, 433–444.

(116) Gillispie, G. J.; Sah, E.; Krishnamurthy, S.; Ahmidouch, M. Y.; Zhang, B.; Orr, M. E. Evidence of the Cellular Senescence Stress Response in Mitotically Active Brain Cells-Implications for Cancer and Neurodegeneration. *Life (Basel)* **2021**, *11*, DOI: 10.3390/life11020153.

(117) Frank-Cannon, T. C.; Alto, L. T.; McAlpine, F. E.; Tansey, M. G. Does neuroinflammation fan the flame in neurodegenerative diseases? *Mol Neurodegener* **2009**, *4*, 47.

(118) Si, Z.; Wang, X.; Zhang, Z.; Wang, J.; Li, J.; Li, L.; Li, Y.; Peng, Y.; Sun, C.; Hui, Y.; Gao, X. Heme Oxygenase 1 Induces Tau Oligomer Formation and Synapse Aberrations in Hippocampal Neurons. *J Alzheimers Dis* **2018**, *65*, 409–419.

(119) Franceschi, C. Inflammaging as a major characteristic of old people: can it be prevented or cured? *Nutr Rev* **2007**, *65*, S173–6.

(120) Chung, H. Y.; Cesari, M.; Anton, S.; Marzetti, E.; Giovannini, S.; Seo, A. Y.; Carter, C.; Yu, B. P.; Leeuwenburgh, C. Molecular inflammation: underpinnings of aging and age-related diseases. *Ageing Res Rev* **2009**, *8*, 18–30.

(121) Yankner, B. A.; Lu, T.; Loerch, P. The aging brain. *Annu Rev Pathol* **2008**, *3*, 41–66.

(122) Si, Z.; Sun, L.; Wang, X. Evidence and perspectives of cell senescence in neurodegenerative diseases. *Biomed Pharmacother* **2021**, *137*, 111327.

(123) Swenson Barbara, L.; Meyer, C. F.; Bussian, T. J.; Baker, D. J. Senescence in aging and disorders of the central nervous system. *Translational Medicine of Aging* **2019**, *3*, 17–25.

(124) Tigges, J.; Krutmann, J.; Fritsche, E.; Haendeler, J.; Schaal, H.; Fischer, J. W.; Kalfalah, F.; Reinke, H.; Reifenberger, G.; Stühler, K.; Ventura, N.; Gundermann, S.; Boukamp, P.; Boege, F. The hallmarks of fibroblast ageing. *Mechanisms of Ageing and Development* **2014**, *138*, 26–44.

(125) Takahashi, K.; Yamanaka, S. Induction of Pluripotent Stem Cells from Mouse Embryonic and Adult Fibroblast Cultures by Defined Factors. *Cell* **2006**, *126*, 663–676.

(126) Ocampo, A.; Reddy, P.; Belmonte, J. C. I. Anti-Aging Strategies Based on Cellular Reprogramming. *Trends in molecular medicine* **2016**, *22*, 725–738.

(127) Mahmoudi, S. et al. Heterogeneity in old fibroblasts is linked to variability in reprogramming and wound healing. *Nature* **2019**, *574*, 553–558.

(128) Lynch, M. D.; Watt, F. M. Fibroblast heterogeneity: implications for human disease. *The Journal of clinical investigation* **2018**, *128*, 26–35.

(129) Shook, B. A.; Wasko, R. R.; Rivera-Gonzalez, G. C.; Salazar-Gatzimas, E.; López-Giráldez, F.; Dash, B. C.; Muñoz-Rojas, A. R.; Aultman, K. D.; Zwick, R. K.; Lei, V.; Arbiser, J. L.; Miller-Jensen, K.; Clark, D. A.; Hsia, H. C.; Horsley, V. Myofibroblast proliferation and heterogeneity are supported by macrophages during skin repair. *Science* **2018**, *362*, DOI: 10.1126/science.aar2971.

(130) Guerrero-Juarez, C. F.; Dedhia, P. H.; Jin, S.; Ruiz-Vega, R.; Ma, D.; Liu, Y.; Yamaga, K.; Shestova, O.; Gay, D. L.; Yang, Z.; Kessenbrock, K.; Nie, Q.; Pear, W. S.; Cotsarelis, G.; Plikus, M. V. Single-cell analysis reveals fibroblast heterogeneity and myeloid-derived adipocyte progenitors in murine skin wounds. *Nature Communications* **2019**, *10*, DOI: 10.1038/s41467-018-08247-x.

(131) Chang, H. Y.; Chi, J. T.; Dudoit, S.; Bondre, C.; Van De Rijn, M.; Botstein, D.; Brown, P. O. Diversity, topographic differentiation, and positional memory in human fibroblasts. *Proceedings of the National Academy of Sciences of the United States of America* **2002**, *99*, 12877–12882.

(132) LeBleu, V. S.; Neilson, E. G. Origin and functional heterogeneity of fibroblasts. *The FASEB Journal* **2020**, *34*, 3519–3536.

(133) Plikus, M. V.; Wang, X.; Sinha, S.; Forte, E.; Thompson, S. M.; Herzog, E. L.; Driskell, R. R.; Rosenthal, N.; Biernaskie, J.; Horsley, V. Fibroblasts: Origins, definitions, and functions in health and disease. *Cell* **2021**, *184*, 3852–3872.

(134) Pakshir, P.; Alizadehgiashi, M.; Wong, B.; Coelho, N. M.; Chen, X.; Gong, Z.; Shenoy, V. B.; McCulloch, C. A.; Hinz, B. Dynamic fibroblast contractions attract remote macrophages in fibrillar collagen matrix. *Nat Commun* **2019**, *10*, 1850.

(135) Hinz, B. The myofibroblast: paradigm for a mechanically active cell. *J Biomech* **2010**, *43*, 146–155.

(136) Tschumperlin, D. J. Fibroblasts and the ground they walk on. *Physiology (Bethesda)* **2013**, *28*, 380–390.

(137) Van Linthout, S.; Miteva, K.; Tschöpe, C. Crosstalk between fibroblasts and inflammatory cells. *Cardiovasc Res* **2014**, *102*, 258–269.

(138) Ferrer, R. A.; Saalbach, A.; Grünwedel, M.; Lohmann, N.; Forstreuter, I.; Saupe, S.; Wandel, E.; Simon, J. C.; Franz, S. Dermal Fibroblasts Promote Alternative Macrophage Activation Improving Impaired Wound Healing. *J Invest Dermatol* **2017**, *137*, 941–950.

(139) Nakaya, M. et al. Cardiac myofibroblast engulfment of dead cells facilitates recovery after myocardial infarction. *J Clin Invest* **2017**, *127*, 383–401.

(140) Armulik, A.; Genové, G.; Betsholtz, C. Pericytes: developmental, physiological, and pathological perspectives, problems, and promises. *Dev Cell* **2011**, *21*, 193–215.

(141) Hung, C.; Linn, G.; Chow, Y. H.; Kobayashi, A.; Mittelsteadt, K.; Altemeier, W. A.; Gharib, S. A.; Schnapp, L. M.; Duffield, J. S. Role of lung pericytes and resident fibroblasts in the pathogenesis of pulmonary fibrosis. *Am J Respir Crit Care Med* **2013**, *188*, 820–830.

(142) Sava, P.; Ramanathan, A.; Dobronyi, A.; Peng, X.; Sun, H.; Ledesma-Mendoza, A.; Herzog, E. L.; Gonzalez, A. L. Human pericytes adopt myofibroblast properties in the microenvironment of the IPF lung. *JCI Insight* **2017**, *2*, DOI: 10.1172/jci.insight.96352.

(143) Kuppe, C. et al. Decoding myofibroblast origins in human kidney fibrosis. *Nature* **2021**, *589*, 281–286.

(144) Darby, I. A.; Hewitson, T. D. Fibroblast differentiation in wound healing and fibrosis. *International review of cytology* **2007**, *257*, 143–179.

(145) Darby, I.; Skalli, O.; Gabbiani, G. α-Smooth muscle actin is transiently expressed by myofibroblasts during experimental wound healing. *Laboratory Investigation* **1990**, *63*, 21–29.

(146) Desmouliere, A.; Redard, M.; Darby, I.; Gabbiani, G. Apoptosis mediates the decrease in cellularity during the transition between granulation tissue and scar. *American Journal of Pathology* **1995**, *146*, 56–66.

(147) Takahashi-Iwanaga, H. The three-dimensional cytoarchitecture of the interstitial tissue in the rat kidney. *Cell and Tissue Research* **1991**, *264*, 269–281.

(148) Sappino, A. P.; Schurch, W.; Gabbiani, G. Differentiation repertoire of fibroblastic cells: expression of cytoskeletal proteins as marker of phenotypic modulations. *Laboratory Investigation; a Journal of Technical Methods and Pathology* **1990**, *63*, 144–161.

(149) Rinn, J. L.; Bondre, C.; Gladstone, H. B.; Brown, P. O.; Chang, H. Y. Anatomic demarcation by positional variation in fibroblast gene expression programs. *PLoS Genetics* **2006**, *2*, 1084–1096.

(150) Paine, R.; Ward, P. A. Cell adhesion molecules and pulmonary fibrosis. *American Journal of Medicine* **1999**, *107*, 268–279.

(151) Florin, L.; Maas-Szabowski, N.; Werner, S.; Szabowski, A.; Angel, P. Increased keratinocyte proliferation by JUN-dependent expression of PTN and SDF-1 in fibroblasts. *Journal of Cell Science* **2005**, *118*, 1981–1989.

(152) Werner, S.; Krieg, T.; Smola, H. Keratinocyte-fibroblast interactions in wound healing. *Journal of Investigative Dermatology* **2007**, *127*, 998–1008.

(153) Kazlauskas, A. PDGFs and their receptors. *Gene* **2017**, *614*, 1–7.

(154) Massagué, J. TGFβ signalling in context. *Nat Rev Mol Cell Biol* **2012**, *13*, 616–630.

(155) Lodyga, M.; Hinz, B. TGF-β1 - A truly transforming growth factor in fibrosis and immunity. *Semin Cell Dev Biol* **2020**, *101*, 123–139.

(156) MacDonald, B. T.; Tamai, K.; He, X. Wnt/beta-catenin signaling: components, mechanisms, and diseases. *Dev Cell* **2009**, *17*, 9–26.

(157) Wong, V. W.; Rustad, K. C.; Akaishi, S.; Sorkin, M.; Glotzbach, J. P.; Januszyk, M.; Nelson, E. R.; Levi, K.; Paterno, J.; Vial, I. N.; Kuang, A. A.; Longaker, M. T.; Gurtner, G. C. Focal adhesion kinase links mechanical force to skin fibrosis via inflammatory signaling. *Nature Medicine* **2012**, *18*, 148–152.

(158) Mikesh, L. M.; Aramadhaka, L. R.; Moskaluk, C.; Zigrino, P.; Mauch, C.; Fox, J. W. Proteomic anatomy of human skin. *Journal of Proteomics* **2013**, *84*, 190–200.

(159) Wong, R.; Geyer, S.; Weninger, W.; Guimberteau, J.-C.; Wong, J. K. The dynamic anatomy and patterning of skin. *Experimental Dermatology* **2016**, *25*, 92–98.

(160) Cabral, A.; Voskamp, P.; Cleton-Jansen, A. M.; South, A.; Nizetic, D.; Backendorf, C. Structural Organization and Regulation of the Small Proline-rich Family of Cornified Envelope Precursors Suggest a Role in Adaptive Barrier Function. *Journal of Biological Chemistry* **2001**, *276*, 19231–19237.

(161) Kwiecien, K.; Zegar, A.; Jung, J.; Brzoza, P.; Kwitniewski, M.; Godlewska, U.; Grygier, B.; Kwiecinska, P.; Morytko, A.; Cichy, J. Architecture of antimicrobial skin defense. *Cytokine and growth factor reviews* **2019**, *49*, 70–84.

(162) Brandner, J. M.; Zorn-Kruppa, M.; Yoshida, T.; Moll, I.; Beck, L. A.; De Benedetto, A. Epidermal tight junctions in health and disease. *Tissue Barriers* **2015**, *3*, DOI: 10.4161/21688370.2014.974451.

(163) Di Meglio, P.; Perera, G. K.; Nestle, F. O. The multitasking organ: recent insights into skin immune function. *Immunity* **2011**, *35*, 857–869.

(164) Gonzales, K. A. U.; Fuchs, E. Skin and Its Regenerative Powers: An Alliance between Stem Cells and Their Niche. *Developmental cell* **2017**, *43*, 387–401.

(165) Kirker, K. R.; James, G. A.; Fleckman, P.; Olerud, J. E.; Stewart, P. S. Differential effects of planktonic and biofilm MRSA on human fibroblasts. *Wound Repair and Regeneration* **2012**, *20*, 253–261.

(166) Tong, P. L.; Roediger, B.; Kolesnikoff, N.; Biro, M.; Tay, S. S.; Jain, R.; Shaw, L. E.; Grimbaldeston, M. A.; Weninger, W. The skin immune atlas: Three-dimensional analysis of cutaneous leukocyte subsets by multiphoton microscopy. *Journal of Investigative Dermatology* **2015**, *135*, 84–93.

(167) Wolf, K.; Müller, R.; Borgmann, S.; Bröcker, E. B.; Friedl, P. Amoeboid shape change and contact guidance: T-lymphocyte crawling through fibrillar collagen is independent of matrix remodeling by MMPs and other proteases. *Blood* **2003**, *102*, 3262–3269.

(168) Kabashima, K.; Honda, T.; Ginhoux, F.; Egawa, G. The immunological anatomy of the skin. *Nature reviews. Immunology* **2019**, *19*, 19–30.

(169) Heilborn, J. D.; Frohm Nilsson, M.; Kratz, G.; Weber, G.; Sørensen, O.; Borregaard, N.; Ståhle-Bäckdahl, M. The cathelicidin anti-microbial peptide LL-37 is involved in re-epithelialization of human skin wounds and is lacking in chronic ulcer epithelium. *Journal of Investigative Dermatology* **2003**, *120*, 379–389.

(170) Koczulla, R. et al. An angiogenic role for the human peptide antibiotic LL-37/hCAP-18. *Journal of Clinical Investigation* **2003**, *111*, 1665–1672.

(171) Wang, Z.; Lai, Y.; Bernard, J. J.; MacLeod, D. T.; Cogen, A. L.; Moss, B.; Di Nardo, A. Skin Mast Cells Protect Mice against Vaccinia Virus by Triggering Mast Cell Receptor S1PR2 and Releasing Antimicrobial Peptides. *The Journal of Immunology* **2012**, *188*, 345–357.

(172) Van Kilsdonk, J. W. J.; Jansen, P. A. M.; van den Bogaard, E. H.; Bos, C.; Bergers, M.; Zeeuwen, P. L. J. M.; Schalkwijk, J. The Effects of Human Beta-Defensins on Skin Cells in vitro. *Dermatology* **2017**, *233*, 155–163.

(173) Brauchle, M.; Angermeyer, K.; Hübner, G.; Werner, S. Large induction of keratinocyte growth factor expression by serum growth factors and pro-inflammatory cytokines in cultured fibroblasts. *Oncogene* **1994**, *9*, 3199–3204.

(174) Strieter, R. M.; Burdick, M. D.; Gomperts, B. N.; Belperio, J. A.; Keane, M. P. CXC chemokines in angiogenesis. *Cytokine and Growth Factor Reviews* **2005**, *16*, 593–609.

(175) Schmidt, B. A.; Horsley, V. Intradermal adipocytes mediate fibroblast recruitment during skin wound healing. *Development* **2013**, *140*, 1517–1527.

(176) Chen, S. X.; Zhang, L. J.; Gallo, R. L. Dermal White Adipose Tissue: A Newly Recognized Layer of Skin Innate Defense. *The Journal of investigative dermatology* **2019**, *139*, 1002–1009.

(177) Gaur, M.; Dobke, M.; Lunyak, V. V. Mesenchymal Stem Cells from Adipose Tissue in Clinical Applications for Dermatological Indications and Skin Aging. *Int J Mol Sci* **2017**, *18*, DOI: 10.3390/ijms18010208.

(178) Nguyen, K. D.; Qiu, Y.; Cui, X.; Goh, Y. P. S.; Mwangi, J.; David, T.; Mukundan, L.; Brombacher, F.; Locksley, R. M.; Chawla, A. Alternatively activated macrophages produce catecholamines to sustain adaptive thermogenesis. *Nature* **2011**, *480*, 104–108.

(179) Lee, S. D.; Tontonoz, P. Eosinophils in fat: pink is the new brown. *Cell* **2014**, *157*, 1249–1250.

(180) Fjeldborg, K.; Pedersen, S. B.; Møller, H. J.; Christiansen, T.; Bennetzen, M.; Richelsen, B. Human adipose tissue macrophages are enhanced but changed to an anti-inflammatory profile in obesity. *Journal of Immunology Research* **2014**, *2014*, DOI: 10.1155/2014/309548.

(181) Amisten, S.; Neville, M.; Hawkes, R.; Persaud, S. J.; Karpe, F.; Salehi, A. An atlas of G-protein coupled receptor expression and function in human subcutaneous adipose tissue. *Pharmacology and Therapeutics* **2015**, *146*, 61–93.

(182) Reed, R. K.; Rubin, K. Transcapillary exchange: role and importance of the interstitial fluid pressure and the extracellular matrix. *Cardiovascular Research* **2010**, *87*, 211–217.

(183) MacK, J.; Squier, W.; Eastman, J. T. Anatomy and development of the meninges: implications for subdural collections and CSF circulation. *Pediatric radiology* **2009**, *39*, 200–210.

(184) Patel, N.; Kirmi, O. Anatomy and imaging of the normal meninges. *Semin Ultrasound CT MR* **2009**, *30*, 559–564.

(185) Haines, D. E.; Harkey, H. L.; Al-Mefty, O. The "Subdural" Space. *Neurosurgery* **1993**, *32*, 111–120.

(186) Mitsuhashi, Y.; Hayasaki, K.; Kawakami, T.; Nagata, T.; Kaneshiro, Y.; Umaba, R.; Ohata, K. Dural Venous System in the Cavernous Sinus: A Literature Review and Embryological, Functional, and Endovascular Clinical Considerations. *Neurologia medico-chirurgica* **2016**, *56*, 326–339.

(187) Swyden, S.; Carter, C.; Shah, S. u. Intracranial Hypotension. *StatPearls* **2021**.

(188) Zhang, E. T.; Inman, C. B.; Weller, R. O. Interrelationships of the pia mater and the perivascular (Virchow-Robin) spaces in the human cerebrum. *Journal of anatomy* **1990**, *170*, 111–123.

(189) Fox, R. J.; Walji, A. H.; Mielke, B.; Petruk, K. C.; Aronyk, K. E. Anatomic Details of Intradural Channels in the Parasagittal Dura: A Possible Pathway for Flow of Cerebrospinal Fluid. *Neurosurgery* **1996**, *39*, 84–91.

(190) Ikushima, I.; Korogi, Y.; Makita, O.; Yamura, M.; Kawano, H.; Kohama, M.; Arikawa, K.; Takahashi, M. MRI of arachnoid granulations within the dural sinuses using a FLAIR pulse sequence. *British Journal of Radiology* **1999**, *72*, 1046–1051.

(191) Feurer, D. J.; Weller, R. O. Barrier functions of the leptomeninges: a study of normal meninges and meningiomas in tissue culture. *Neuropathology and Applied Neurobiology* **1991**, *17*, 391–405.

(192) Jiang, X.; Iseki, S.; Maxson, R. E.; Sucov, H. M.; Morriss-Kay, G. M. Tissue origins and interactions in the mammalian skull vault. *Developmental Biology* **2002**, *241*, 106–116.

(193) Yoshida, T.; Vivatbutsiri, P.; Morriss-Kay, G.; Saga, Y.; Iseki, S. Cell lineage in mammalian craniofacial mesenchyme. *Mechanisms of Development* **2008**, *125*, 797–808.

(194) Dasgupta, K.; Jeong, J. Developmental biology of the meninges. *Genesis* **2019**, *57*, e23288–e23288.

(195) Spector, J. A.; Greenwald, J. A.; Warren, S. M.; Bouletreau, P. J.; Detch, R. C.; Fagenholz, P. J.; Crisera, F. E.; Longaker, M. T. Dura mater biology: autocrine and paracrine effects of fibroblast growth factor 2. *Plast Reconstr Surg* **2002**, *109*, 645–654.

(196) Warren, S. M.; Brunet, L. J.; Harland, R. M.; Economides, A. N.; Longaker, M. T. The BMP antagonist noggin regulates cranial suture fusion. *Nature* **2003**, *422*, 625–629.

(197) Levi, B.; Wan, D. C.; Wong, V. W.; Nelson, E.; Hyun, J.; Longaker, M. T. Cranial Suture Biology. *Journal of Craniofacial Surgery* **2012**, *23*, 13–19.

(198) Borrell, V.; Marín, O. Meninges control tangential migration of hem-derived Cajal-Retzius cells via CXCL12/CXCR4 signaling. *Nature Neuroscience* **2006**, *9*, 1284–1293.

(199) Choe, Y.; Siegenthaler, J. A.; Pleasure, S. J. A Cascade of Morphogenic Signaling Initiated by the Meninges Controls Corpus Callosum Formation. *Neuron* **2012**, *73*, 698–712.

(200) Zhu, Y.; Yu, T.; Zhang, X. C.; Nagasawa, T.; Wu, J. Y.; Rao, Y. Role of the chemokine SDF-1 as the meningeal attractant for embryonic cerebellar neurons. *Nature Neuroscience* **2002**, *5*, 719–720.

(201) Bagri, A.; Gurney, T.; He, X.; Zou, Y.-R.; Littman, D. R.; Tessier-Lavigne, M.; Pleasure, S. J. The chemokine SDF1 regulates migration of dentate granule cells. *Development* **2002**, *129*, 4249–4260.

(202) Stumm, R. K.; Zhou, C.; Ara, T.; Lazarini, F.; Dubois-Dalcq, M.; Nagasawa, T.; Höllt, V.; Schulz, S. CXCR4 regulates interneuron migration in the developing neocortex. *Journal of Neuroscience* **2003**, *23*, 5123–5130.

(203) Paredes, M. F.; Li, G.; Berger, O.; Baraban, S. C.; Pleasure, S. J. Stromal-derived factor-1 (CXCL12) regulates laminar position of Cajal-Retzius cells in normal and dysplastic brains. *Journal of Neuroscience* **2006**, *26*, 9404–9412.

(204) Li, G.; Kataoka, H.; Coughlin, S. R.; Pleasure, S. J. Identification of a transient subpial neurogenic zone in the developing dentate gyrus and its regulation by Cxcl12 and reelin signaling. *Development* **2009**, *136*, 327–335.

(205) Chou, F. S.; Li, R.; Wang, P. S. Molecular components and polarity of radial glial cells during cerebral cortex development. *Cellular and molecular life sciences : CMLS* **2018**, *75*, 1027–1041.

(206) Halfter, W.; Dong, S.; Yip, Y. P.; Willem, M.; Mayer, U. A critical function of the pial basement membrane in cortical histogenesis. *Journal of Neuroscience* **2002**, *22*, 6029–6040.

(207) Beggs, H. E.; Schahin-Reed, D.; Zang, K.; Goebbels, S.; Nave, K. A.; Gorski, J.; Jones, K. R.; Sretavan, D.; Reichardt, L. F. FAK deficiency in cells contributing to the basal lamina results in cortical abnormalities resembling congenital muscular dystrophies. *Neuron* **2003**, *40*, 501–514.

(208) Guénette, S.; Chang, Y.; Hiesberger, T.; Richardson, J. A.; Eckman, C. B.; Eckman, E. A.; Hammer, R. E.; Herz, J. Essential roles for the FE65 amyloid precursor protein-interacting proteins in brain development. *The EMBO Journal* **2006**, *25*, 420–431.

(209) Zarbalis, K.; Siegenthaler, J. A.; Choe, Y.; May, S. R.; Peterson, A. S.; Pleasure, S. J. Cortical dysplasia and skull defects in mice with a Foxc1 allele reveal the role of meningeal differentiation in regulating cortical development. *Proceedings of the National Academy of Sciences of the United States of America* **2007**, *104*, 14002–14007.

(210) Inoue, T.; Ogawa, M.; Mikoshiba, K.; Aruga, J. Zic deficiency in the cortical marginal zone and meninges results in cortical lamination defects resembling those in type II lissencephaly. *Journal of Neuroscience* **2008**, *28*, 4712–4725.

(211) Labelle-Dumais, C.; Dilworth, D. J.; Harrington, E. P.; de Leau, M.; Lyons, D.; Kabaeva, Z.; Manzini, M. C.; Dobyns, W. B.; Walsh, C. A.; Michele, D. E.; Gould, D. B. COL4A1 Mutations Cause Ocular Dysgenesis, Neuronal Localization Defects, and Myopathy in Mice and Walker-Warburg Syndrome in Humans. *PLoS Genetics* **2011**, *7*, e1002062–e1002062.

(212) Ichikawa-Tomikawa, N.; Ogawa, J.; Douet, V.; Xu, Z.; Kamikubo, Y.; Sakurai, T.; Kohsaka, S.; Chiba, H.; Hattori, N.; Yamada, Y.; Arikawa-Hirasawa, E. Laminin α1 is essential for mouse cerebellar development. *Matrix Biology* **2012**, *31*, 17–28.

(213) Siegenthaler, J. A.; Ashique, A. M.; Zarbalis, K.; Patterson, K. P.; Hecht, J. H.; Kane, M. A.; Folias, A. E.; Choe, Y.; May, S. R.; Kume, T.; Napoli, J. L.; Peterson, A. S.; Pleasure, S. J. Retinoic acid from the meninges regulates cortical neuron generation. *Cell* **2009**, *139*, 597–609.

(214) Bonney, S.; Harrison-Uy, S.; Mishra, S.; MacPherson, A. M.; Choe, Y.; Li, D.; Jaminet, S. C.; Fruttiger, M.; Pleasure, S. J.; Siegenthaler, J. A. Diverse functions of retinoic acid in brain vascular development. *Journal of Neuroscience* **2016**, *36*, 7786–7801.

(215) Mishra, S.; Choe, Y.; Pleasure, S. J.; Siegenthaler, J. A. Cerebrovascular defects in Foxc1 mutants correlate with aberrant WNT and VEGF—A pathways downstream of retinoic acid from the meninges. *Developmental Biology* **2016**, *420*, 148–165.

(216) Decimo, I.; Fumagalli, G.; Berton, V.; Krampera, M.; Bifari, F. Meninges: from protective membrane to stem cell niche. *American journal of stem cells* **2012**, *1*, 92–105.

(217) Bifari, F.; Decimo, I.; Chiamulera, C.; Bersan, E.; Malpeli, G.; Johansson, J.; Lisi, V.; Bonetti, B.; Fumagalli, G.; Pizzolo, G.; Krampera, M. Novel stem/progenitor cells with neuronal differentiation potential reside in the leptomeningeal niche. *Journal of Cellular and Molecular Medicine* **2009**, *13*, 3195–3208.

(218) Bifari, F.; Berton, V.; Pino, A.; Kusalo, M.; Malpeli, G.; Di Chio, M.; Bersan, E.; Amato, E.; Scarpa, A.; Krampera, M.; Fumagalli, G.; Decimo, I. Meninges harbor cells expressing neural precursor markers during development and adulthood. *Frontiers in Cellular Neuroscience* **2015**, *9*, 383.

(219) Bifari, F. et al. Neurogenic Radial Glia-like Cells in Meninges Migrate and Differentiate into Functionally Integrated Neurons in the Neonatal Cortex. *Cell Stem Cell* **2017**, *20*, 360–373.e7.

(220) Colombo, J. A.; Napp, M. I.; Puissant, V. Leptomeningeal and skin fibroblasts: Two different cell types? *International Journal of Developmental Neuroscience* **1994**, *12*, 57–61.

(221) Sievers, J.; Pehlemann, F. W. Influences of meningeal cells on brain development. Findings and hypothesis. *Naturwissenschaften* **1986**, *73*, 188–194.

(222) Rakic, P. Specification of cerebral cortical areas. *Science* **1988**, *241*, 170–176.

(223) DeSisto, J.; O'Rourke, R.; Jones, H. E.; Pawlikowski, B.; Malek, A. D.; Bonney, S.; Guimiot, F.; Jones, K. L.; Siegenthaler, J. A. Single-Cell Transcriptomic Analyses of the Developing Meninges Reveal Meningeal Fibroblast Diversity and Function. *Developmental Cell* **2020**, *54*, 43–59.e4.

(224) Decimo, I.; Dolci, S.; Panuccio, G.; Riva, M.; Fumagalli, G.; Bifari, F. Meninges: A Widespread Niche of Neural Progenitors for the Brain. *Neuroscientist* **2021**, *27*, 506–528.

(225) Nakagami, H.; Nakagawa, N.; Takeya, Y.; Kashiwagi, K.; Ishida, C.; Hayashi, S. I.; Aoki, M.; Matsumoto, K.; Nakamura, T.; Ogihara, T.; Morishita, R. Model of vasculogenesis from embryonic stem cells for vascular research and regenerative medicine. *Hypertension* **2006**, *48*, 112–119.

(226) Atala, A. Regenerative medicine strategies. *Journal of Pediatric Surgery* **2012**, *47*, 17–28.

(227) Brunt, K. R.; Weisel, R. D.; Li, R. K. Stem cells and regenerative medicine - future perspectives. *Canadian Journal of Physiology and Pharmacology* **2012**, *90*, 327–335.

(228) Okano, H.; Nakamura, M.; Yoshida, K.; Okada, Y.; Tsuji, O.; Nori, S.; Ikeda, E.; Yamanaka, S.; Miura, K. Steps toward safe cell therapy using induced pluripotent stem cells. *Circulation research* **2013**, *112*, 523–533.

(229) Sancho-Martinez, I.; Baek, S. H.; Izpisua Belmonte, J. C. Lineage conversion methodologies meet the reprogramming toolbox. *Nature cell biology* **2012**, *14*, 892–899.

(230) Ieda, M. Direct Reprogramming into Desired Cell Types by Defined Factors. *The Keio Journal of Medicine* **2013**, *62*, 74–82.

(231) Matsui, T.; Takano, M.; Yoshida, K.; Ono, S.; Fujisaki, C.; Matsuzaki, Y.; Toyama, Y.; Nakamura, M.; Okano, H.; Akamatsu, W. Neural Stem Cells Directly Differentiated from Partially Reprogrammed Fibroblasts Rapidly Acquire Gliogenic Competency. *STEM CELLS* **2012**, *30*, 1109–1119.

(232) Margariti, A.; Winkler, B.; Karamariti, E.; Zampetaki, A.; Tsai, T. N.; Baban, D.; Ragoussis, J.; Huang, Y.; Han, J. D. J.; Zeng, L.; Hu, Y.; Xu, Q. Direct reprogramming of fibroblasts into endothelial cells capable of angiogenesis and reendothelialization in tissue-engineered vessels. *Proceedings of the National Academy of Sciences of the United States of America* **2012**, *109*, 13793–13798.

(233) Efe, J. A.; Hilcove, S.; Kim, J.; Zhou, H.; Ouyang, K.; Wang, G.; Chen, J.; Ding, S. Conversion of mouse fibroblasts into cardiomyocytes using a direct reprogramming strategy. *Nature Cell Biology* **2011**, *13*, 215–222.

(234) Kim, J.; Efe, J. A.; Zhu, S.; Talantova, M.; Yuan, X.; Wang, S.; Lipton, S. A.; Zhang, K.; Ding, S. Direct reprogramming of mouse fibroblasts to neural progenitors. *Proceedings of the National Academy of Sciences of the United States of America* **2011**, *108*, 7838–7843.

(235) Kim, J.; Ambasudhan, R.; Ding, S. Direct lineage reprogramming to neural cells. *Current opinion in neurobiology* **2012**, *22*, 778–784.

(236) Xu, Y.; Shi, Y.; Ding, S. A chemical approach to stem-cell biology and regenerative medicine. *Nature* **2008**, *453*, 338–344.

(237) Li, W.; Ding, S. Small molecules that modulate embryonic stem cell fate and somatic cell reprogramming. *Trends in pharmacological sciences* **2010**, *31*, 36–45.

(238) Hou, P.; Li, Y.; Zhang, X.; Liu, C.; Guan, J.; Li, H.; Zhao, T.; Ye, J.; Yang, W.; Liu, K.; Ge, J.; Xu, J.; Zhang, Q.; Zhao, Y.; Deng, H. Pluripotent stem cells induced from mouse somatic cells by small-molecule compounds. *Science* **2013**, *341*, 651–654.

(239) Federation, A. J.; Bradner, J. E.; Meissner, A. The use of small molecules in somatic-cell reprogramming. *Trends in cell biology* **2014**, *24*, 179–187.

(240) Qin, H.; Zhao, A.; Fu, X. Small molecules for reprogramming and transdifferentiation. *Cellular and molecular life sciences : CMLS* **2017**, *74*, 3553–3575.

(241) Cole, M. F.; Johnstone, S. E.; Newman, J. J.; Kagey, M. H.; Young, R. A. Tcf3 is an integral component of the core regulatory circuitry of embryonic stem cells. *Genes and Development* **2008**, *22*, 746–755.

(242) Tam, W.-L.; Lim, C. Y.; Han, J.; Zhang, J.; Ang, Y.-S.; Ng, H.-H.; Yang, H.; Lim, B. T-Cell Factor 3 Regulates Embryonic Stem Cell Pluripotency and Self-Renewal by the Transcriptional Control of Multiple Lineage Pathways. *Stem Cells* **2008**, *26*, 2019–2031.

(243) Silva, J.; Barrandon, O.; Nichols, J.; Kawaguchi, J.; Theunissen, T. W.; Smith, A. Promotion of reprogramming to ground state pluripotency by signal inhibition. *PLoS Biol* **2008**, *6*, e253.

(244) Li, X. et al. Small-Molecule-Driven Direct Reprogramming of Mouse Fibroblasts into Functional Neurons. *Cell Stem Cell* **2015**, *17*, 195–203.

(245) Yang, M.; Ding, Q.; Zhang, M.; Moon, C.; Wang, H. Forebrain overexpression of type 1 adenylyl cyclase promotes molecular stability and behavioral resilience to physical stress. *Neurobiology of Stress* **2020**, *13*, 100237.

(246) Kumar, A.; Narayanan, K.; Chaudhary, R. K.; Mishra, S.; Kumar, S.; Vinoth, K. J.; Padmanabhan, P.; Gulyás, B. Current Perspective of Stem Cell Therapy in Neurodegenerative and Metabolic Diseases. *Molecular neurobiology* **2017**, *54*, 7276–7296.

(247) Hyun, I. et al. New ISSCR guidelines underscore major principles for responsible translational stem cell research. *Cell stem cell* **2008**, *3*, 607–609.

(248) Rosemann, A. Stem cell treatments for neurodegenerative diseases: challenges from a science, business and healthcare perspective. *Neurodegenerative Disease Management* **2015**, *5*, 85–87.

(249) Hayakawa, K.; Snyder, E. Y.; Lo, E. H. Meningeal Multipotent Cells: A Hidden Target for CNS Repair? *Neuromolecular medicine* **2021**, *23*, 339–343.

(250) Guaita, A.; Colombo, M.; Vaccaro, R.; Fossi, S.; Vitali, S. F.; Forloni, G.; Polito, L.; Davin, A.; Ferretti, V. V.; Villani, S. Brain aging and dementia during the transition from late adulthood to old age: design and methodology of the "Invece.Ab" population-based study. *BMC Geriatr* **2013**, *13*, 98.

(251) Gere, C. A brief history of brain archiving. *J Hist Neurosci* **2003**, *12*, 396–410.

(252) Klioueva, N. M.; Rademaker, M. C.; Dexter, D. T.; Al-Sarraj, S.; Seilhean, D.; Streichenberger, N.; Schmitz, P.; Bell, J. E.; Ironside, J. W.; Arzberger, T.; Huitinga, I. BrainNet Europe's Code of Conduct for brain banking. *J Neural Transm (Vienna)* **2015**, *122*, 937–940.

(253) Poloni, T. E. et al. Abbiategrasso Brain Bank Protocol for Collecting, Processing and Characterizing Aging Brains. *Journal of Visualized Experiments* **2020**, *2020*, 1–25.

(254) Lee, K.; Saetern, O. C.; Nguyen, A.; Rodriguez, L.; Schüle, B. Derivation of leptomeninges explant cultures from postmortem human brain donors. *Journal of Visualized Experiments* **2017**, *2017*, 55045.

(255) Orzechowska, B.; Pabijan, J.; Wiltowska-Zuber, J.; Zemła, J.; Lekka, M. Fibroblasts change spreading capability and mechanical properties in a direct interaction with keratinocytes in conditions mimicking wound healing. *Journal of Biomechanics* **2018**, *74*, 134–142.

(256) Duarte-Neves, J.; Pereira de Almeida, L.; Cavadas, C. Neuropeptide Y (NPY) as a therapeutic target for neurodegenerative diseases. *Neurobiology of disease* **2016**, *95*, 210–224.

(257) Shevach, E. M.; Stephens, G. L. The GITR-GITRL interaction: co-stimulation or contrasuppression of regulatory activity? *Nature reviews. Immunology* **2006**, *6*, 613–618.

(258) Lacal, P. M.; Petrillo, M. G.; Ruffini, F.; Muzi, A.; Bianchini, R.; Ronchetti, S.; Migliorati, G.; Riccardi, C.; Graziani, G.; Nocentini, G. Glucocorticoid-induced tumor necrosis factor receptor family-related ligand triggering upregulates vascular cell adhesion molecule-1 and intercellular adhesion molecule-1 and promotes leukocyte adhesion. *Journal of Pharmacology and Experimental Therapeutics* **2013**, *347*, 164–172.

(259) Gao, J.; Wang, S.; Liu, S. The involvement of protein <scp>TNFSF18</scp> in promoting <scp>p-STAT1</scp> phosphorylation to induce coronary microcirculation disturbance in atherosclerotic mouse model. *Drug Development Research* **2021**, *82*, 115–122.

(260) Kuleshov, M. V.; Jones, M. R.; Rouillard, A. D.; Fernandez, N. F.; Duan, Q.; Wang, Z.; Koplev, S.; Jenkins, S. L.; Jagodnik, K. M.; Lachmann, A.; McDermott, M. G.; Monteiro, C. D.; Gundersen, G. W.; Ma'ayan, A. Enrichr: a comprehensive gene set enrichment analysis web server 2016 update. *Nucleic acids research* **2016**, *44*, W90–W97.

(261) Mueller, M. M.; Fusenig, N. E. Tumor-stroma interactions directing phenotype and progression of epithelial skin tumor cells. *Differentiation; research in biological diversity* **2002**, *70*, 486–497.

(262) Werner, S.; Smola, H. Paracrine regulation of keratinocyte proliferation and differentiation. *Trends in cell biology* **2001**, *11*, 143–146.

(263) Costea, D. E.; Loro, L. L.; Dimba, E. A. O.; Vintermyr, O. K.; Johannessen, A. C. Crucial Effects of Fibroblasts and Keratinocyte Growth Factor on Morphogenesis of Reconstituted Human Oral Epithelium. *Journal of Investigative Dermatology* **2003**, *121*, 1479–1486.

(264) Eming, S. A.; Krieg, T.; Davidson, J. M. Inflammation in wound repair: molecular and cellular mechanisms. *The Journal of investigative dermatology* **2007**, *127*, 514–525.

(265) Hecht, J. H.; Siegenthaler, J. A.; Patterson, K. P.; Pleasure, S. J. Primary cellular meningeal defects cause neocortical dysplasia and dyslamination. *Annals of Neurology* **2010**, *68*, 454–464.

(266) Haushalter, C.; Schuhbaur, B.; Dolle, P.; Rhinn, M. Meningeal retinoic acid contributes to neocortical lamination and radial migration during mouse brain development. *Biology Open* **2017**, *6*, 148–160.

(267) Boucherie, C.; Boutin, C.; Jossin, Y.; Schakman, O.; Goffinet, A. M.; Ris, L.; Gailly, P.; Tissir, F. Neural progenitor fate decision defects, cortical hypoplasia and behavioral impairment in Celsr1-deficient mice. *Molecular Psychiatry* **2018**, *23*, 723–734.

(268) Singh, M.; Sharma, A. K. Outgrowth of fibroblast cells from goat skin explants in three different culture media and the establishment of cell lines. *In Vitro Cell Dev Biol Anim* **2011**, *47*, 83–88.

(269) Vangipuram, M.; Ting, D.; Kim, S.; Diaz, R.; Schüle, B. Skin punch biopsy explant culture for derivation of primary human fibroblasts. *Journal of visualized experiments : JoVE* **2013**, 3779.

(270) Ruoslahti, E. RGD and other recognition sequences for integrins. *Annual review of cell and developmental biology* **1996**, *12*, 697–715.

(271) Hacking, S. A.; Khademhosseini, A. In *Biomaterials Science (Third Edition)*, Buddy, D. R., Hoffman, A. S., Schoen, F. J., Lemons, J. E., Eds., Third Edit; Academic Press: 2013, pp 408–427.

(272) Ruoslahti, E.; Reed, J. C. Anchorage dependence, integrins, and apoptosis. *Cell* **1994**, *77*, 477–478.

(273) Lago, J. C.; Puzzi, M. B. The effect of aging in primary human dermal fibroblasts. *PLoS ONE* **2019**, *14*, DOI: 10.1371/journal.pone.0219165.

(274) Katoh, K. FAK-Dependent Cell Motility and Cell Elongation. *Cells* **2020**, *9*, 192.

(275) Sriram, G.; Bigliardi, P. L.; Bigliardi-Qi, M. Fibroblast heterogeneity and its implications for engineering organotypic skin models in vitro. *European journal of cell biology* **2015**, *94*, 483–512.

(276) Gilyarov, A. V. Nestin in central nervous system cells. *Neuroscience and Behavioral Physiology* **2008**, *38*, 165–169.

(277) Dehmelt, L.; Halpain, S. The MAP2/Tau family of microtubule-associated proteins. *Genome biology* **2005**, *6*, DOI: 10.1186/GB-2004-6-1-204.

(278) Da Mesquita, S.; Fu, Z.; Kipnis, J. The Meningeal Lymphatic System: A New Player in Neurophysiology. *Neuron* **2018**, *100*, 375–388.

(279) Insel, P. A.; Ostrom, R. S. Forskolin as a tool for examining adenylyl cyclase expression, regulation, and G protein signaling. *Cellular and molecular neurobiology* **2003**, *23*, 305–314.

(280) Larigot, L.; Juricek, L.; Dairou, J.; Coumoul, X. AhR signaling pathways and regulatory functions. *Biochimie open* **2018**, *7*, 1–9.

(281) Price, K. M.; Wigg, K. G.; Feng, Y.; Blokland, K.; Wilkinson, M.; He, G.; Kerr, E. N.; Carter, T.-C.; Guger, S. L.; Lovett, M. W.; Strug, L. J.; Barr, C. L. Genome-wide association study of word reading: Overlap with risk genes for neurodevelopmental disorders. *Genes, Brain and Behavior* **2020**, *19*, e12648–e12648.

(282) Okamoto, N.; Miya, F.; Kitai, Y.; Tsunoda, T.; Kato, M.; Saitoh, S.; Kanemura, Y.; Kosaki, K. Homozygous ADCY5 mutation causes early-onset movement disorder with severe intellectual disability. *Neurological Sciences* **2021**, 1–4.

(283) Xu, Z.; Su, S.; Zhou, S.; Yang, W.; Deng, X.; Sun, Y.; Li, L.; Li, Y. How to reprogram human fibroblasts to neurons. *Cell and bioscience* **2020**, *10*, DOI: 10.1186/S13578-020-00476-2.

(284) Ahmad, F.; Chung, Y. W.; Tang, Y.; Hockman, S. C.; Liu, S.; Khan, Y.; Huo, K.; Billings, E.; Amar, M. J.; Remaley, A. T.; Manganiello, V. C. Phosphodiesterase 3B (PDE3B) regulates NLRP3 inflammasome in adipose tissue. *Scientific reports* **2016**, *6*, DOI: 10.1038/SREP28056.

(285) Karam, S. et al. Cardiac Overexpression of PDE4B Blunts β-Adrenergic Response and Maladaptive Remodeling in Heart Failure. *Circulation* **2020**, *142*, 161–174.

(286) Wang, Y.; Adjaye, J. A Cyclic AMP Analog, 8-Br-cAMP, Enhances the Induction of Pluripotency in Human Fibroblast Cells. *Stem Cell Reviews and Reports* **2011**, *7*, 331–341.

(287) Sackett, D. L.; Ozbun, L.; Zudaire, E.; Wessner, L.; Chirgwin, J. M.; Cuttitta, F.; Martínez, A. Intracellular proadrenomedullin-derived peptides decorate the microtubules and contribute to cytoskeleton function. *Endocrinology* **2008**, *149*, 2888–2898.

(288) Tixier, E.; Leconte, C.; Touzani, O.; Roussel, S.; Petit, E.; Bernaudin, M. Adrenomedullin protects neurons against oxygen glucose deprivation stress in an autocrine and paracrine manner. *Journal of Neurochemistry* **2008**, *106*, 1388–1403.

(289) Ferrero, H.; Larrayoz, I. M.; Gil-Bea, F. J.; Martínez, A.; Ramírez, M. J. Adrenomedullin, a Novel Target for Neurodegenerative Diseases. *Molecular neurobiology* **2018**, *55*, 8799–8814.

(290) Hurtado, O.; Serrano, J.; Sobrado, M.; Fernández, A. P.; Lizasoain, I.; Martínez-Murillo, R.; Moro, M. A.; Martínez, A. Lack of adrenomedullin, but not complement factor H, results in larger infarct size and more extensive brain damage in a focal ischemia model. *Neuroscience* **2010**, *171*, 885–892.

(291) Ochoa-Callejero, L.; Pozo-Rodrigálvarez, A.; Martínez-Murillo, R.; Martínez, A. Lack of adrenomedullin in mouse endothelial cells results in defective angiogenesis, enhanced vascular permeability, less metastasis, and more brain damage. *Scientific Reports* **2016**, *6*, 1–12.